INVESTIGATION OF ACID/BASE INTERACTIONS IN ADHESION

by

Paul Alan Koning

Dissertation submitted to the Faculty of the

Virginia Polytechnic Institute and State University

in partial fulfillment of the requirements for the degree of

Doctorate

in

Chemistry

APPROVED:

Thomas C. Ward, Chairman

James E. McGrath

James P. Wightman

Jack D. Graybeal

Halbert F. Brinson

January, 1988

Blacksburg, Virginia

INVESTIGATION OF ACID/BASE INTERACTIONS IN ADHESION

by

Paul Alan Koning

Thomas C. Ward, Chairman

Chemistry

(ABSTRACT)

The fundamental study of Lewis acid/base interactions presented in this dissertation demonstrates the role of these interactions in adhesive phenomena. The model systems investigated were representative of real substrates and soft, viscoelastic adhesives where, in one case, favorable acid/base interactions were possible which were not possible in the other. Inverse gas chromatography (IGC) and Infrared spectroscopy (IR) techniques were used to analyze the model adhesive in terms of its acid/base nature. The results of both experiments indicated, through negative enthalpies of acid/base interaction with acidic solvents, that the model adhesive poly(2-ethyl hexyl methacrylate) (PEHMA) exhibits the properties of a Lewis base. The near quantitative agreement of the results from both experiments validate these methods of determining acid/base interactions in polymeric systems. Fitting the enthalpies for acid/base interaction to Drago's and Gutmann's models brought out the importance of the electrostatic component of the interactions investigated. Furthermore, they illustrated the need to expand the existing data sets beyond organo-metallic compounds, and include more common organic solvents.

Results from X-ray photoelectron spectroscopy (XPS) and scanning transmission electron microscopy (STEM) analysis of the model substrate, grade 2 titanium, pretreated via chromic acid (CAA) or sodium hydroxide anodization (PSHA), confirmed that oxides of very similar topology can be produced. Indicator dye studies revealed the CAA-Ti had a surface pH of below 3.0 and the PSHA-Ti had a surface pH of above 8.0.

Bonds constructed from these analyzed materials were tested in peel and both systems exhibited good adhesion. However, the bonds in which favorable interactions were possible demonstrated superior interfacial performance. This improvement was seen in the bond's ability to resist adhesive (interfacial) failure at debond rates at which other bonds failed. When the test

geometry was changed such that the stress intensity at the interface was increased, the bonds in which acid/base interactions were favorable supported a higher peel load.

Acknowledgements

This dissertation represents the result of a coordinated effort on the part of many people and organizations. I, the author, wish to acknowledge these people and express my sincere gratitude for their efforts. Without them, this work would not have been possible.

The author would first like to thank his advisor, Dr. T. C. Ward, for his inspiration, support, encouragement, for providing the opportunities to attend meetings and meet prominent scientists, and lastly for his patience during the writing of this dissertation.

The author would like to thank his committee members Dr. H. F. Brinson, Dr. J. D. Graybeal, Dr. J. E. McGrath, Dr. T. C. Ward, and Dr. J. P. Wightman for serving on his committee and for their individual contributions to my graduate experience. Also, I would like to thank them for their continuing efforts to make the program at Virginia Tech one the author is proud to be associated with.

I would like to thank the Center for Adhesion Science for providing a graduate fellowship, funds for attending meetings, and for providing an arena of interaction with scientists of other disciplines. I would also like to thank the Polymer Materials and Interface Laboratories for the industrial interactions and travel funding which this organization provided. The author also gratefully acknowledges the support of the Office of Naval Research and the Adhesives and Sealants Council for their support of this work.

I would like to thank for their cooperation and synthetic experience in preparing the model adhesive systems; for her long discussions and suggestions in the area of surface science; for help with the

chromatography; for many hours on the STEM; , who kept the surface analysis equipment running;

for their various skills; and for their excellent editing of this dissertation.

The author would like to thank the Polymer Physical Chemistry Group and his friends at Virginia Tech, particularly the incoming class of 1982, for their helpful discussions and comradery. Finally, I would like to thank my wife, for her excellent typing, patience, understanding, and loving support throughout the "dissertation experience."

Table of Contents

List of Figures

List of Tables

1.0 INTRODUCTION

When two materials are brought into intimate contact, an interphase region is created, marking the transition from one material to the other. Understanding the nature of this interphase is critical in the study of interactions between two materials. Of primary interest in this work is the phenomenon of adhesion, and the interphase is thought to play a critical role.

According to Webster, the definition of adhesion is:

ad • he • sion, noun 1. an adhering or sticking together

2. body tissues abnormally joined

Concentrating on the first definition, what appears to be missing is the "why": what are the forces active in the interphase which cause the two materials to adhere? There are four general theories of adhesion[1-3]: diffusional, electrostatic, mechanical and adsorptive. The diffusion theory of adhesion, in essence, states that during the bonding process portions of polymeric adhesive will diffuse into the substrate, and vice versa. The interphase, therefore, is a physical mixture of the substrate and adhesive. This view of adhesion works well in describing the bonding of a polymer to itself or polymer/polymer bonding, but fails to explain adequately bonding in mutually insoluble systems (i.e., polymer-metal bonds).

The electrostatic theory of adhesion treats a bond as a capacitor, with the adhesive acting as one plate and the substrate as the other. To separate the plates (corresponding to bond failure), work must be done against any charge voltage differential. This theory ignores any other contribution to the work of adhesion. While some contributions from electrostatics may *result*

from failing a high strength bond, it is difficult to envision a load-bearing bond in which this would be the sole "cause" of adhesion.

The mechanical theory of adhesion proposes a mechanical keying or interlocking of the adhesive into irregularities of the substrate's surface as the major source of intrinsic adhesion. This interlocking prevents direct "pull out" of the adhesive off the surface. It also provides a less abrupt change in modulus across the interphase, allowing more effective transfer of stress from the substrate to the adhesive. However, good bond strengths can be obtained on smooth substrates where mechanical interlocking is minimal, thus, the mechanical interlocking theory alone cannot provide a comprehensive description of adhesion.

The adsorption theory of adhesion states that for maximum adhesion to occur, the adhesive must come into intimate contact with the substrate. If the materials are in intimate contact, one can use thermodynamic principles to define a work of adhesion W_A. This "thermodynamic adhesion" is the work required to separate a unit area of the two materials, and can be related to the surface free energies of the substrate and adhesive by the Dupre Equation[1-3]. In the absence of chemisorption, mechanical interlocking and interdiffusion, the reversible work of adhesion is expressed as:

$$W_A = \gamma_S + \gamma_{Adh} - \gamma_{S,Adh} \qquad [1.1]$$

where γ_s is the surface tension of the substrate, γ_{Adh} the surface tension of the adhesive and $\gamma_{S,Adh}$ the interfacial surface tension between the substrate and adhesive. It is important to note two items, revealed by the Dupre Equation and basic to the adsorption theory of adhesion. As the work of adhesion is expressed by "surface terms," then W_A, as expressed by Equation [1.1], concerns itself primarily with interfacial bond strengths. The equation as expressed does not account for any non-interfacial processes (i.e., viscoelastic contributions) which will add to the observed W_A. The strength of this model is that it recognizes that specific interactions across the interface can contribute to interfacial bond strength. This contribution is contained in the term $\gamma_{S,Adh}$.

1.1 Acid/Base Concepts in Adhesion

Using the adsorption theory of adhesion and the Dupre Equation as guides for the understanding of adhesion phenomena, the term $\gamma_{S,Adh}$ is of particular interest. It suggests that there are additional or perhaps "new" interactions occurring across the interphase as a result of placing the two materials into contact. Good[4], Grifalco[4], and Fowkes[5] were pioneers in attempting to understand the specific interactions which express themselves in the $\gamma_{S,Adh}$ term. The general approach used by these investigators was to break down the $\gamma_{S,Adh}$ into separate contributions from intermolecular forces. Such a treatment of the interfacial surface tension could then be expressed in a simple additive model:

$$\gamma_{S,Adh} = \gamma^{D}_{S,Adh} + \gamma^{dd}_{S,Adh} + \gamma^{I}_{S,Adh} + \gamma^{A/B}_{S,Adh} + \ldots\ldots \qquad [1.2]$$

where D represents the dispersion force term, dd the dipole-dipole, I the ionic and A/B the acid/base contribution.

Fowkes has championed the importance of acid/base interaction. He postulated that the work of adhesion, and, therefore, the interfacial performance of an adhesive bond, is dominated by the acid/base interaction and the dispersion forces. If this is true, then the interfacial surface tension can be expressed as:

$$\gamma_{S,Adh} = \gamma^{A/B}_{S,Adh} + \gamma^{D}_{S,Adh} \qquad [1.3]$$

with the other terms of Equation [1.2] making negligible contributions. The work of adhesion can be expressed as:

$$W_A = W_A^{A/B} + W_A^{D} \qquad [1.4]$$

As evidence of this view, Fowkes cites research involving the adsorption of polymers onto inorganic fillers. For a polymer in solution to spontaneously adsorb onto a filler, the change in the Gibbs free energy of the process must be negative ($\Delta G^{ads} < 0$). The adsorption process involves a decrease in entropy as the polymer chain has fewer possible configurations in the adsorbed state

than in solution. Therefore, for ΔG^{ads} to be negative, the enthalpy ΔH^{abs} must be sufficiently negative (exothermic) to overcome the unfavorable entropic contribution.

Mostafa[6] and Fowkes[6,7] have shown that acidic post-chlorinated poly(vinyl chloride), (CPVC), will strongly adsorb onto calcium carbonate (a basic filler), but will *not* adsorb onto silica (an acidic filler). When basic poly(methyl methacrylate), (PMMA), is used, the situation is reversed. These data, summarized in Figure 1.1, illustrate the thermodynamic prediction that adsorption will only occur when exothermic acid/base interactions are possible.

The data presented in Figure 1.2 indicate that even slight changes in the magnitude of acid/base interactions will affect the amount of polymer that will adsorb. In this experiment, Mostafa and Fowkes have shown that maximum adsorption of PMMA onto acidic silica occurs only in neutral solvents such as carbon tetrachloride. In solvents such as methylene chloride and chloroform, which are Lewis acids, competition of the acidic solvent with the acidic silica for the basic polymer reduces the amount adsorbed. In solvents such as dioxane and tetrahydrofuran, which are Lewis bases, competition between the basic solvent and the polymer for the acidic sites on the silica again reduced adsorption.

The above experiments clearly demonstrate the importance of exothermic acid/base interactions in adsorption phenomena. One can then safely postulate, using the adsorption theory of adhesion, that they should also play a major role in achieving optimum adhesive performance.

Fowkes has attempted to quantify acid/base interactions by extending an empirical relation first proposed by Drago *et al.*[8,9]. By means of a extensive set of enthalpy-of-reaction measurements, Drago developed a set of empirical constants, E_A, C_A and E_B, C_B , which allow prediction of the enthalpies of interaction for acidic and basic species. Drago and coworkers were then able to show that:

$$-\Delta H_{fA/B} = C_A C_B + E_A E_B \qquad [1.5]$$

where $\Delta H_{fA/B}$ is the enthalpy for the formation of acid/base interactions. A more thorough discussion of Drago's model can be found in Section 3.4. While Drago's work was limited to the interaction of low molecular weight compounds in solution, Fowkes has extended this model to

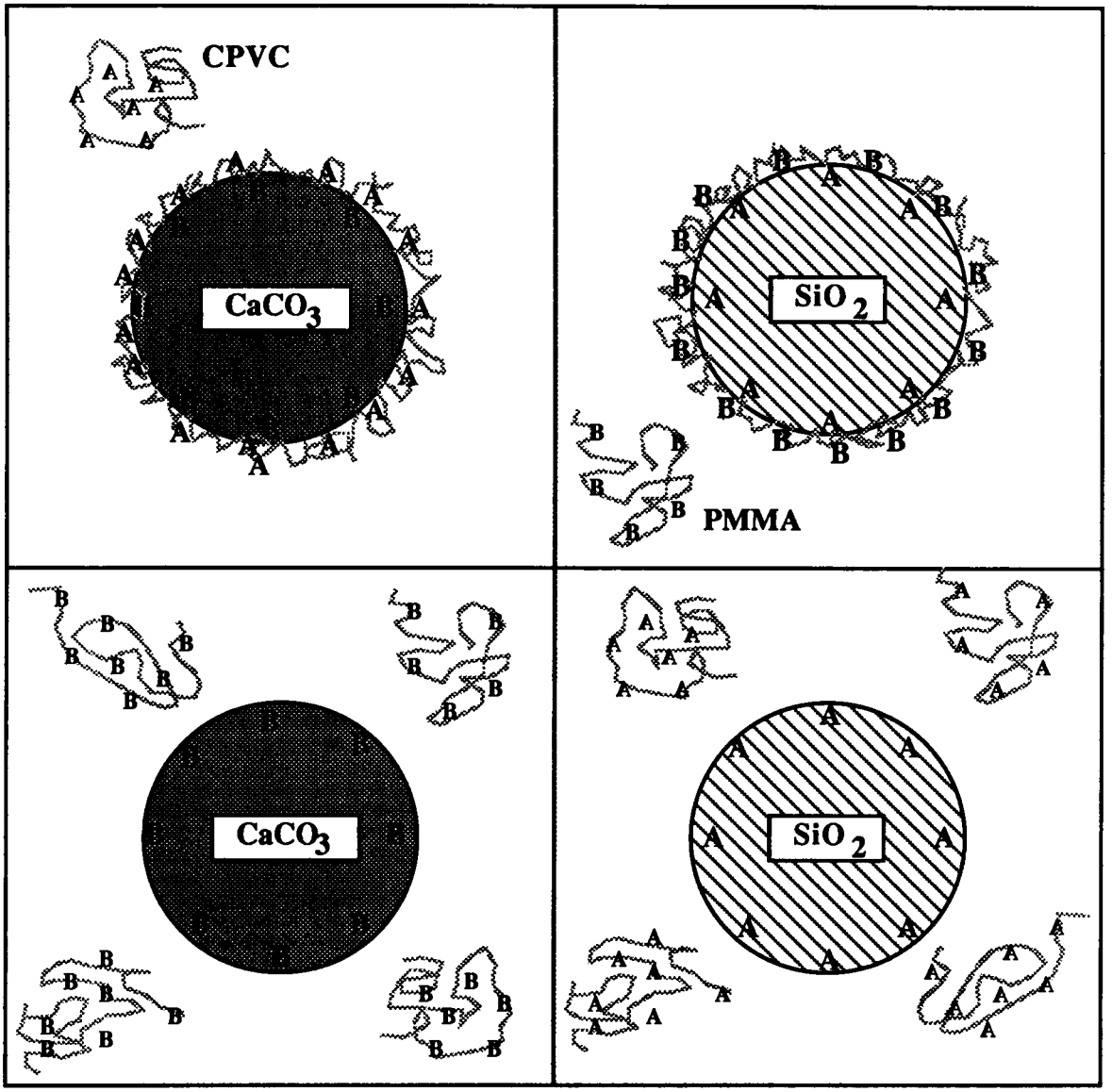

Figure 1.1 Effect of acid/base interaction on adsorption of polymers from solution (redrawn from Fowkes and Mostafa [6,7]).

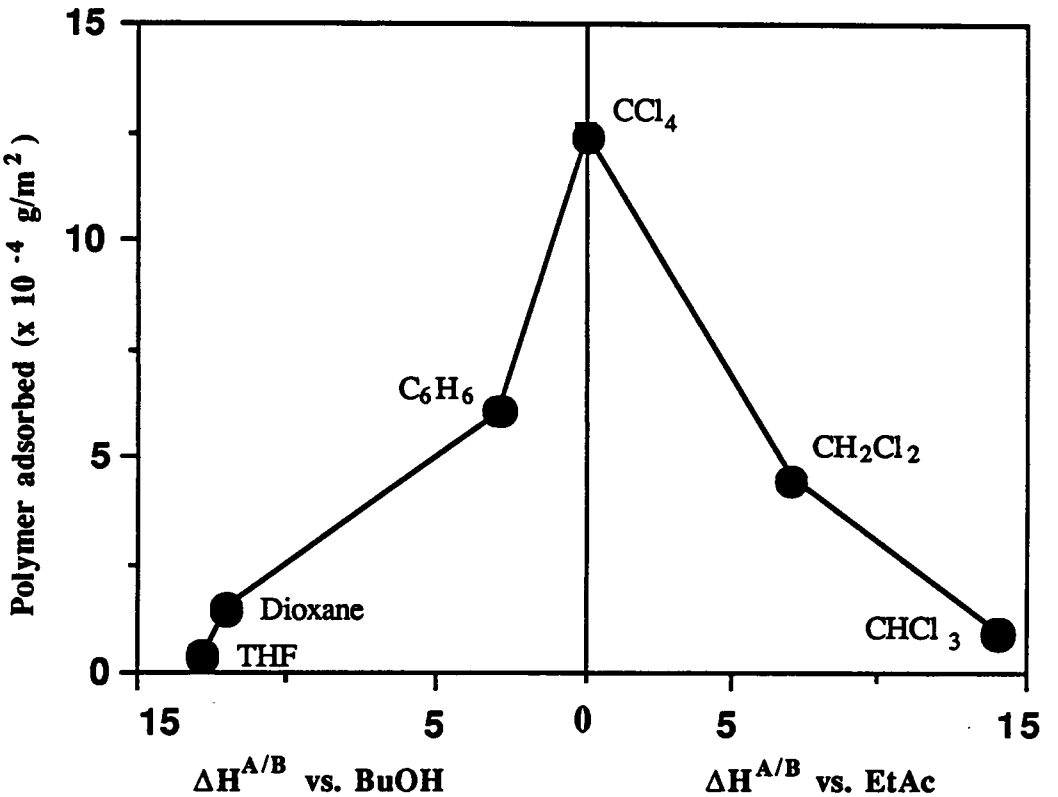

Figure 1.2 Basic PMMA adsorbs onto the acidic silica most strongly from neutral solvents, but with increasing basic or acidic solvents adsorption is diminished because of competition (redrawn from Fowkes and Mostafa [6,7]).

predict acid/base interactions *vis-a-vis* adhesion. The acids and base can now be viewed as the substrate and adhesive. If these C and E constants are known, the enthalpic contribution to the work of adhesion theoretically can be quantified.

Gutmann has also developed an empirical model which allows the estimation of enthalpies for acid/base interactions[10,11]. He proposes that these enthalpies can be calculated by one of the following relations:

$$\Delta H_{f\,A|B} = -f_A\,DN \qquad [1.6]$$

$$\Delta H_{f\,A|B} = -f_B\,AN \qquad [1.7]$$

$$\Delta H_{f\,A|B} = (-f_A\,DN) + (-f_B\,AN) \qquad [1.8]$$

In these equations, DN is the donor number for a Lewis base, AN the acceptor number for a Lewis acid, f_A the acceptor strength of an unknown acid, and f_B the donor strength of an unknown base.

Three equations are used in order to account for three possible situations. Equation [1.6] is used when a Lewis base interacts with an unknown acceptor; Equation [1.7] when a Lewis acid interacts with an unknown donor, and Equation [1.8] when a solvent exhibiting both acidic and basic properties (amphoteric) interacts with an unknown. A more detailed discussion of this model can be found in Section 3.5. Gutmann's work has been applied to low molecular weight compounds with great success and most recently by Schultz to epoxy/carbon fiber composites[12]. Schultz observed excellent correlation between the donor and acceptor strengths of epoxies and carbon fibers and the interfacial shear stress (τ) of the resulting composite material. His work clearly indicates the importance of acid/base interactions in composite materials.

The study presented in the following chapters is concerned with evaluating the contribution of acid/base interactions to adhesion. The aim of these investigations was to analyze a model adhesive and substrate with respect to their acid/base nature, and to demonstrate the macroscopic effect of these interactions in bonds.

1.2 References

1. W. D. Wake; *Adhesion and the Formulation of Adhesives, 2nd Ed.*, Applied Science Publishers (1982).
2. A. J. Kinloch; *Durability of Structural Adhesives*, Applied Science Publishers (1982).
3. S. R. Hartshorn; *Structural Adhesives*, Plenum Press (1986).
4. R. J. Good and L. A. Girifalco; *J. Phys. Chem. 64*, 561 (1960).
5. F. M. Fowkes; *J. Phys. Chem. 66*, 382 (1962).
6. F. M. Fowkes and M. A. Mostafa; *Ind. Eng. Chem. Prod. Res. Dev. 17 (1)*, 3 (1978).
7. F. M. Fowkes; *J. Adhesion Sci. Tech. 1 (1)*, 7 (1987).
8. F. M. Fowkes, D. O. Tischler, J. A. Wolfe, L. A. Lannigan, C. M. Ademu-John and M. J. Halliwell; *J. Polym. Sci.: Polym. Chem. Ed., 22*, 547 (1984).
9. R. S. Drago, G. C. Vogel and T. E. Needham; *J. Am. Chem. Soc. 93 (23)*, 6014 (1971).
10. V. Gutmann; *Electrochim. Acta. 21*, 661 (1976).
11. V. Gutmann; *The Donor-Acceptor Approach to Molecular Interactions*, Plenum Press (1978).
12. J. Schultz, L. Lavielle and C. Martin; *J. Adhesion 23*, 45 (1987).

2.0 APPLICATION OF INVERSE GAS CHROMATOGRAPHY IN THE STUDY OF THE ACID-BASE NATURE OF ADHESIVES

2.1 Overview of IGC

The uses of gas chromatography may be broadly divided into three classes: Analytical uses, preparative uses, and a method of determining physio-chemical properties.

The analytical uses of GC have become so widespread and commonplace that it is surprising to find a modern chemical laboratory without this capability. Preparative GC has found its greatest utility in industrial processing of petroleum streams and in laboratory purification of organics on the microscale. The development of GC as a method of determining thermodynamic properties, however, has been relatively slow. This is particularly true in the study of polymeric materials where their inherent negligible volatility has hindered progress. As a result, most early studies were confined to analysis of residual monomer or additives. An alternate solution to volatility problems was developed through pyrolysis GC. By this "enhancement" of the volatiles the resulting low molecular weight fragments could now be analyzed by traditional GC, and information on the structure and composition of the polymer could be derived.

The direct approach to the study of polymeric systems was initiated by Smidsvød and Guillet[1] in 1969. In these experiments, the polymer served as the stationary phase, and its interaction with known, volatile solutes was recorded. From the magnitude and temperature dependence of the interaction, physio-chemical properties of the polymer-solvent system, as well as those of the pure

polymer, can be measured. By convention, the term "probe" is given to the volatile solvent as its function is to probe the polymer and, by analysis of its behavior, yield thermodynamic information. The name "Inverse Gas Chromatography" (IGC) is customarily given to this technique.

The experimental quantities measured in IGC are temperature, retention times, flow rates, pressures, and percent loading of polymer. These are conveniently expressed in one parameter, the specific retention volume:

$$V_g^o = \frac{273.16 V_N}{T w_1} = \left(\frac{t_r}{w_1}\right) F J_2^3 \qquad [2.1]$$

where V_N is the net retention volume at temperature T, w_1 the mass of polymer on the column, F the corrected flow rate and J_2^3 the correction for gas compressibility. The first expresion for V_g^o uses terms conventional to GC theory; the second expression is an equivalent form more convenient for "number crunching" the raw data. A more detailed discussion of Equation [2.1] can be found in Section 2.4 and Appendix A.

These data are plotted in a generalized retention diagram of ln V_g^o vs. the reciprocal of the absolute temperature (1/T). A typical curve for a semi-crystalline polymer is shown in Figure 2.1. The explanation for the shape of this curve has been given by Guillet and coworkers[1-3] and is summarized below.

In the temperature region AB, the polymer is below its glass transition, and the probe molecule cannot penetrate the bulk. The curve approximates a straight line where the slope can be related to:

$$\frac{\partial \ln V_g^o}{\partial 1/T} = \frac{\Delta H_v - \Delta H_a}{R} \qquad [2.2]$$

where ΔH_v is the latent enthalpy of vaporization of the probe and ΔH_a is the enthalpy of adsorption onto the polymer surface.

The deviation from linearity at point B can be related to the T_g of the polymer. The region BC corresponds to non-equilibrium adsorption of the probe. The rate of diffusion in this

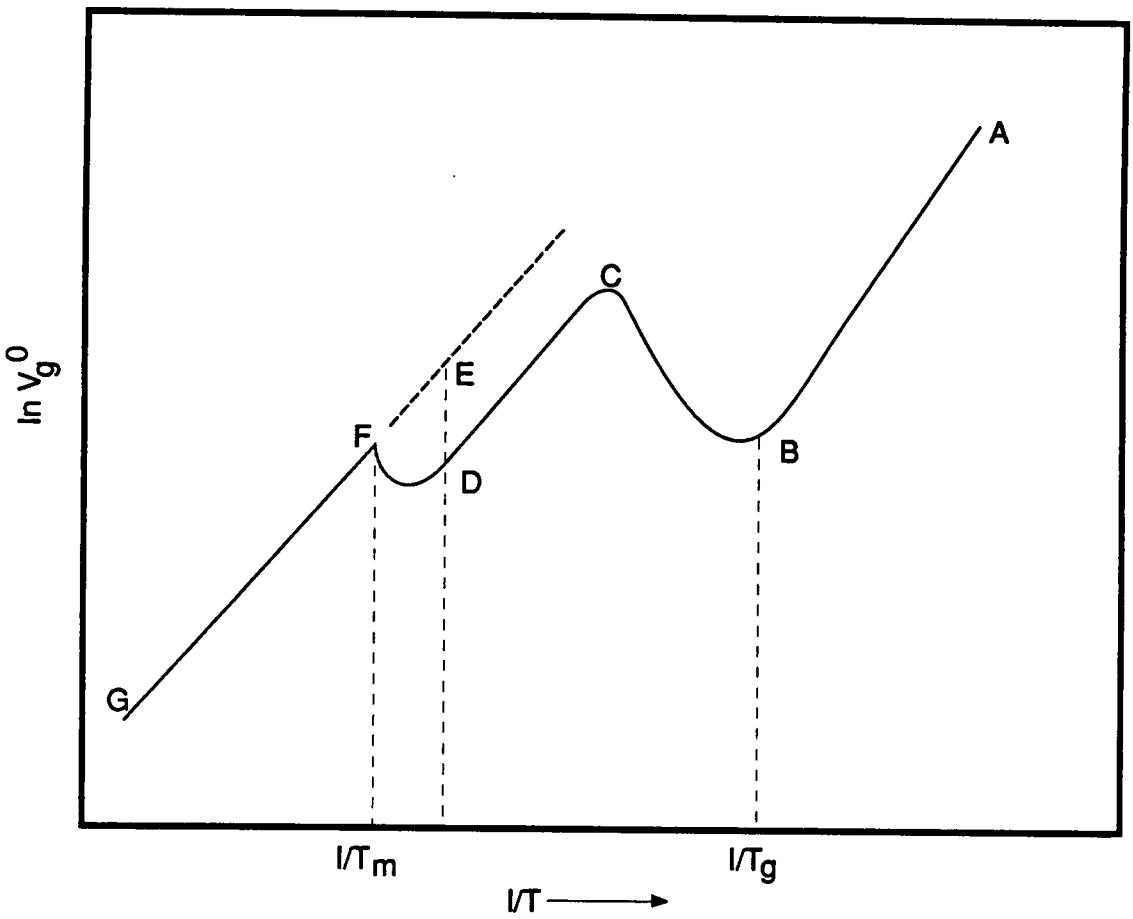

Figure 2.1. Generalized retention diagram.

temperature range is too slow to allow equilibrium to be established between the mobile and stationary phases.

Equilibrium absorption of the probe molecules throughout the amorphous phase of the polymer occurs in the region CD. The slope can be related to the heat of solution by the Equation:

$$\frac{-\Delta H_s}{R} = \frac{\partial \ln V_g^o}{\partial (1/T)} \qquad [2.3]$$

In semi-crystalline polymers, there can be some interference by adsorption of the probe onto crystallites. In such a case, Equation [2.3] cannot be rigorously applied until the polymer is completely amorphous (above T_m). Another source of interference would be the adsorption of the probe onto the solid support. This can be minimized by using thick polymer film ($\simeq$13% loading) and an inert solid support.

Upon melting, the fraction of amorphous material increases in region DF, causing an increase in the specific retention volume. At temperatures above the melting point, region FG, a linear retention diagram, corresponding to bulk adsorption into the now completely amorphous polymer, is obtained. By extrapolation of this line, FE, the crystalline content of the polymer can be determined by comparison of the experimental and extrapolated retention volumes.

As witnessed by the expanding literature in the field, IGC has been developed into a powerful tool for the investigation of polymer physical chemistry. The area is also well served by many excellent review articles[4-9]. A brief list of additional information which can be obtained from an IGC experiment is given in Table 2.1.

2.2 Acid/Base Information from IGC

While there is a great body of IGC work on the general thermodynamics of polymer-solvent systems, there is a notable lack of information for polar polymer-solvent systems. Inverse gas chromatography has been shown to be a technique ideally suited for obtaining physiochemical information about polymer-solvent systems at infinite dilution of the probe, and in particular for

Table 2.1. Listing of Parameters Available via IGC.

Parameter	Symbol	Reference
Enthalpies of Solution	ΔH_s	7
Hildebrand Solubility Parameter	δ_2	10
Weight Fraction Activity Coefficient	Ω_1^∞	11
Flory-Huggins Interaction Parameter	χ_{12} and χ_{23}	11,12,13
Glass Transition Temperature	T_g	1
Crystalline Melting Point	T_m	14
Percent Crystallinity	% C	15
Diffusion Coefficient	d_f	16

Note: In all these parameters, the subscript 1 refers to the solvent and 2 (or higher) to the polymer, hence χ_{12} is specific to a solvent-polymer system, while δ_2 is particular to the polymer alone.

studying the thermodynamics of specific interactions. Some authors suggest that this specific interaction can be ascribed to polar effect and in special cases charge transfer complexing[17]. In this work, the specific interaction term will be related to Lewis acid/base interactions. It is important to note that while this assignment is reasonable with respect to the systems of this study, this will not be universally correct for all polymer-solvent systems. Ionomers and reactive polymer systems (i.e. partially cured epoxies) could have chemical interactions with the probes that fall outside the scope of simple acid/base theory. It is important to keep this in mind when interpreting IGC data.

The thermodynamic parameter of interest in this work is the enthalpy for the formation of specific interactions, and, in particular, Lewis acid/base interactions. Two approaches[17,18] have been proposed to isolate the enthalpies for specific interactions. Both of these approaches decompose the overall enthalpies of solution into components resulting from dispersion forces, a component dipole/dipole interactions and a component for "specific" interactions. The first approach decomposes the enthalpy of solution into a general function of the polarizability (α_1), the dipole moment (μ_1) of the solvent and the specific interactions between the solvent and polymer (X) using the relation[17]:

$$-\Delta H_s = f(\alpha_1,\ \mu_1) + X \qquad [2.4]$$

In demonstrating this method, Dincer and Bonner used an ethylene-vinyl acetate copolymer as the stationary phase, and fit the enthalpies of solutions for a series of n-alkanes to quadratic curves. Since n-alkanes would only interact through the polarizabilities, the equation was found to be:

$$-\Delta H_{s(polarizability)} = \left[0.597\alpha_1 + 0.123\alpha_1^2\right] kJ\ mol^{-1} \qquad [2.5]$$

The dependence of the enthalpies of solution on the dipole moment of a solvent was determined using a series of alphatic ethers and nitriles. The enthalpic contribution from the polarizability was calculated from Equation [2.5] and the remaining enthalpy was totally assigned to dipole interactions. This relationship was found to be:

$$-\Delta H_s(dipole\ moment) = 1.78x10^{24}\,\mu_1\ kJmol^{-1} \qquad [2.6]$$

Combining Equations [2.5] and [2.6] yields the general form:

$$-\Delta H_s = 0.597\alpha_1 + 0.123\alpha_1^2 + 1.78x10^{24}\mu + X \qquad [2.7]$$

This equation was then used to fit the enthalpies of solution of 22 solvents with the ethylene-vinyl acetate copolymer. The logical conclusion arising from observing this equation is that any extra enthalpy that cannot be accounted for by α_1 and μ_1 must arise from specific interactions. While this equation is useful in gaining insight into the relative contribution of α and μ , it is far from exact. The authors acknowledge that Equation [2.5] is dependent not only on α_1, but also the class of the solvent. That is, n-alkane and aromatic compounds have separate and distant quadratic curves. They also admit the data set for which Equation [2.6] was obtained had significnt scatter and that perhaps the use of weaker dipoles and/or the inclusion of higher multipole moments would help.

An overview of the second approach to isolate acid/base interaction is described below. The injection of a small quantity of an electron-pair donor (acid probe) into a large excess of an electron-pair acceptor (basic polymer) gives rise to a heat term due to specific Lewis acid/base interactions and terms due to the action of non-specific forces such as dispersion forces or permanent dipole interaction.

It is possible to correct for non-specific interaction and thus obtain estimates of Lewis acid/base by choosing a suitable model compound for the probe and recording its interaction with the polymer under study. Such a model probe would be difficult to define as it must be identical to the probe in all physical properties except for the specific interaction group. Any mismatch would give rise to a small heat term due to the difference in non-specific interaction between the probe and its model. The magnitude of this difference can be measured and corrected for expanding the experiment and allowing both the probe and model to interact with a neutral polymer. A neutral polymer is defined as a polymer which has no Lewis acid/base or strong permanent dipoles. The difference in the ΔH_s between the solvent and probe with the neutral polymer will then be due only to their non-specific interactions, not to any acid/base interaction with the substrate.

This leads us to write the following relation for the estimation of Lewis acid/base interactions from overall heats of solution[18]:

$$\Delta H_{f(A/B)} = \left(\Delta H_s^P - \Delta H_s^M\right)_{sam} - \left(\Delta H_s^P - \Delta H_s^M\right)_{ref} \qquad [2.8]$$

where A, B, P and M refer to acid, base, probe and model compounds. A more detailed discussion of Equation [2.8] is found in Appendix B.

2.3 Experimental

Perhaps the most essential piece of equipment in the experimental setup is the investigator. To obtain reliable data, one must design and perform the experiments with awareness of the assumptions and limitations of the theory. There are many small numerical corrections and seemingly overzealous techniques that individually seem insignificant; however, when taken as a whole they can determine the success or failure of the experiment. The author feels it is because of the general lack of proper experimental technique that IGC has faded into obscurity after great activity in the area in the 1970's.

2.3.1 Materials

The solid support onto which the polymer is deposited was 60-80 mesh Chromosorb W-HP. This support was selected because it is one of the most inert available. Specific interaction between polymer/support and the solvent probe/support can interfere with the data interpretation (i.e., non-symmetric peaks) and therefore must be minimized. Powered Teflon supports are available, but generally not used due to problems in coating the support and the possibility of Teflon's own thermal transitions affecting the results ($T_\gamma = -80°C$, $T_{\beta 1} = 19°C$, $T_{\beta 2} = 30°C$, $T_\alpha = 126°C$, $T_m = 327°C$).

The solvents used for depositing the polymer onto the support for IGC analysis were reagent grade xylene and carbon tetrachloride, both neutral solvents. All solvents used as probes were gold-label grade from Aldrich Chemical and stored over activated 4 Å molecular sieves. Chloroform, methylene chloride and tetrahydrofuran were further purified by the method described

in Perrin *et al.*[19] to remove the stabilization agent. These light sensitive solvents were stored under N_2, in amber bottles and in a darkened dessicator. If more than two months passed, these solvents were redistilled before use. Poly(2-ethyl hexyl methacrylate), (PEHMA), was the polymer selected for this study. There were four major reasons why it was chosen. First, the polymer does exhibit adhesive properties. In order to apply the information gained in the IGC studies to adhesion phenomena, this is a requirement. Second, the polymer is totally amorphous. A crystalline phase in the polymer would complicate interpretation of the IGC data. Also, the necessity of reproducing exact crystalline morphologies in all experiments, using different substrates, would pose severe difficulties. Third, the low T_g of PEHMA ($\simeq$0°C) allowed the IGC experiment to be carried out in a convenient temperature range (40-65°C). When working with higher T_g materials (> 120°C), the commonly used solvent probes elute too quickly. Many times the elution peaks for the solvent probes partially or totally overlap with the peak for the marker gas. This makes accurate determination of the retention time and estimation of peak tailing difficult. Lastly, PEHMA contains only one type of functional group, the carbonyl group, which should be active in acid/base interactions.

The monomer, 2-ethyl hexyl methacrylate, was obtained from Polysciences, Inc. This monomer was polymerized, without further purification, in bulk via a free radical reaction by Tim Long and Craig DePorter of the Polymer Synthesis group at Virginia Tech. The resulting polymer had a number average molecular weight of 322,000 daltons, a polydispersity of 1.9. The triad tacticity revealed by ^{13}C and ^{1}H NMR was 60% syndiotactic and 40% heterotactic. Upon receiving the PEHMA, it was dissolved in THF, precipitated into a 50/50 methanol water mixture, dissolved in toluene, filtered and reprecipitated into methanol. This purification scheme assured removal of residual monomer, salts, and any particulate impurities. Polyethylene (PE) was chosen as the reference polymer in this study. It contains no strong Lewis acid/base sites and no permanent dipoles. Low density polyethylene (0.88 g/cm^3), free from antioxidant, was obtained from Scientific Polymer Products, Inc. The helium used for the carrier gas was first passed through a drying tube and an oxygen scrubber. The oxygen was scrubbed to the ppm level to assure that minimal degradation would occur as the column was left at elevated temperatures for long periods of time.

2.3.2 *IGC Techniques and Instrumentation*

The polymers to be analyzed were first dissolved in a suitable solvent and filtered. A quantity of inert support was then weighed out to achieve a final product of ≃25 grams of a 15 wt/wt % stationary phase. The inert support and filtered polymer solution were then placed into a 500 ml "hedgehog" flask. The hedgehog flask is a 500 ml pear-shaped flask with vigreux fingers extending into its interior. The solvent was removed by slow evaporation using a rotary evaporator. The rotary motion in combination with the hedgehog flask assures gentle but adequate agitation needed for complete and uniform coverage. After removal of the solvent, the free-flowing support was vacuum dried for 24 hours at 110°C. This supported stationary phase was resieved to 60-80 mesh, which removed large agglomerates and "fines" (fractured solid support). This step is important as agglomerates and fines reduce packing efficiently, cause peak-tailing and will expose uncoated, non-neutralized surfaces. The support was then packed into a 0.25" (o.d.) stainless-steel column (premium grade from Supelco) with the aid of a column vibrator. Silane treated glass wool was used to plug the column ends. The column was then coiled and placed in the chromatograph with only its inlet port connected. After a 30-minute purge with helium gas, the column was taken to 10° above the T_g or T_m of the polymeric phase, whichever was highest, and held there for 12 hours. This procedure removed any residual solvent and solvent-induced morphologies present in the polymer.

IGC measurements were carried out using a HP-5890 gas chromatograph equipped with a FID detector. A schematic is shown in Figure 2.2. The FID detector allows much lower detection limits (≃ 100x) and a greater linear response range than a TCD. This affords a much better approximation of infinite dilution. Helium was the carrier gas to assure near-ideal gas behavior, and methane was the non-interacting probe. Retention times for both the marker and probe molecules were determined from their peak maxima using a HP-3392A integrator. The reported area of the peak was plotted against retention time to assure that the retention time was independent of sample size (i.e., infinite dilution) (Figure 2.3).

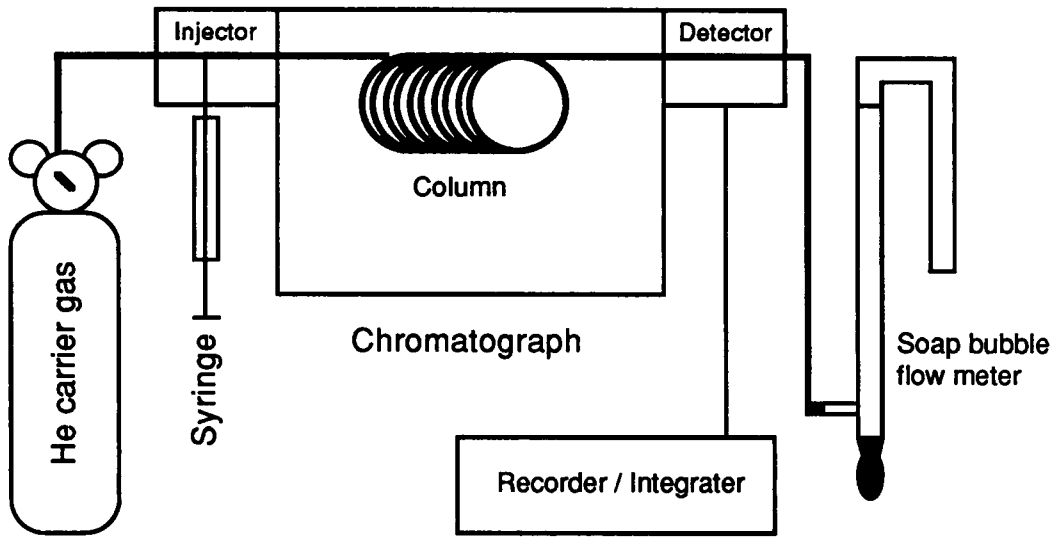

Figure 2.2. Schematic of IGC apparatus.

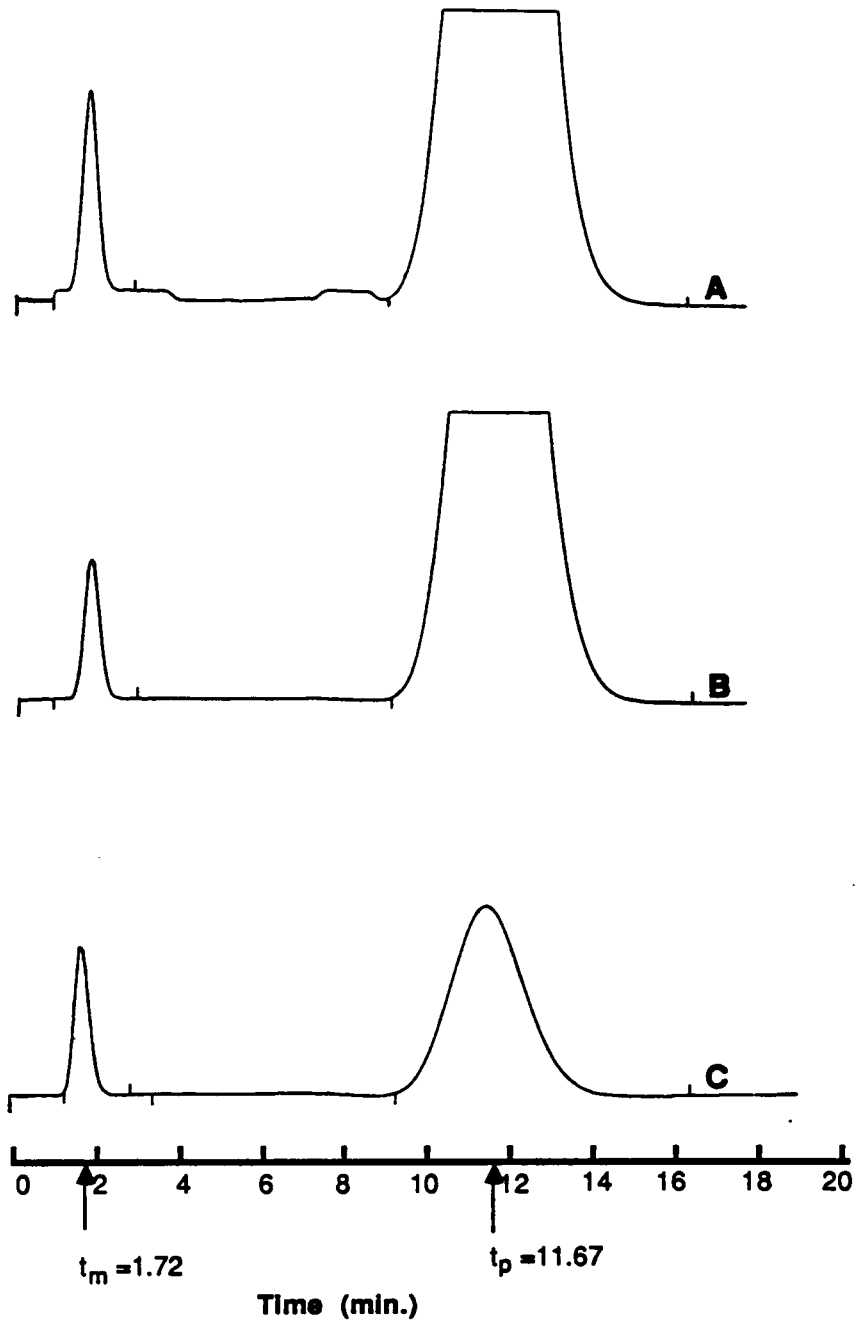

Figure 2.3. Typical IGC chromatogram showing independence of retention time (t_p) on the sample size. Integrated areas range from 4,100,000 for A to 700,000 for C.

Flow rates were measured from the column end using a soap bubble flow meter modified with an inverted U-tube on top. The U-tube allowed the flow meter to be purged with the carrier gas prior to measurement. This is important, as diffusion of helium through a bubble to the air-rich side will cause errors in measurement at these slow flow rates (5-10 ml/min). The walls of the flow meter were thoroughly dampened by passing 20 bubbles its entire length before any measurement was made. An average of four readings was taken to assure accuracy. Pressures at the inlet of the column were measured with a mercury manometer. The outlet pressure (atmospheric) was measured using a mercury and brass barometer applying the appropriate correction[20]. Oven and ambient temperatures were measured with an Omega Instruments Pt resistance thermometer. Both the probe and marker were injected simultaneously with a Hamilton 10 $\mu\ell$ gas-tight syringe. The following injection technique was adopted in order to insure the injection "0" sample size. Initially the syringe was flushed out many times with solvent *vapor*. Approximately 1 $\mu\ell$ of solvent vapor with 1 $\mu\ell$ of a $\simeq$0.08 vol% mixture of methane in He was injected into the chromatograph and its response recorded. Further, 1 $\mu\ell$ injection of the methane/He mixture was made until the peak for the residual solvent vapor was no longer recorded. This allowed a regression of many sample sizes (via the peak area) on the retention time to assure they were independent (i.e., slope = 0).

The weight of polymer on the support was determined by ashing using a Perkin Elmer-TGA. The coated support (10 mg) was loaded into the TGA sample pan and the temperature raised to 550°C in oxygen. Measurements on the coated and uncoated support were made in triplicate to assure accuracy. The method of Soxhet extraction to determine sample loading was not used as it is longer, more cumbersome and less accurate. This method, however, would be necessary with polymers which form refractor oxides (i.e., siloxanes).

The amount of loading was typically 3% lower than that expected from the initial weight of polymer and support. This is due to coating of the glassware with the polymer. The optimum loading lies between 6-15 wt/wt %. Several workers[21,22] have shown that below 4-6% loading contribution due to adsorption on uncoated support can be detected, while at higher loadings (> 15%), diffusion through the thick polymer coating becomes a problem.

2.4 Data Reduction

The specific retention volume, V_g^0, was calculated from the relation:

$$V_g^0 = \left(\frac{t_r}{w_l}\right) F J_2^3 \qquad [2.9]$$

where t_r is the net retention time, w_l the mass of polymer in the column, F the corrected flow rate and J_2^3 the correction for pressure drop across the column[4,23,24]. The flow rate F has been corrected in regard to two terms: vapor pressure of water in the flow meter and 0°C. The relation is given by[25]:

$$F = \frac{273.16 f (P_o - P_{H_2O})}{P_o (273.16 + T_A)} \qquad [2.10]$$

where P_o is the atmospheric pressure (mm Hg), f the flow rate measured from the column end (ml/min), and P_{H_2O} the pressure of water (mm Hg) at the temperature T_A (°C) of the flowmeter.

J_2^3 is the James-Martin correction factor for gas compressibility and is given by the relation[24,26]:

$$J_2^3 = \frac{3}{2}\left[\frac{\left(\frac{P_i}{P_o}\right)^2 - 1}{\left(\frac{P_i}{P_o}\right)^3 - 1}\right] \qquad [2.11]$$

where P_i is the pressure (mm Hg) at the injector.

The enthalpies of solution at infinite dilution were calculated from the temperature dependence of the specific retention volumes[4]:

$$\Delta H_s = R \frac{\partial \ln (V_g^0)}{\partial \ln \left(\frac{1}{T}\right)} \qquad [2.12]$$

A more detailed description of Equation [2.12] can be found in Appendix A. The enthalpies of formation for acid/base interaction can be obtained from enthalpies of solution using a relation developed by Arnett *et al.*[27] for classical calorimetry and first applied to IGC by DiPaola-Baranyi and Guillet[1]:

$$\Delta H_{f(A/B)} = \left[\Delta H_s^P - \Delta H_s^M\right]_{sample} - \left[\Delta H_s^P - \Delta H_s^M\right]_{ref.} \qquad [2.13]$$

where A, B, P and M refer to acid, base, probe and model compounds, respectively.

A more detailed discussion of Equation [2.13] can be found in Appendix B. In this study, PEHMA was the sample polymer and low density PE, the reference polymer. The reference polymer and model compound were chosen with the requirement that they contain neither a strong, permanent dipole nor a Lewis acid/base site, hence PE and carbon tetrachloride are logical choices[28].

Flory-Huggins interaction parameters at infinite dilution were calculated from the relation[4]:

$$\chi_{12}^{\infty} = \ln\left(\frac{273.16\,R\,v_2}{V_1\,V_g^o\,P_1^o}\right) - \left(1 - \left(\frac{V_1}{\overline{M}_n\,v_2}\right)\right) - \frac{P_1^o}{RT}\left(B_{11} - V_1\right) \qquad [2.14]$$

where V_1, P_1^0 and B_{11} are the molar volume, vapor pressure and second virial coefficient of the probe, v_2 and $\overline{M}_n$ are the specific volume and number-average molecular weight of the polymer. Values for V_1, P_1^0 and B_{11} were obtained from the recent data compilation of Boublik[29], Smith[30] and Dymond[31]. The more traditional sources for this information, Reid[32], Olabisi[33], Timmermans[34], Dreisbach[35], Orwoll and Flory[36], Guggenheim[37] and McGlashan[38], were consulted if the data did not appear in the more recent compilations. Values for v_2, the specific volume of the polymer, were estimated using the methods of Van Krevelan[39]. A more detailed discussion of Equation [2.14] can be found in Appendix A.

2.5 Results and Discussion

The experimental specific retention volumes were determined over a range of 45° to 65°C. The typical temperature dependence, ln V_g^o , is shown in Figure 2.4. The linearity of this plot indicated that the enthalpy of solution was constant over this temperature range. A summary of the enthalpies of solution calculated from Equation [2.13] are shown in Table 2.2. As can be seen, the enthalpies of solution for all four probes with both polymers were negative. This result indicated that at low concentrations of solvent (i.e., infinite dilution), the overall heat of solution was favorable to mixing.

Calculated enthalpies for acid/base interactions are shown in Table 2.2. Tetrahydrofuran and acetone were classified as Lewis bases due to the lone pair electrons on oxygen which could be donated. This is consistent with Drago's classification of the compounds[40]. PEHMA also contains oxygen atoms in its ester group and is expected to exhibit a basic nature. An analog of PEHMA, poly(methyl methacrylate), has been shown to be a Lewis base[41]. The enthalpy for the formation of the base/base interaction was shown to be positive, hence endothermic. This result was expected since the interaction of two bases would be predicted to be thermodynamically unfavorable.

In the case of the two acidic probes, chloroform and methylene chloride, the enthalpy for the acid/base interaction was negative, hence exothermic. This is again the expected result since an acid/base interaction would be thermodynamically favorable. The ranking of the two solvents, indicating methylene chloride is a stronger acid than chloroform, is of concern. One would expect chloroform with more electronegative chlorines attached to the carbon to be the stronger Lewis acid. A possible explanation of these results would be that one of the solvents contained some water. Water can act as an acid or base and could therefore interfere with these measurements. If the chloroform were wet, water, being a weaker acid, could lower the observed enthalpy of interaction.

Flory-Huggins parameters calculated from Equation [2.14] are shown in Table 2.4. As χ_{12}^{∞} was nearly constant over the temperature range, the reported χ_{12}^{∞} is an average over 45-65°C. The negative values of χ_{12}^{∞} indicated strong interaction or thermodynamically "good" solutions. The

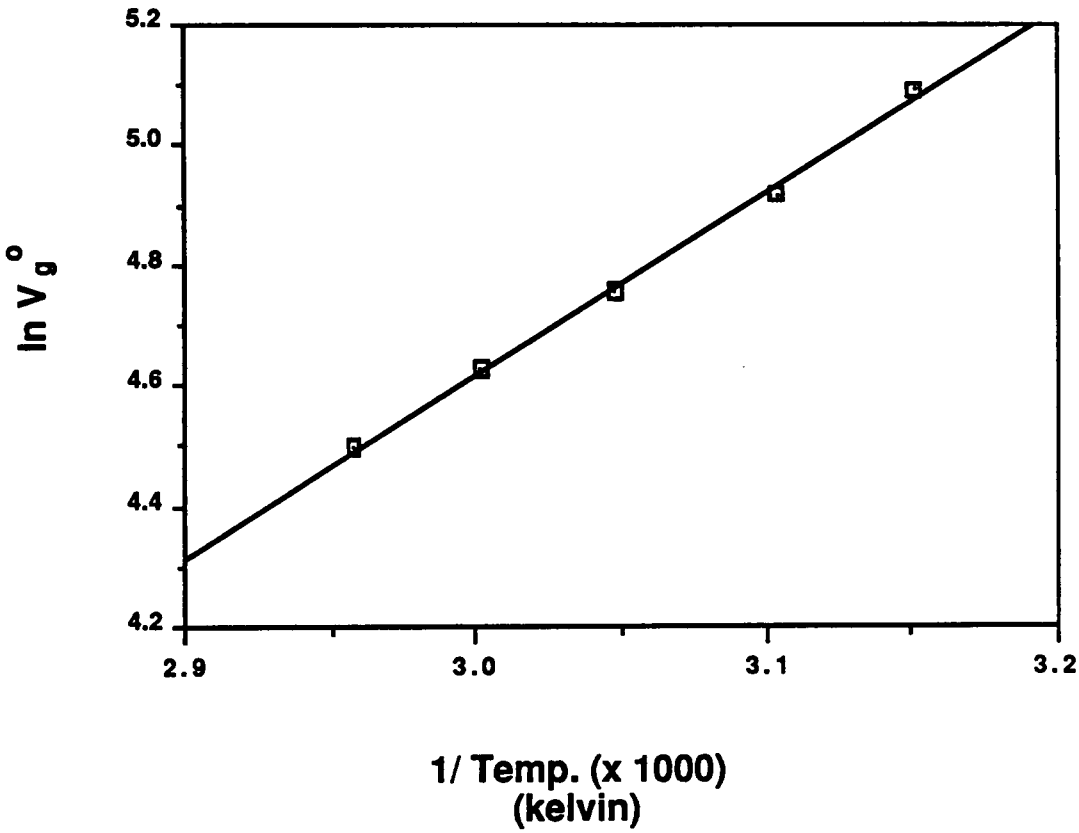

Figure 2.4. Typical IGC data showing the temperature dependence of the specific retention volume. The slope is proportional to the ΔH_S (Equation [2.12]).

Table 2.2. Enthalpies of Solution via IGC (PEHMA & PE).

	ΔH_s (PEHMA)	ΔH_s (PE)
Acetone	-28.8	-34.8
THF	-31.8	-27.6
CCl_4	-32.4	-25.2
$CHCl_3$	-36.6	-26.6
CH_2Cl_2	-30.0	-18.6

(all enthalpies in kJ/mol)

Table 2.3. Acid/Base Results via IGC.

	$\Delta H_{f\,A/B}$	*Interaction Type*
Acetone	13.1	B x B
THF	2.9	B x B
$CHCl_3$	-2.9	A x B
CH_2Cl_2	-4.3	A x B

(all enthalpies in kJ/mol)

amorphous PEHMA is readily soluble in all of the listed solvents, so strong χ_{12}^{∞} were expected. However "normal" PE is not soluble in these solvents, thus, the negative χ_{12}^{∞} seems inconsistent. This concern can be allayed if one considers two items: First, the polyethylene used in this experiment is exceptional due to its very low density (0.88 g/cm^3), very low molecular weight (1100 g/mol), high branching (50-60 methyl groups/1,000 carbon atoms) and low crystallinity (< 30%)[42]. This is very different from "normal" PE with typical densities in the range of 0.91-0.97 g/cm^3, molecular weights 50,000 to 500,000, less than 20 methyls per 1,000 carbon atoms and crystallinities above 80%. Second, when performing IGC below the T_m of the polymer, the probe molecule only "samples" the amorphous regions. Chain ends, branch points and other defects tend to be excluded from the crystalline regions and concentrate in the amorphous phase. With these facts in mind, the negative χ_{12}^{∞}'s do not seem so unreasonable.

The macroscopic solution properties support the χ_{12}^{∞} for the polymers. PEHMA is completely and readily soluble in all the solvents, as expected. The low density PE is semi-crystalline, therefore, complete solution is not expected until the temperature exceeds T_m (90°C). In all listed solvents, with one exception, the polymer swelled extensively. The exception was acetone where the swelling was moderate. When these solutions were heated to their boiling point, the polymer, originally a waxy mass, dispersed into the solvent. Their appearance was that of many small "pin point" swollen particles in an otherwise clear solution. Upon cooling all solutions became cloudy, indicating some fraction of the polymer had been in true solution.

2.6 Summary

The results presented indicate that inverse gas chromatography data, when analyzed using the described procedures, can yield information on the acid/base nature of polymeric adhesives. Our results show that PEHMA is a basic polymer. The result is consistent with the fact that an analogous polymer, PMMA, has been shown to be a Lewis base.

Only limited information is available on acid/base interactions in polymeric systems, and it will be necessary to extend the experiments described herein to other polymer solvent combinations.

Table 2.4. Flory-Huggins Interaction Parameters for Various Solutes in PEHMA and PE (45-65°C).

	χ_{12}^{∞} (*PEHMA*)	χ_{12}^{∞} (*PE*)
Acetone	-0.88	-0.59
THF	-1.74	-1.67
CCl_4	-1.99	-1.48
$CHCl_3$	-1.94	-1.43
CH_2Cl_2	-1.62	-0.74

Complementary spectroscopic experiments are reported in Chapter 3 and the data there compared as an additional check of the reliability of the acid/base measurements. These acid/base measurements can be further analyzed using Drago's two-parameter or Gutmann's one-parameter system of expressing acid/base strength. These methods permit a calculation of the predicted enthalpies with other species. This analysis is discussed in Chapter 3.

The negative values of χ_{12}^{∞} indicated strong interaction or thermodynamically "good" solutions with both PEHMA and PE in the region of infinite dilution of probe. While surprising in the case of the PE, if one considers the special nature of this PE and its macroscopic solution behavior in these solvents, these results seem reasonable.

2.7 Future Directions

The fact that one can get reliable information on the acid/base nature of polymeric adhesives opens new directions for using IGC to study adhesion phenomena. The extension to other low T_g methacrylate/acrylate adhesives is obvious. It will be desirable to utilize different neutral and model compounds, however. The low density polyethylene currently used has a T_m of 90°C, limiting its usefulness. An amorphous polymer such as hydrogenated isoprene, [poly(ethylene-alt-propylene)], has a low T_g, good thermal stability and could also serve as a neutral adhesive in mechanical test, a great bonus. There is some evidence that the model probe molecule, CCl_4, can exhibit an acidic nature. While it is not known if this is due to impurities or intrinsic properties, switching to n-pentane or n-hexane would circumvent these difficulties. Furthermore, when studying systems with higher T_g's, a low boiling probe may elute too quickly to be useful; higher n-alkanes would be readily available in high purity.

Investigations of high T_g engineering thermoplastics would also be a fruitful area of study. The backbone of these polymers is more rigid than the low T_g pressure sensitive adhesive. Thus, while the $\Delta H_f(A/B)$ measure with a highly mobile small molecule may be large, it may not necessarily translate to enhanced interfacial properties as the number of polymer conformations is

limited. Shultz[43] has shown that the analysis of the acid base nature of carbon fibers is also possible using IGC. This allows analysis of both matrix and fiber using the same instrument.

2.8 References

1. O. Smidsrød and J. E. Guillet; *Macromol., 2 (3)*, 272-277 (1969).
2. A. Lavoie and J. E. Guillet; *Macromol., 2*, 443 (1969).
3. A. N. Stein and J. E. Guillet; *Macromol., 3*, 102 (1970).
4. J. E. G. Lipson and J. E. Guillet; *Development in Polymer Characterization - 3*, ed. J. V. Dawkins, Applied Science Pub. (1982).
5. J. S. Aspler; *Pyrolysis and GC in Polymer Analysis*, Marcel Dekker Inc. (1985).
6. J. M. Braum and J. E. Guillet; *Advances in Polymer Science, Vol. 21*, Springer-Verlag.
7. J. E. Guillet; *New Development in Gas Chromatography*, John Wiley & Sons (1973).
8. D. G. Gray; *Prog. Polym. Sci., 5 (1)*, 1-60 (1977).
9. D. C. Bonner; *J. Macromol. Sci.-Revs. Macromol. Chem., C13 (2)*, 263-319 (1975).
10. K. Ito and J. E. Guillet; *Macromol. 12 (6)* (1979).
11. D. Patterson, Y. B. Tewari, H. P. Schreiber and J. E. Guillet; *Macromol., 4 (3)*, 356 (1971).
12. Z. Y. Al-Saigh and Petr Munk; *Macromol., 17 (4)* (1984).
13. G. DiPaola-Baranyi and P. Degre; *Macromol. 14 (5)* (1981).
14. D. G. Gray and J. E. Guillet; *Macromol. 4 (1)* (1970).
15. J. E. Guillet and A. N. Stein; *Macromol. 3 (1)* (1970).
16. D. G. Gray and J. E. Guillet; *Macromol. 6 (2)* (1973).
17. S. Dincer and D. C. Bonner; *Macromol., 11 (1)*, 107-113 (1978).
18. G. DiPaola-Baranyi, J. E. Guillet, H. Jeberien and J. Klein; *Makromol. Chem., 181*, 215-226 (1980).
19. D. D. Perrin, W. L. F. Armarego and D. R. Perrin; *Purification of Laboratory Chemicals, 2nd Ed.*, Pergamon Press (1980).
20. *CRC Handbook of Chemistry and Physics, 55th Ed.*, E-40, CRC Press (1975).
21. W. R. Summers, Y. B. Tewari and H. P. Schreiber; *Macromol., 5 (1)*, 12-16 (1972).
22. J. M. Braun and J. E. Guillet; *Macromol., 8 (6)*, 882-888 (1975).
23. A. B. Littlewood, C. S. G. Phillips and D. T. Price; *J. Chem. Soc., 1480* (1955).
24. A. B. J. Cruickshank, M. L. Windsor and C. L. Young, *Proc. R. Soc. London, A295*, 259-270 (1966).
25. G. D. Paola-Baranyi; *Macromol., 14 (3)*, 683-687 (1981).
26. A. T. James and A. J. P. Martin; *Biochem. J., 50*, 679-690 (1952).
27. E. M. Arnett, L. Joris, E. Mitchell, T. S. R. Murty, T. M. Govrie and P. V. R. Schleyer; *J. Am. Chem. Soc., 92*, 2365 (1970).

28. Carbon tetrachloride was chosen as a model neutral solvent based on Drago's selection of it as his neutral solvent. It has recently come to the author's attention that CCl_4 can exhibit an amphoteric or weakly acidic nature. It is not known if this is due to common impurities found in CCl_4 or if this is an inherent property. In the future an n-alkane should be used if possible.

29. T. Boublik, V. Fried and E. Hala; *The Vapour Pressures of Pure Substances, Physical Sciences Data 17*, Elsevier (1984).

30. B. Smith and R. Srivastava; *Thermodynamic Data for Pure Compounds, Physical Sciences Data 25 A & B*, Elsevier (1986).

31. J. H. Dymond and E. B. Smith; *The Virial Coefficients of Pure Gases and Mixtures*, Oxford University Press (1980).

32. R. C. Reid, J. M. Prausnitz and T. K. Sherwood; *The Properties of Gases and Liquids*, McGraw-Hill (1977).

33. O. Olabisi; *J. Appl. Poly. Sci., 22*, 1021 (1978).

34. J. Timmermans; *Physico-Chemical Constants of Pure Organic Compounds*, Elsevier (1950), ibid. 1962.

35. D. R. Dreisbach; *Adv. Chem. Soc.* No. 15, ibid. No. 22, ibid. No. 29.

36. R. A. Orwoll, P. J. Flory; *J. Am. Chem. Soc., 89*, 6814 (1967).

37. E. A. Guggenheim and C. J. Wormald; *J. Chem. Phys., 42*, 3775 (1965).

38. M. L. McGlashan, D. J. B. Potter; Proc. R. Soc. London Ser. *A267*, 478 (1962).

39. D. W. Van Krevelen and P. J. Hoftyzer; *Properties of Polymers: Their Estimation and Correlation with Chemical Structure*, Elsevier (1976).

40. R. S. Drago, G. C. Vogel, T. E. Needham; *J. Am. Chem. Soc., 93 (23)*, 6014-6026 (1971).

41. F. M. Fowkes, D. O. Tischler, J. A. Wolfe, L. A. Lannigan, C. M. Ademu-John and M. J. Halliwell; *J. Poly. Sci., Poly. Chem. Ed., 22*, 547-566 (1984).

42. Molecular weight was determined by Vapor Phase Osmometry; branching and crystallinity were estimated from the melting point and density.

43. J. Schultz, L. Lavielle and C. Martin; *J. Adhesion 23*, 45 (1987).

3.0 APPLICATIONS OF INFRARED SPECTROSCOPY

3.1 Introduction to Infrared Spectroscopy

Infrared spectroscopy is a field in which the absorption of various wavelengths of incident infrared (IR) radiation into the vibrational normal modes of a molecule is analyzed. As the possible vibrational modes in polyatomic molecules can be quite complex, so the absorption spectrum is also highly complex. The spectrum is thereby very information-rich, with various functional groups and atomic configurations giving rise to characteristic absorptions and patterns of absorption.

For a functional group to be "IR active," it must fulfill two major conditions. First, the energy spectrum of the photons in incident radiation must contain a portion which coincides with the energy level difference of that group's vibrational mode. Second, that absorption must cause a change in the electrical dipole moment of the group. This restriction distinguishes between systems which are infrared and Raman active.

The location of the absorption for a functional group is not a random event, but defined by the laws of quantum mechanics. A simple mathematical expression, assuming a harmonic oscillator, allows estimation of the absorption maxima and is given by[1,2]:

$$\bar{\nu} = \frac{1}{2\pi c}\sqrt{\frac{k}{\mu}} \qquad [3.1]$$

where $\bar{\nu}$ is the wavenumber of absorption, c the velocity of light, k the force constant of the chemical bond and μ the reduced mass of the atoms involved. As can be seen if the reduced mass

is kept relatively constant and the force constant of the chemical bond is changed, the frequency of absorption will become higher. An example of this is shown in Table 3.1. Ranges, rather than single values, are reported in Table 3.1 since Equation [3.1] only gives an approximate position of the IR band. The exact location of the absorption maxima may be shifted from the calculated value by intramolecular resonance effects, hybridization, and intermolecular specific interactions which may be operating in molecules. It is the shift due to specific interaction which contains the information on acid/base interactions.

3.2 Acid/Base Information From IR Spectroscopy

It is observed that if the IR spectrum of a compound is obtained in a series of solvents, there will be a shift in the frequency of the absorption maxima for many of its functional groups dependent on the solvent used. This phenomenon is known as "solvent shift" and is an example of intermolecular interactions (e.g., solvent-sample) giving rise to a change in the IR absorption.

The primary cause of the solvent shift effect has long been a topic of study. An excellent series of articles which details studies on the solvent shift has been written by Bellamy and co-workers[3-7] (1958-1960), Allerhand and Schleyer[8] (1963) and Fowkes[9] (1984). These works generally focused on the study of X-H or X=O functional groups. Common to all these studies is the assignment of a reference-state, free compound frequency for the IR absorption band. This state is defined as the low pressure vapor phase, and the corresponding absorption maxima (the free compound frequency) is given the symbol ν^{ref}. This reference-state, free compound frequency assumes no intermolecular interaction will be active in the low pressure vapor as the molecules approach high dilution. The intramolecular interactions inherent to the molecule are assumed to be constant.

Bellamy *et al.*[3-7] attempted to assign all solvent shift from ν^{ref} to specific hydrogen bonding interactions. While his model works well in acid/base active solvents, it fails to adequately explain solvent shift in inert, neutral solvent. To account for this, it seemed that an additional non-specific interaction term was needed. This fact was recognized by Allerhand *et al.*[8] and, most recently, by

Table 3.1. Force Constants and Stretching Frequencies for a Series of Carbon Oxygen Bonds.

Functional Group	k*	$\bar{\nu}$*
C-O	5.0 x 10^5 dyn cm^{-1}	1300-800 cm^{-1}
C=O	10 x 10^5 dyn cm^{-1}	1900-1500 cm^{-1}
C≡O	15 x 10^5 dyn cm^{-1}	2300-2000 cm^{-1}

*Data taken from Silverstein *et al.*[2]

Fowkes *et al.*[9]. Fowkes proposed that omni-directional dispersion forces, active in all materials, formed the basis for the non-specific portion of the solvent shift. From his work with doubly bonded oxygen groups, in particular the carbonyl group C=O, he demonstrates that the solvent shift can be estimated by:

$$\left[\nu_{X=O}^{ref} - \nu_{X=O}^{obs}\right] = \Delta\nu_0 = \Delta\nu_D + \Delta\nu_{A/B} \qquad [3.2]$$

where $\nu_{X=O}^{obs}$ is the experimentally observed absorption maxima, $\Delta\nu_D$ the shift due to the dispersion forces of the solvent and $\Delta\nu_{A/B}$ the shift due to Lewis acid/base interactions. Fowkes has used the more general Lewis definition of acids and bases to describe the hydrogen bonding shift. He has also shown that the dispersion force shift, $\Delta\nu_D$, correlates well with γ^d, the dispersion force component of the surface tension (Figure 3.1)[9].

While Equation [3.2] works very well with low molecular weight compound, a problem is encountered in applying it to polymeric systems. The reference state frequency $\nu_{X=O}^{ref}$ is a low pressure vapor phase experiment. Polymers typically have negligible vapor pressure, so a value for $\nu_{X=O}^{ref}$ seems impossible to obtain. Fowkes has shown a simple solution to this problem. In solvents in which acid/base interactions are not active (i.e., inert solvents), Equation [3.2] becomes[9]:

$$\nu_{C=O}^{ref} - \nu_{C=O}^{obs} = \Delta\nu_D \qquad [3.3]$$

Upon rearrangement:

$$\nu_{C=O}^{ref} = \Delta\nu_D + \nu_{C=O}^{obs} \qquad [3.4]$$

From Equation [3.4], it can be seen that, as $\Delta\nu_D \rightarrow 0$:

$$\nu_{C=O}^{obs} = \nu_{C=O}^{ref} \qquad [3.5]$$

The graph shown in Figure 3.2 takes advantage of this relation. The experimentally observed absorption maxima for ethyl acetate and poly(methyl methacrylate) are plotted against the dispersion force component of the surface tension of the neutral solutions, γ^d. In the case of the

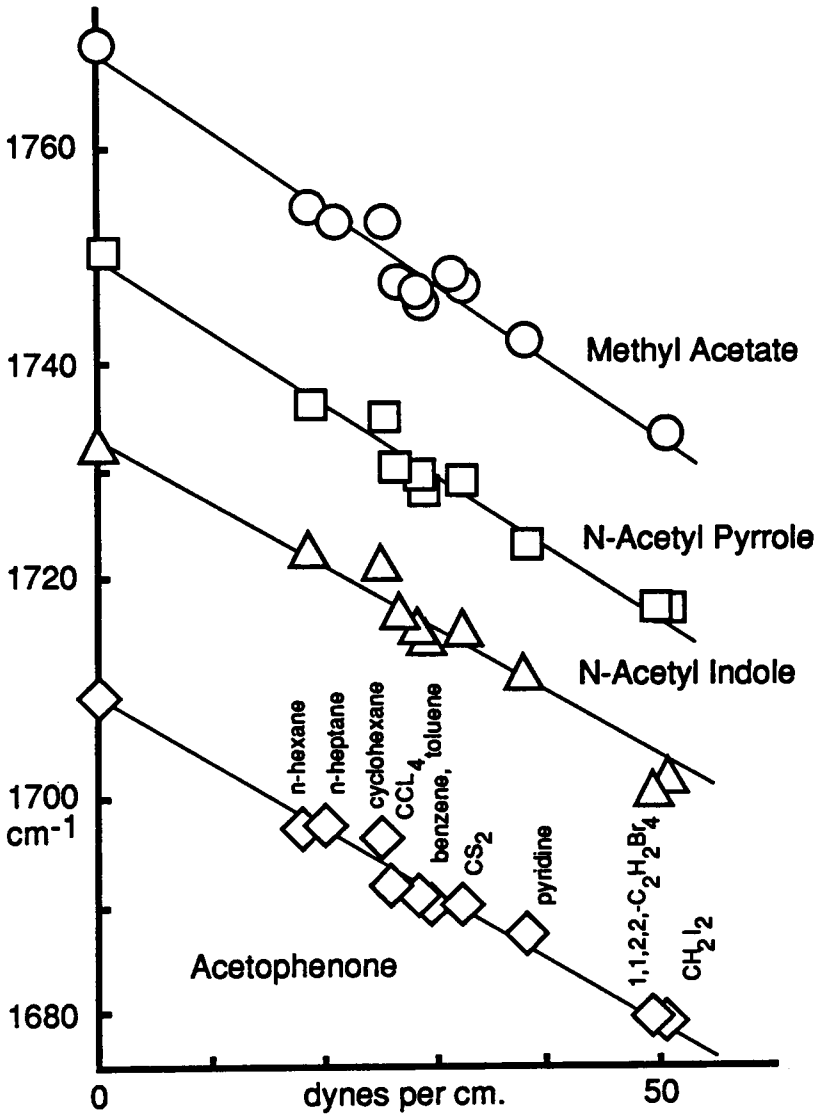

Figure 3.1. Solvent shifts of the carbonyl stretching frequency for four carbonyl containing compounds in non-acidic solvents of various surface tensions (redrawn from Fowkes[9]).

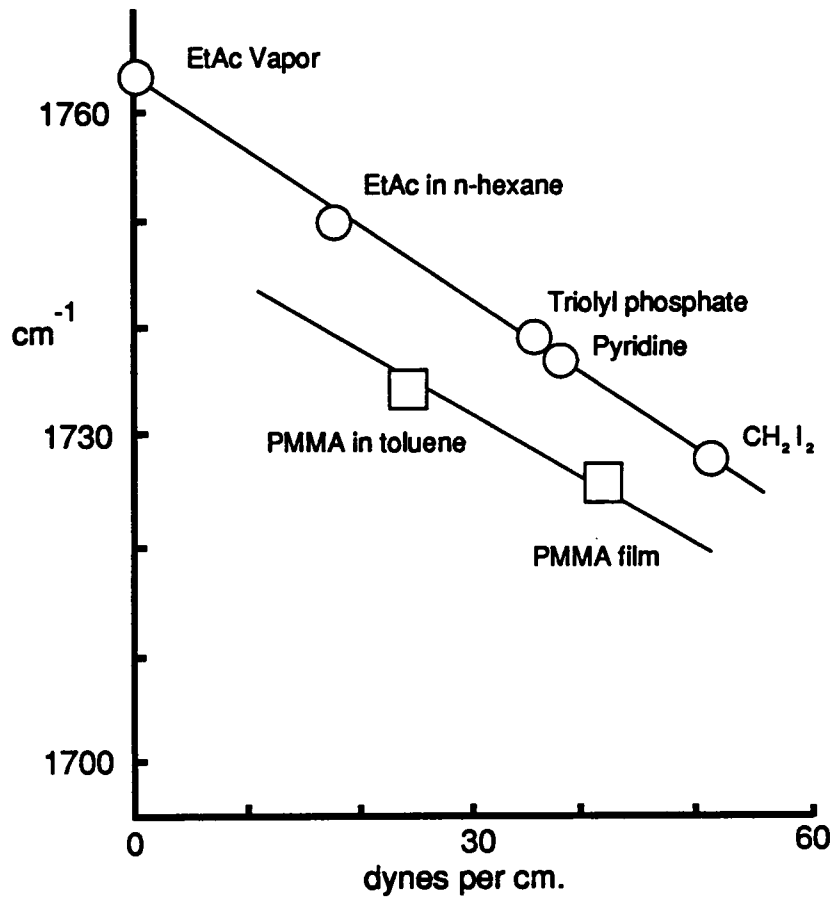

Figure 3.2. Dependence of the carbonyl stretching frequency for ethyl acetate and PMMA on the dispersion forces component of the surface tension γ^d (redrawn from Fowkes[9]).

low molecular weight ethyl acetate, it is seen that as $\gamma^d \rightarrow 0$ (and therefore $\Delta\nu_D \rightarrow 0$), $\Delta\nu_{C=O}^{obs}$ approaches the reference state or free carbonyl frequency $\nu_{C=O}^{ref}$. Therefore, for poly(methyl methacrylate), or any carbonyl containing polymer, the vapor phase absorption maxima need not be directly observed. It can be accurately estimated by extrapolating the observed carbonyl frequency, $\gamma^d \rightarrow 0$, and using the ordinate intercept value for $\nu_{C=O}^{ref}$. Also, since the plot used to determine $\nu_{C=O}^{ref}$ was constructed from solution spectra in which only dispersion forces were active, the shift for dispersion forces, $\Delta\nu_D$ can be calculated directly from the same plot. It will simply be the difference in frequency between the reference state carbonyl and the observed carbonyl maximum.

To calculate the shift due to chemical acid/base interactions, $\Delta\nu_{C=O}^{A/B}$, one first must know the γ^d of the solution. The expected carbonyl maxima due to dispersion forces ($\nu_{ref} - \Delta\nu_D$) can then be read off the graph as described above. If acid/base interactions are likewise active in the solution, the experimentally observed carbonyl frequency will be vertically shifted for the expected carbonyl frequency (Figure 3.6). This shift arises from the lone pair electrons on the carbonyl oxygen being donated in the interaction. This causes the carbon-oxygen double bond to start to assume more single bond characteristics. Referring to Table 3.1, one would expect the carbonyl maxima to be shifted to lower wavenumbers. Rearranging Equation [3.2], it can be seen that

$$\Delta\nu_0 - \Delta\nu_D = \Delta\nu_{A/B} \qquad [3.6]$$

The magnitude of this shift from the "expected frequency" is $\Delta\nu_{C=O}^{A/B}$ and can be directly related to the strength of the acid/base interaction.

3.3 Converting Spectral $\Delta\nu_{A/B}$ to Thermodynamic Information

It would be convenient to convert the spectral information, $\Delta\nu_{A/B}$, to thermodynamic information, specifically $\Delta H_{fA/B}$. A comparison of the spectral results of acid/base interactions with other methods of obtaining $\Delta H_{fA/B}$ would act as confirmation of the technique and add credibility to the measurements. Fowkes has proposed a simple relation which allows this conversion[9]:

$$\Delta H_{f\,A/B} = K\,\Delta v_{C=0}^{A/B} \qquad [3.7]$$

where K is an experimentally determined constant with units of (energy per mole • cm^{-1}).

The constant K for a low molecular weight compound is determined as follows. The acid/base solvent shift, $\Delta v_{C=0}^{A/B}$, is determined in a series of solvents in which acid/base interactions are active. The enthalpies of acid/base interaction, $\Delta H_{f\,A/B}$, are then calorimetrically determined in the same series of solvents. Then $\Delta H_{f\,A/B}$ is divided by $\Delta v_{C=0}^{A/B}$ and the average value of the ratio is assumed to be K.

For a polymeric species, K is determined using an expanded method. First, a low molecular weight model of the polymer is selected and its constant, K, is determined in the above described manner. Then, $\Delta v_{C=O}^{A/B}$ for the polymer is determined in the same series of solvents, and the acid/base solvent shift for the polymeric species is ratioed to the acid/base solvent shift for the low molecular weight model. Finally, K_{model} is scaled by this ratio as shown in Equation [3.8]. This new value of K is the "polymeric" constant to convert acid/base solvent shifts to enthalpies of acid/base interaction.

$$\left[\frac{\Delta v_{C=O,\,polymer}^{A/B}}{\Delta v_{C=O,\,model}^{A/B}}\right] \bullet K_{model} = K_{polymeric} \qquad [3.8]$$

3.4 Drago's C&E Model of Acid/Base Interactions

A useful relation for modeling the enthalpy of acid/base has been proposed by Drago *et al.*[11,12], and is shown in Equation [3.9]:

$$-\Delta H_{f\,A/B} = C_A\,C_B + E_A\,E_B \qquad [3.9]$$

In this relation, two empirically determined parameters, C_A and E_A, are assigned to the acid, and two, C_B and E_B, are assigned to the base. C_A and C_B may be loosely interpreted as the susceptibility of the acid and base to form covalent bonds, and E_A and E_B the susceptibility to

undergo electrostatic interactions. Ratios of C/E for a given acid or base can be related to the Hard-Soft Acid/Base (HSAB) model. If the ratio is relatively large, then the acid or base would be classified as soft. If the ratio is small, the species would be classified as hard.

The C and E model is empirical. To form the basis for this model, Drago first assigned reference values to three compounds: iodine $E_A = 1.00$, $C_A = 1.00$; dimethylacetamide $E_B = 1.32$; and diethyl sulfide $C_B = 7.40$. Using these predefined constants, he statistically fit C and E values to 74 other compounds. This involved obtaining over 280 enthalpies of adduct formation from the general literature. Drago's linear transformation matrix method of fitting C and E values to the experimental data is quite sophisticated and is described in Reference 12.

To calculate C_B and E_B parameters for poly (2-ethyl hexyl methacrylate) (PEHMA), a different method of data manipulation was used. To use Drago's matrix method, the original data for *all* the 280 enthalpies is required, and all 148 C and E parameters would be statistically adjusted to obtain estimates for C_B and E_B for PEHMA. As this was well beyond the scope of this work, present values of C_A and E_A for the acidic solvent were assumed to be accurate.

Equation 3.9 can be rewritten in a linear form:

$$E'_B = \frac{-\Delta H_{f\,A|B}}{E_A} - C'_B\left(\frac{C_A}{E_A}\right) \qquad [3.10]$$

where

$$\frac{-\Delta H_{f\,A|B}}{E_A} = \textit{ordinate intercept} \qquad [3.11]$$

$$-\left(\frac{C_A}{E_A}\right) = \textit{slope} \qquad [3.12]$$

and E'_B, C'_B are trial values for the actual values of E_B, C_B of the unknown Lewis base. These actual values occur at one point on the straight line. If lines are drawn for more than one set of E_A and C_A values (i.e., experiments with other known Lewis acids), then these lines should intersect at the true E_B and C_B for the Lewis base.

Another method of estimating C_B and E_B for PEHMA is to put Equation [3.9] into a standard form for multiple regression:

$$-\Delta H_{f(A/B)} = X_1 C_B + X_2 E_B + \beta \qquad [3.13]$$

where X_1 is the C_A value for the acidic solvent, X_2 the E_A value and β an intercept. By forcing β to zero and performing the multiple regression, values of C_B and E_B can be obtained. The benefit of the multiple regression approach is that it is a more rigorous statistical method. Not only are estimates of C_B and E_B obtained, but also information on how well the Drago model fits the experimental data. By making use of t-statistics and hypothesis testing, it is possible to gain insight into the relative importance of the electrostatic and covalent components of the reaction.

A problem with both the graphical and multiple regression methods of estimation is that both have the underlying assumption that the values of C_A and E_A for the solvent are independent variables. In reality, they are random variables with a sizeable uncertainty associated with them. This does not invalidate these methods of estimation, but serves as a reminder that statistical liberties have been taken and that one could expect large uncertainties (i.e., errors about the mean) associated with the estimates.

3.5 Gutmann's Donor-Acceptor Model of Acid/Base Interactions

Another model which can be used to quantify acid/base interaction is Gutmann's Donor-Acceptor approach[13-15]. In this empirical model, Gutmann proposes three equations by which the enthalpy of acid/base interaction can be estimated:

$$\Delta H_{f\,A/B} = -f_A\, DN \qquad [3.14]$$

$$\Delta H_{f\,A/B} = -f_B\, AN \qquad [3.15]$$

$$\Delta H_{f\,A/B} = (-f_A\, DN) + (-f_B\, AN) \qquad [3.16]$$

where DN is the donor number of a Lewis base, AN the acceptor number of a Lewis acid, f_A the acceptor strength of an "unknown acid" and f_B the donor strength of an "unknown base".

These equations are used to cover three possible scenarios for the interaction. Equation [3.14] covers the interaction of a known Lewis base (i.e., DN is known) with an "unknown acceptor". It is important to note that $f_A \neq AN$, therefore even if AN is known, f_A must still be experimentally determined. Equation [3.15] handles the reverse situation where a known Lewis acid interacts with an unknown donor (similarly $f_B \neq DN$). Equation [3.16] states that some materials are amphoteric; they exhibit the properties of both an acid *and* a base. The potential for this type of behavior is not included in Drago's model.

The donor number is defined as the molar enthalpy for the reaction of the donor (D) with $SbCl_5$ (antimony pentachloride) as a reference acceptor in a 10^{-3} M solution of dichloroethane.

$$D + SbCl_5 \rightleftarrows D \cdot SbCl_5 \; (-\Delta H_{D \cdot SbCl_5} \equiv DN) \qquad [3.17]$$

The acceptor number is based on the ^{31}P NMR chemical shift (δ) of triethylphosphine oxide[16]. The δ value used for calculating the acceptor number has been extrapolated to infinite dilution, referred to hexane as a neutral reference solvent ($AN \equiv 0$), and corrected for differences in volume susceptabilities between hexane and the solvent in which the experiment is run. This corrected δ value is then ratioed to the corrected value for antimony pentachloride ($AN \equiv 100$) and the final acceptor number is given by:

$$AN \equiv \frac{\delta_{corr} \cdot 100}{\delta_{corr}\,(Et_3PO \cdot SbCl_5)} \qquad [3.18]$$

3.6 Comparison of Drago's and Gutmann's Methods

If one compares Gutmann's and Drago's models, it is apparent that Gutmann's approach is a simplified two parameter approximation of Drago's four parameter model. Gutmann's simplifying assumption is that all acid/base interactions are roughly the same. This view ignores

all of Pearson's "hard/soft" principles[17,18]. Gutmann's empirical model is also based on a different reference acid, base and neutral than Drago's.

Gutmann, Drago, Pearson, and others have hotly debated the relative strengths and weaknesses of their models, without reconciliation. The author feels it safe to state that there is no universally satistifactory way of measuring the strengths of acids and bases. Drago's model allows deeper insight into the nature (electrostatic and covalent) of the acid/base interaction, and also seems more satisfactory from the theoretical point of view. The Gutmann model allows materials to be amphoteric; this is a clear advantage when dealing with complex systems (i.e. copolymer, mixed oxide, etc.). It is a two parameter model and therefore can be "fit" with less experimental data.

There is no clear choice as to which model is best. For a practical approach, Gutmann's model allows analysis of complex, amphoteric systems. However, to understand the chemistry and the nature of the interfacial bonding, Drago's model would be better.

3.7 Experimental

3.7.1 Materials

All solvents used were gold-label grade from Aldrich Chemical and stored over activated 4 $\mathring{A}$ molecular sieves. Chloroform, methylene chloride, and tetrahydrofuran were further purified by the method described in Perrin *et al.* to remove the stabilization agent[19]. These light sensitive solvents were stored under N_2, in amber bottles and in a darkened dessicator. If more than two months had passed, these solvents were redistilled before use. The polymer selected, poly(2-ethyl hexyl methacrylate), (Figure 3.3), was the same polymer used in the IGC experiments (Chapter 2). There are five reasons why PEHMA was an advantageous choice in the light of the IR experiments. First, the carbonyl group is a very strong IR absorber, and is quite easy to identify and quantify even at low concentrations. Second, the carbonyl group's solvent shift, $\Delta\nu^{A/B}_{C=O}$, has been one of the primary groups previously used in the study of this phenomenon and its behavior has been well

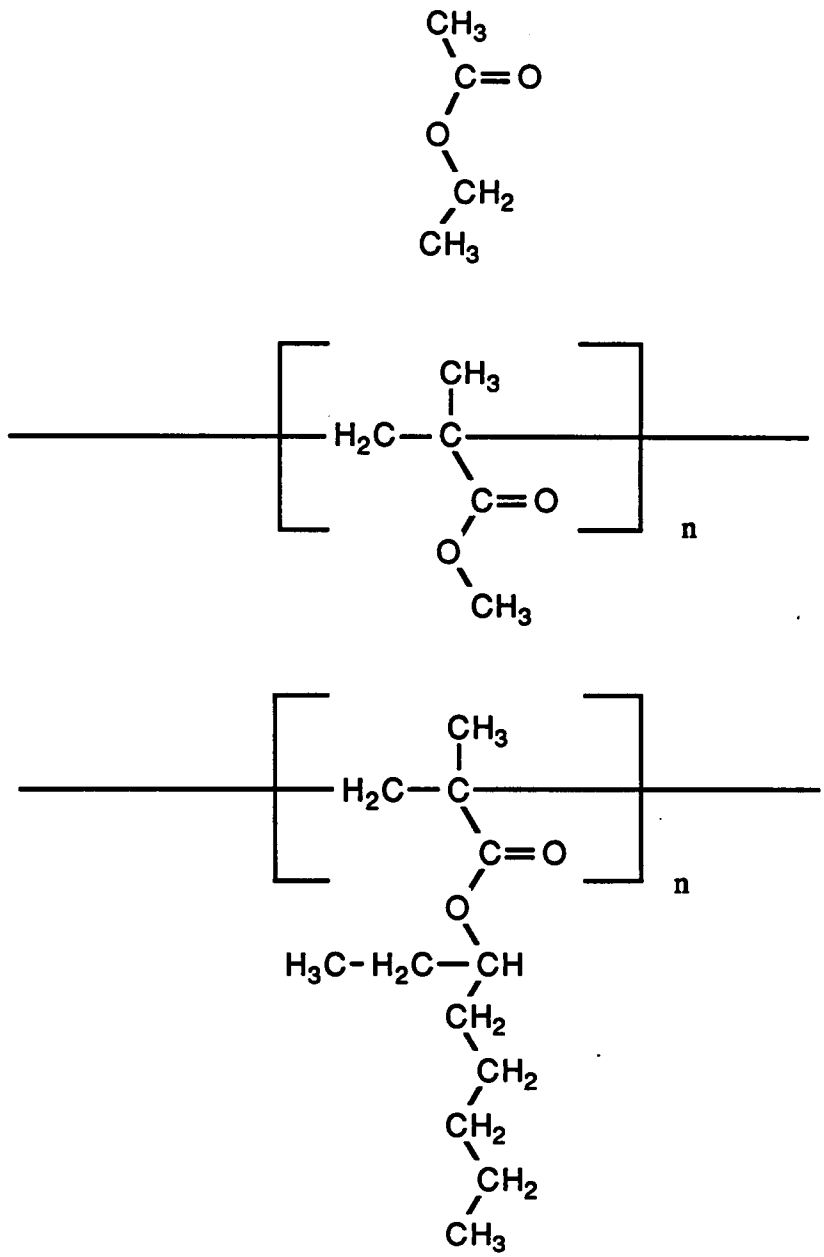

Figure 3.3. Structure for ethyl acetate, poly(methyl methacrylate) and poly(2-ethyl hexyl methacrylate).

documented. Third, the first reported study of $\Delta v^{A/B}_{C=O}$ for polymeric systems was done with poly(methyl methacrylate) PMMA[9], and, since PEHMA is so structurally similar, its behavior should be closely related. Fourth, the polymer is completely soluble in a wide variety of solvents. This allows for a great deal of freedom in selecting the solvents for this study. A polymer of limited solubility will restrict the selection of neutral and acidic solvents for these experiments. Lastly, PEHMA is amorphous which allows the spectra to be obtained at room temperature, rather than having to exceed the crystalline melting point to assure true solution.

In this set of experiments, the low molecular weight model selected for PEHMA was ethyl acetate. There were four reasons why this model was selected. First, and most obvious, ethyl acetate is an aliphatic ester, as is PEHMA, and its behavior in acidic solvents should be very similar. Second, ethyl acetate was one of the Lewis bases originally analyzed by Drago[12], its enthalpies of acid/base interaction had been measured with a wide variety of Lewis acids, and its C and E values are well defined (C_B = 1.74, E_B = 0.975). Third, ethyl acetate was the low molecular weight model used in Fowkes' work, and thus allowed a direct comparison of this author's data and calculated values for $v^{gl}_{C=0}$, $\Delta v^{D}_{C=0}$, and $\Delta v^{A/B}_{C=0}$ as a check of experimental technique. Lastly, ethyl acetate was readily available in high purity and in an anhydrous state.

3.7.2 IR Techniques and Instrumentation

Solutions for IR analysis were prepared in 4 ml sample vials fitted with Teflon/rubber septa. A layer of activated 4$\mathring{A}$ sieves were placed in the vial was added, then 2-3 ml of dry solvent was added, followed by sufficient PEHMA to achieve a 1% (wt/wt) solution. The vials were then purged with dry nitrogen gas, capped, and the gap between the lid and bottle sealed with a Teflon tape. All samples were allowed to sit overnight to assure complete dissolution.

The IR sample cell was a Wilmad 116-1 liquid cell mount equipped with 13 mm CaF_2 windows. CaF_2 was chosen as it is non-hydroscopic, resistant to most solvents, acids and bases; has a low refractive index, thereby minimizing interference fringes in short path lengths; and has a wide transmission range (60,000 to 950 cm^{-1}). The path length through the cell was controlled

by the use of Teflon spacers. The optimum path length was found to be 0.2 mm. This gave an absorption intensity in the range of 0.1-1 absorption units and a signal-to-noise ratio of approximately 10^3. The internal volume of the cell was approximately .03 ml.

All handling of the IR sample cell and solutions were performed in a nitrogen dry box. The samples were loaded into the IR cell in a nitrogen dry box using a Hamilton 1 ml gastight syringe. The cell was first flushed twice with 1 ml of solvent, then 1 ml of polymer solution was passed through. The cell was then capped and visually checked for entrapped air bubbles immediately prior to the spectrum being obtained. The cell was then removed from the dry box and immediately loaded into the spectrometer.

The infrared spectra were obtained using a Nicolet 6000C FT spectrometer. The spectrometer was purged with the dry nitrogen gas for 10 minutes after the sample cell was introduced to assure a reproducible background. Thirty-two scans were collected per spectral file. Absorbance spectra were obtained by ratioing files containing spectral information on the pure solvent and a solvent/polymer solution. The carbonyl region (1760-1690 cm^{-1}) of the resulting file was then plotted in absorbance units (Figure 3.4). Peak maxima were determined by triangulation.

3.8 Data Reduction

IR spectra were obtained in a series of neutral solvents (n-hexane, n-octane, carbon tetrachloride, benzene and toluene) in which only dispersion forces were active; this data is summarized in Table 3.2. The observed maxima for the carbonyl were linearly regressed on the γ^d of the solvents, and the resulting plots are shown in Figure 3.5. The γ^d of solution was taken to be the γ^d of the pure solvents. At this low concentration (1% or less) of both model and polymer polymer, γ^d for the pure solvent should be a reasonable estimate for the γ^d of the solution. An attempt was made to measure γ^d for PEHMA using the Zismann series of liquids and plotting the data according to the Good-Girfalco-Fowkes-Young equation[10]. The polymer, however, underwent swelling when placed in contact with these solvents, negating the results. From the

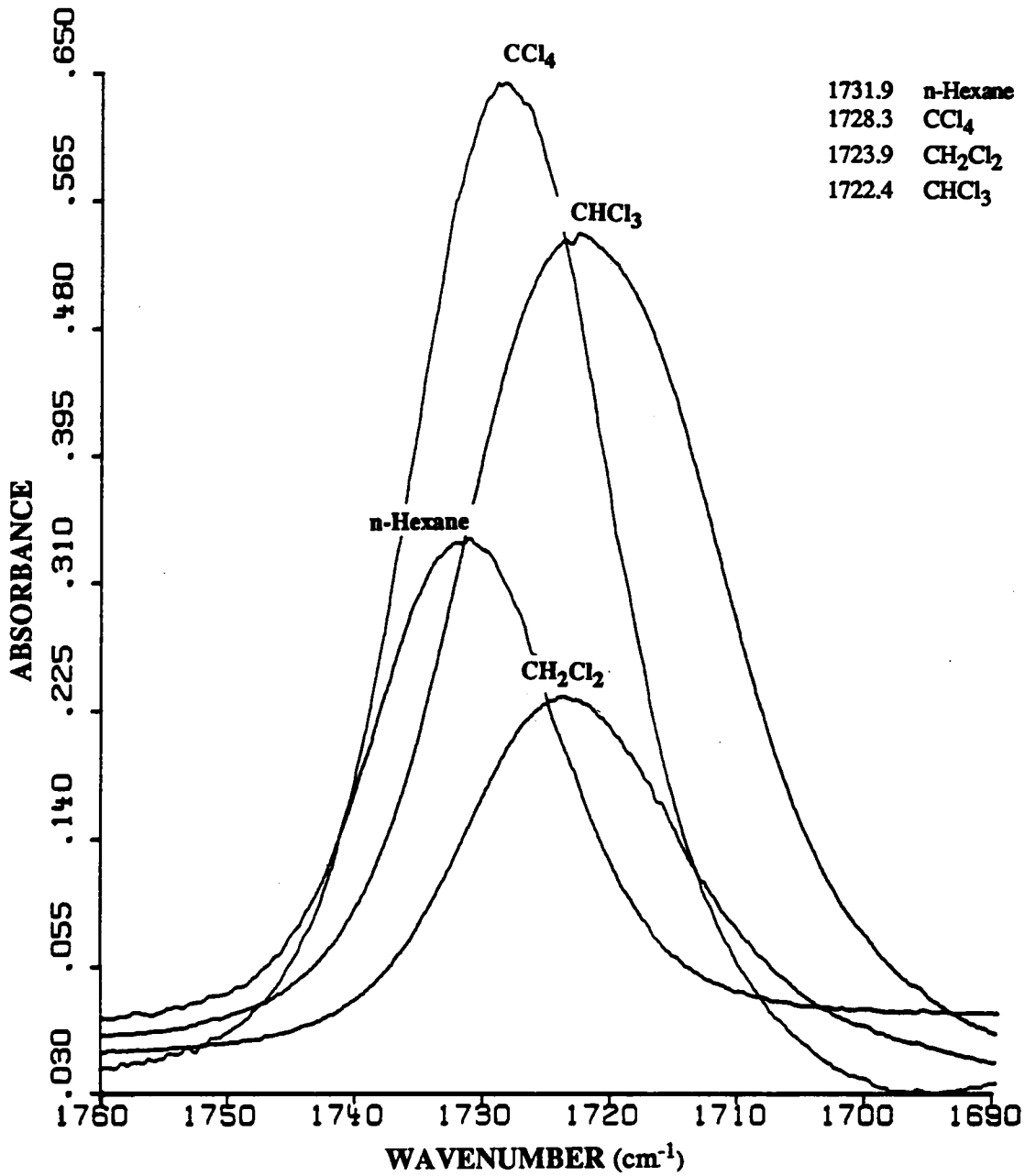

Figure 3.4. Typical FTIR data showing the shift in the carbonyl band of PEHMA in two neutral solvents and two acidic solvents.

ordinate intercepts shown in Figure 3.5, the estimate of the reference-state, free carbonyl for PEHMA, $\nu^{ref}_{C=O} = 1740.2\, cm^{-1}$, and for ethyl acetate, $\nu^{ref}_{C=O} = 1764.3\ cm^{-1}$ were obtained.

The IR spectra of PEHMA was also obtained in acidic solvents (chloroform, methylene chloride, t-butyl alcohol/toluene and iodine/n-hexane). Mixed solvents were used in the case of t-butyl alcohol and iodine as PEHMA was not soluble in the neat compound. The dispersion force component of the surface tension, γ^d , for the mixed solvents was calculated on a volume faction basis using the literature[20-22] values of γ^d for pure compounds. If only Hildebrand solubility parameters (δ) were available, then γ^d could be estimated using a relation established by Beerbower[23] and Becher[24]:

$$\delta_d^2 = 13.9 \frac{cal}{erg} \frac{\gamma^d}{V_s^{1/2}} \qquad [3.19]$$

where V_s is the molar volume of the compound.

Knowing γ^d for the acidic solvents, the expected carbonyl frequency due to dispersion forces alone was interpolated from the graph in Figure 3.5. The differences between the experimentally observed frequency and the expected frequency (i.e., the vertical shifts in Figure 3.6) were assigned as the acid/base shift $\Delta\nu^{A/B}_{C=O}$ and are shown in Table 3.3.

The $\Delta\nu^{A/B}_{C=O}$ was related to the enthalpy of formation using Equation [3.6]. These results are shown in Table 3.3. Comparison of these data with previously determined enthalpies for the formation of acid/base interaction (via IGC) was used as a check of the validity of Equation [3.2].

The experimental enthalpies of acid/base interaction obtained from Equation [3.6] were fitted to the Drago model using Equations [3.10] and [3.13]. Using Equation [3.10], estimates of E_B and C_B were taken as the intersection points of the lines. The experimental enthalpies and solvent E_A, C_A values were used in Equation [3.13], and analyzed using the "SAS" statistical package on the main frame computer at Virginia Tech. Estimates of C_B and E_B were obtained from the statistical report.

Table 3.2. Shifts of Carbonyl Stretching Frequency in Neutral Solvents.

Ester	Neutral Solvent	γ^d (dynes/cm)	$\nu^{obs}_{C=O}$ (cm^{-1})
Ethyl acetate	(vapor phase)	0	1764.0*
Ethyl acetate	n-hexane	18.43	1750.0
Ethyl acetate	CCl_4	26.95	1741.9
Ethyl acetate	toluene	28.5	1741.8
Ethyl acetate	benzene	28.85	1739.7
PEHMA	n-hexane	18.43	1731.9
PEHMA	n-octane	21.80	1731.8
PEHMA	CCl_4	26.95	1728.3
PEHMA	toluene	28.5	1728.2
PEHMA	benzene	28.85	1727.4

* Literature value taken from Reference 12.

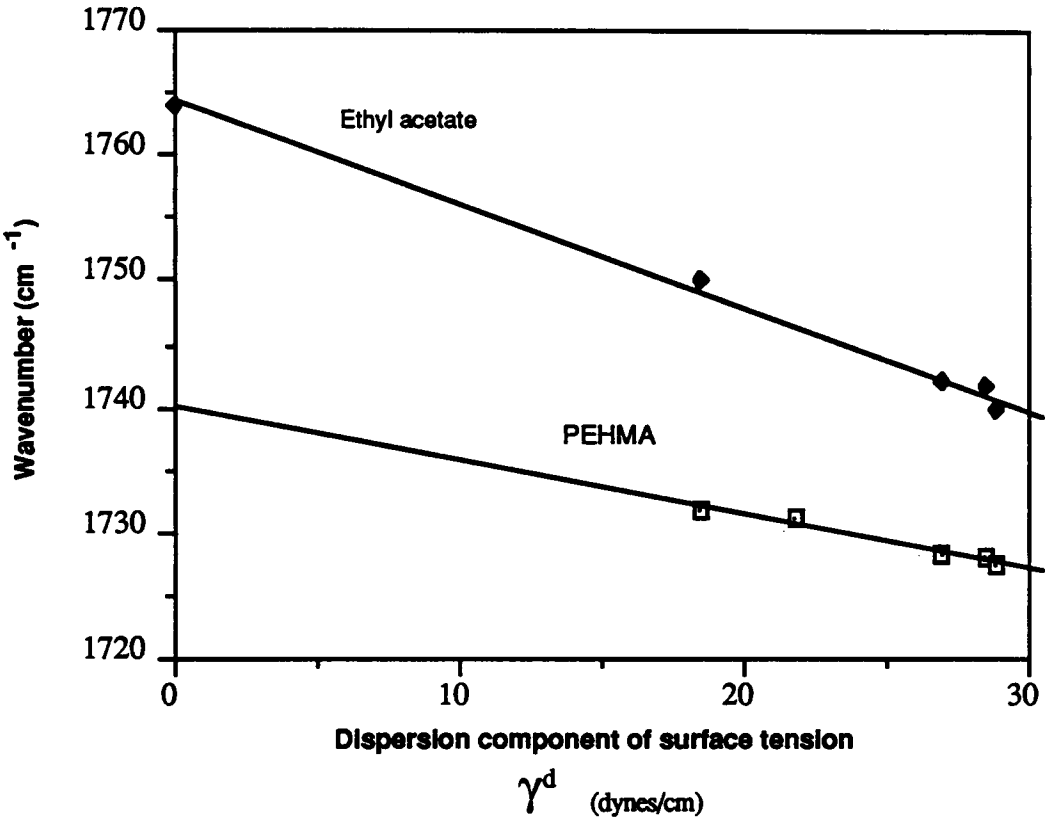

Figure 3.5. Experimental data showing the dependence of the carbonyl stretching frequency of ethyl acetate and PEHMA on the dispersion component of the surface tension.

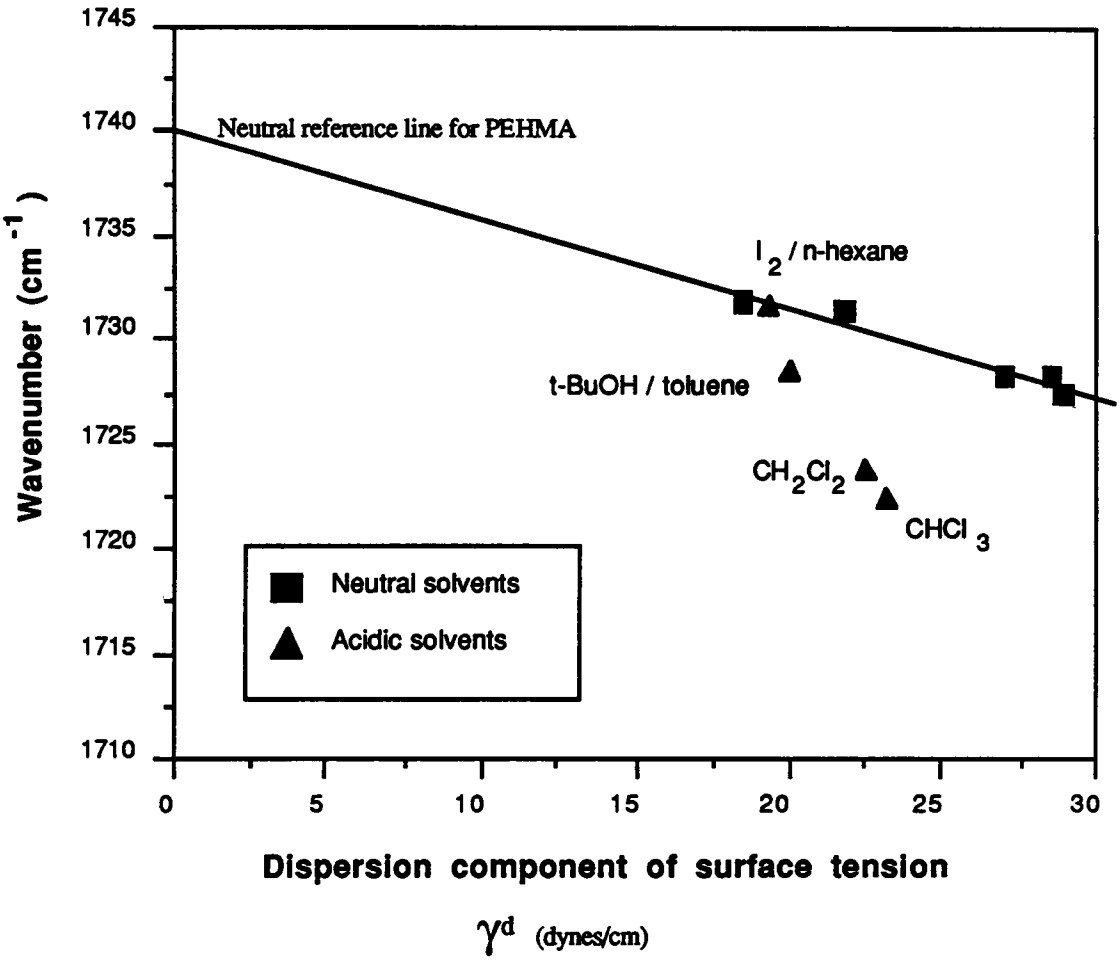

Figure 3.6. Vertical shift off neutral reference line due to Lewis acid/base interactions.

Table 3.3. Acid/Base Results via FTIR and IGC.

Acid	*Solvent*	$\Delta v_{a/b}$	$\Delta H_{f\,A/B}$	$\Delta H_{f\,A/B}$ *(IGC)*
$CHCl_3$	$CHCl_3$	-7.5	-3.0	-2.9
CH_2Cl_2	CH_2Cl_2	-6.5	-2.5	-4.0
I_2	n-hexane	-0.3	-0.1	NA
$(CH_3)_3COH$	toluene	-3.0	-1.1	NA

(all enthalpies in kJ/mol, shifts in cm^{-1}) NA = not available

3.9 Results and Discussion

Data for the spectral shift due to dispersion forces alone are shown in Table 3.3 and Figure 3.5. Fowkes *et al.* has reported that for ethyl acetate, $\nu^{gl}_{C=0} = 1764\,cm^{-1}$, and in n-hexane, $\nu^{observed}_{C=0} = 1750\,cm^{-1}$. The data collected in these experiments reveal that $\nu^{gl}_{C=0} = 1764.3\,cm^{-1}$ and in n-hexane $\nu^{observed}_{C=0} = 1750.0\,cm^{-1}$, in excellent agreement with Fowkes. Fowkes also shows data obtained using the "neutral" solvents tritoyl phosphate, pyridene and methylene iodide, but does not list their numerical values. Due to this and in consideration of the purity and the toxicity of these solvents, a different set of neutrals were used. However, even with a different set of neutrals near quantitative agreement in the extrapolated value for $\nu^{gl}_{C=0}$ was observed, indicating that this procedure for obtaining $\nu^{gl}_{C=0}$ by extrapolation is valid. The constant K_{model} for ethyl acetate was calculated using Equation [3.7] and was 0.99 kJ/mol cm. The calorimetric data used in Equation [3.7] weres taken from Drago *et al.*[11] and Fowkes *et al.*[9].

The graph from which the extrapolated value of $\nu^{gl}_{C=0}$ for PEHMA is calculated is shown in Figure 3.5. As can be seen, the data points fall on a straight line (r = 0.98) with its intercept at 1740.2 cm^{-1}. This intercept value is the reference-state, free carbonyl frequency for PEHMA ($\nu^{gl}_{C=0}$). The acid base shifts, $\Delta\nu^{A/B}_{C=0}$, are shown in Table 3.3 and Figure 3.6. As is seen in Figure 3.6, the stronger the Lewis acid, the greater the shift from the dispersion force predicted carbonyl maxima (i.e., the vertical shift from the line of neutral solvents). This vertical shift is the acid/base shift, $\Delta\nu^{A/B}_{C=0}$, for the various Lewis acids interacting with PEHMA. The constant $K_{polymer}$ for PEHMA was calculated using Equation [3.7] and was found to be 0.38 kJ/mol cm. If IGC determined enthalpies are used to allow independent calculation of $K_{polymer}$ using Equation [3.7], K is found to be 0.37 kJ/mol cm., which is in excellent agreement with the previously obtained value.

The graphical estimation of the Drago C_B and E_B values for PEHMA via Equation [3.10] is shown in Figure 3.7, and the intersection points listed in Table 3.4. If the data perfectly fit the model, all of the lines should intersect at one unique point. This is not the case, as there are six discrete points of intersection. The average value of E_B for PEHMA was $0.30 \pm 0.09 (kcal/mol)^{1/2}$. This value is lower than the typical range of E_B for an alphatic ether of $0.9 - 0.6\,(kcal/mol)^{1/2}$.

The average value of C_B for PEHMA was -1.12 ± 1.09 . This value is not reasonable, as the minimum C_B value of any species should be zero, indicating the functional group has no tendency to covalently bond with any interacting species.

The results of fitting the Drago model to the present data using Equation [3.13] provides insight into the cause of the negative C_B. The statistical report is shown in Table 3.5. The predicted values of the E and C constants are $E_b = 0.25 \pm .05$ and $C_B = -0.30 \pm 0.20$. This E_B value is in good agreement with that obtained from Equation [3.10]. The C_B value of $-0.30\,(kcal/mol)^{1/2}$ differs from the earlier estimation of $-1.12\,(kcal/mol)^{1/2}$. A cause for the negative C_B values can be inferred from the hypothesis testing which Equation [3.13] allows. The null hypothesis is set at $C_B = 0$ and $E_B = 0$; that is, there is no covalent or electrostatic interaction. The statistics indicate that there is a 75% chance that the covalent interactions are negligably small (i.e., $C_B = 0$). If this was the case, and the covalent portions of these particular interactions were small, then four experiments would be insufficient to obtain reliable information. The author believes that this is the most likely explanation of the negative C_B's.

3.10 Summary

From the results, it has been shown that a reference-state free carbonyl frequency can be established for non-volatile compounds such as polymers, which allows the use of the spectral shift method to gain information about acid/base interactions in polymeric systems. From the shift due to acid/base interactions, $\Delta\nu_{C=0}^{A/B}$, it has been shown that PEHMA does exhibit the nature of a Lewis base. The results were reasonable in that $\Delta\nu_{C=0}^{A/B}$ was shifted towards lower wavenumbers, indicating donation of the lone pair electrons, and that the calculated enthalpies for favorable acid/base interactions were exothermic. They also agreed well with enthalpies for acid/base interaction obtained via IGC, in spite of the fact that these two experiments are extremely different in terms of quantities measured and the concentration of the solutions employed. The results are also consistent with the fact that PMMA, an analogous polymer, has been shown to be a Lewis base.

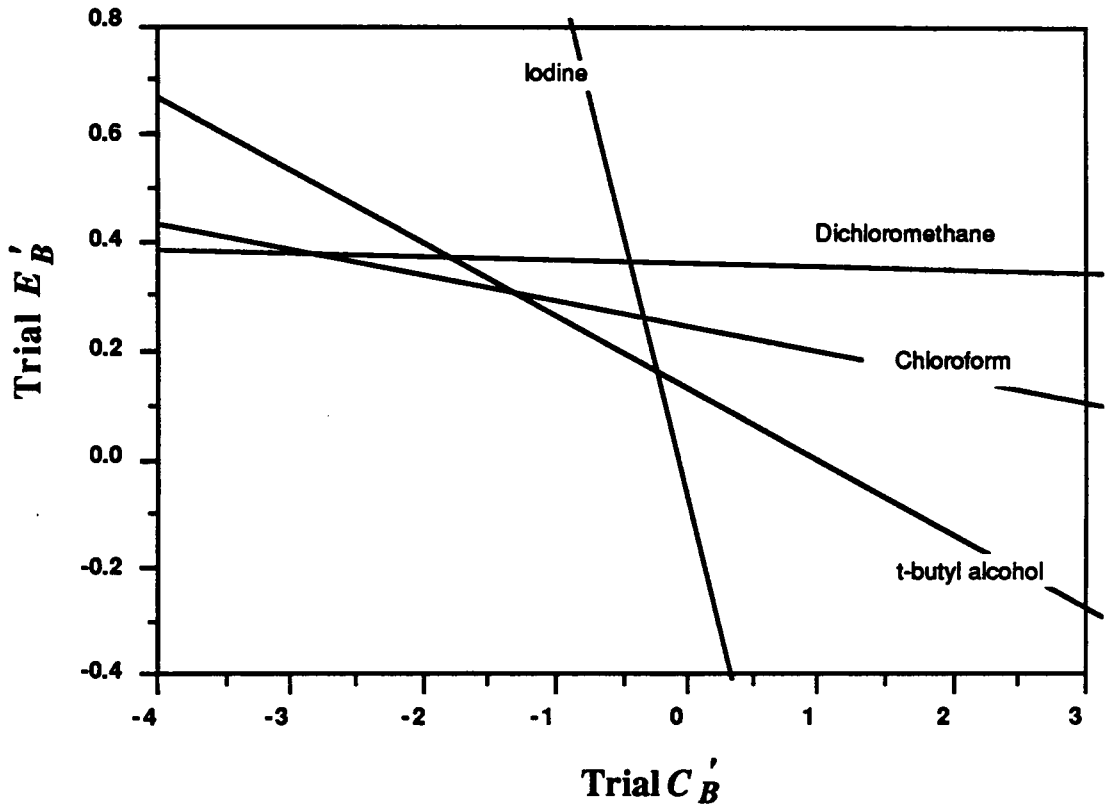

Figure 3.7. Graphical estimation of E_B and C_B for PEHMA using Equation [3.10].

Table 3.4. Graphical Estimation of E_B and C_B for PEHMA using Equation [3.10].

Intersection Point	E_B*	C_B*
I_2 / CH_2Cl_2	0.362	-0.335
I_2 / $CHCl_3$	0.252	-0.250
I_2 / t-BuOH	0.144	-0.143
t-BuOH / $CHCl_3$	0.303	-1.30
t-BuOH / CH_2Cl_2	0.371	-1.80
$CHCl_3$ / CH_2Cl_2	0.377	-2.90
Average Values**	0.301 ± 0.09	-1.12 ± 1.09

*units are $(kcal/mol)^{1/2}$
**± are one standard deviation

Table 3.5. Statistical Report from Regression of Equation [3.13].

Variable	Estimate	DF	Std. Error	t for H_0 = 0 (variable = 0)	Prob > |T|
E_B	0.253	1	0.50	5.04	0.03
C_B	-0.297	1	0.200	-1.51	0.27

Fitting the data to the Drago C&E model met with only limited success. The E_B value of PEHMA in the range of 0.25 to 0.30 $(kcal/mol)^{1/2}$ is slightly lower than that of other alphatic esters (.6-.9 $(kcal/mol)^{1/2}$). It should be noted that only three esters have ever been analyzed using the Drago method; ethyl acetate, methyl acetate, and poly(methyl methacrylate). This is a small data base against which to make comparisons. The prediction of negative C_B values for PEHMA (-1.12 and -0.27) is a more serious shortcoming, and it is believed that two factors contributed to this result. The first is the apparent domination of the electrostatic component in the acid/base interaction. This made the overall enthalpy relatively insensitive to the C_B parameter. The second factor is the small amount of experimental data compared to the type of model tested (i.e., four experiments for a two parameter model).

The donor strength (f_B), based on Gutmann's model of acids and bases obtained from Equation [3.15], was .03 ± .01 arbitrary SI units. There are no available listings of donor strength for comparison to other alphatic esters. Schultz[25] has shown that an untreated carbon fiber has f_B of 0.3-0.4 arbitrary SI units.

3.11 Future Directions

These results show that the IR solvent shift method works well in quantifying acid/base interactions in carbonyl containing polymers. It should be noted, however, that shifts of this nature have also been observed in N=O, S=O, P=O, O-H, N-H function groups. This makes this technique applicable to many other polymer systems. Also, the solvent shifts of small molecules containing these functional groups could be used to probe the acid/base nature of solid surfaces. While one normally does not think of FTIR as a true surface sensitive technique, advances in instrumentation are rapidly changing this premise[26,27].

The spectroscopic method does show promise as an important tool to examine acid/base interactions. This technique should be pushed past simple transmission spectra, using polymer solutions, to direct observation of the polymer/substrate interface. This type of observation is accessible using specular reflectance, diffuse reflectance of metal oxide powders, or photoacoustic

methods. Analysis of the spectral shifts to obtain acid/base information would be complicated by optical effects (i.e., the analytical beam entering and exiting a high refractive index substrate at various angles and the thinness of the polymer films examined, $> 500\mathring{A}$), but these should not prove to be impossible to overcome. Of particular relevance to the analysis of carbon fibers would be photoacoustic spectroscopy. Spectra could be obtained on polymer coated carbon fiber and the spectral shifts analyzed. This data could be correlated to the IGC analysis of carbon fiber pioneered by J. Shultz and being pursued here at Virginia Tech by Anne Bolvari[28].

If one can model a metal oxide surface with a metal oxide powder, diffuse reflectance spectroscopy would be an ideal method for the study of the polymer/metal interface. The acid/base nature of the metal oxide could be studied both by IGC using Shultz's techniques and now spectroscopically.

The relationship (Equation [3.7]) proposed by Fowkes to relate spectral information to enthalpies of interaction seems qualitatively correct, but in applications with weak Lewis acids, seems inadequate. The equation is:

$$\Delta H_{f\,A/B} = K\,\Delta\nu_{C=0}^{A/B} \qquad [3.7]$$

The form of the equation suggests that if one simply ratios the enthalpies to the spectral shift for a series of solvents, the average value K should be the true value for the constant. Fowkes has suggested linearly regressing $\Delta H_{f\,A/B}$ on $\Delta\nu_{C=0}^{A/B}$ and taking the slope of the fit line to be the constant K. This is valid *if* and *only if* the intercept of the regressed line is zero.

$$\Delta H_{f\,A/B} = K\,\Delta\nu_{C=0}^{A/B} + b \qquad [3.14]$$

For all compounds studied by both Fowkes and this author (ethyl acetate, PMMA, PEHMA), the intercept is non-zero on the order of + 1 kJ/mole. Fowkes has ignored this non-zero intercept in all of his work. It is not known if he has simply written it off to experimental error or if he statistically forces the intercept to be zero. In this work the intercept has been statistically forced to be zero in order to meet the constraints of Equation [3.7]. Perhaps fortuitously, this procedure

yields a value of $K_{polymer}$, which is almost identical to the independently determined IGC value for K of .37 kJ/mol cm.

In order to determine if the intercept is non-zero and therefore represents a shortcoming of Equation [3.7], work involving both spectral and calorimetric experiments should be done with both ketones and ester using mild Lewis acids. It is this author's opinion that this intercept is non-zero. It has not been perceived to be important because most spectral shift work has been done with strong Lewis acids (i.e., $(CH_3)_3Al$, $SbCl_5$, etc.), thereby resulting in large acid/base shifts (60 to 100 cm^{-1}). With such large shifts and high enthalpies of interaction, a small intercept of approximately 1 kJ/mole could have been easily overlooked.

These FTIR experiments were designed to complement the IGC experiment described in Chapter 2. Therefore, many of the requirements for "well-behaved" IGC probes were passed on to the spectroscopic study. Strongly basic or acidic are not appropriate IGC probes as they can permanently bond to the metal parts of the chromatographic system, and gas-phase diffusion of these species will result in very broad, unusable peaks during their long elution times in the columns. If FTIR is continued to be useful as a comparison to IGC measurement, the issue of solvent selection requires further study.

3.12 References

1. W. G. Laidlaw; *Introduction to Quantum Concepts in Spectroscopy*, Robert E. Krieger Publishing Company, Inc. (1980).
2. R. M. Silverstein, G. C. Bassler and T. C. Morrill; *Spectrometric Identification of Organic Compounds, 4th Ed.*; John Wiley & Sons (1981).
3. L. J. Bellamy, H. E. Hallam and R. L. Williams; *Trans. Faraday Soc., 54*, 1120 (1958).
4. L. J. Bellamy and R. L. Williams; *Trans. Faraday Soc., 55*, 14 (1959).
5. L. J. Bellamy and H. E. Hallam; *Trans. Faraday Soc., 55*, 220 (1959).
6. L. J. Bellamy and R. L. Williams; *Proc. R. Soc. London Ser. A., 255*, 22 (1960).
7. L. J. Bellamy, C. P. Conduit, R. J. Pace, and R. L. Williams; *Trans. Faraday Soc., 55*, 1677 (1959).
8. A. Allerhand and P. von R. Schleyer; *J. Am. Chem. Soc., 85*, 371 (1963).
9. F. M. Fowkes, D. O. Tischler, J. A. Wolfe, L. A. Lannigan, C. M. Ademu-John and M. J. Halliwell; *J. Polym. Sci.: Polym. Chem. Ed., 22*, 547-566 (1984).
10. J. R. Dann; *J. Colloid and Interface Sci., 32*, 302 (1970).
11. R. S. Drago and B. B. Wayland; *J. Amer. Chem. Soc., 87*, 3571 (1965).
12. R. S. Drago, G. C. Vogel and T. E. Needham; *J. Amer. Chem. Soc., 93*, 6014 (1971).
13. V. Gutmann; *The Donor-Acceptor Approach to Molecular Interactions*, Plenum Press (1978).
14. U. Mayer, V. Gutmann and W. Gerger; *Mh. Chem. 106*, 1235 (1975).
15. V. Gutmann; *Electrochim. Acta. 21*, 661 (1976).
16. V. Gutmann and E. Wychera; *Inorg. Nucl. Chem. Lett. 2*, 257 (1966).
17. R. G. Pearson; *J. Amer. Chem. Soc. 85*, 3533 (1963).
18. R. G. Pearson; *J. Chem. Educ. 45*, 581 & 643 (1968).
19. D. D. Perrin, W. L. F. Armarego and D. R. Perrin; *Purification of Laboratory Chemicals, 2nd Ed.*, Pergamon Press (1980).
20. R. C. Weast; *Handbook of Chemistry and Physics, 55th ed.*, CRC Press (1975).
21. A. T. M. Barton; *Handbook of Solubility Parameters and Other Cohesion Parameters*, CRC Press (1983).
22. J. J. Jasper; *J. Phys. Chem. Ref. Data 1 (4)*, 841 (1972).
23. A. Beerbower; *J. Colloid and Interface Sci 35 (1)*, 126 (1971).
24. P. Becher; *J. Colloid and Interface Sci 38 (2)*, 291 (1972).
25. J. Schultz, L. Lavielle and C. Martin; *J. Adhesion 23*, 45 (1987).
26. M. J. Kelly; *Chemtech*, August (1987).
27. J. Smith and D. Gerson; *Research and Development*, May (1987).

28. A. Bolvari; *Polymer Preprints*, 1988 National ACS Meeting, Toronto, Canada (to be published).

4.0 PRETREATMENT AND ACID/BASE PROPERTIES OF TITANIUM SUBSTRATES

4.1 Titanium

Titanium (atomic no. 22) is a silvery-white metal which resembles steel. It was first discovered by W. Gregor, an English priest, in 1791, and first produced as a pure metal in 1910. It was considered a laboratory curiosity until Kroll, in 1946, demonstrated that it could be produced commercially by reducing titanium tetrachloride with magnesium. It found its first use as an alloy in some steels and aluminums, but has recently become an important engineering material in its own right[1,2].

Titanium is a prominant material in the aerospace industry. It is as strong as steel, yet 45% lighter. Compared to the aluminum alloys, it is 60% heavier, but has twice the strength, and it maintains its mechanical properties at temperatures where these lightweight alloys begin to fall off and fail. Like aluminum, titanium metal is highly reactive and forms a dense, protective oxide on contact with air. It is this oxide coating which imparts high resistance to corrosion in cold acids and sea water making it a prime material for use in high performance naval systems and desalination plants. It is also considered physiologically inert and has found use in prosthetic devices.

Titanium is an allotropic element. The α-phase, is hexagnol close-packed, and is the stable crystalline form up to 882°C, above which the body-centered cubic β-phase is in stable form. The β-phase is harder, stronger, less ductile, and denser than the α-phase. Titanium alloys are typically

$\alpha + \beta$ alloys, with Ti-6Al-4V being an example where aluminum is used to stabilize the α-phase and vanadium stabilizes the β-phase. Such $\alpha + \beta$ alloys show good formability, cold and hot strength, making them an excellent material for high performance structures.

Since titanium is such a useful engineering material, there has been extensive research into effective methods of joining titanium parts. Adhesive bonding has several advantages over mechanical fastening: Weight saving (crucial to the aerospace industry), more effective stress distribution, sealent properties, improved corrosion resistance, and fatigue resistance. As has been stated, titanium is always covered by a protective native oxide, and it is to this oxide that bonding must occur.

4.2 Titanium Oxide

At normal pressures, titanium oxide (TiO_2) occurs in three crystalline forms: Rutile, anatase, and brookite[3-5]. In each form, the central Ti^{4+} cation is surrounded by six O^{2-} anions forming a slightly distorted octahedron. The three forms differ in the nature of this disorder and in the packing of the octahedra into the crystalline lattice. The number of edges shared by the octahedra in the different packings are two for rutile, three for brookite and four for anatase. The number of corners shared are six for rutile, five for brookite and four for anatase. This coordination and the unit cell of rutile is shown in Figure 4.1, and an example of this packing for rutile and anatase is shown in Figure 4.2. Thermodynamically, rutile is the most stable form, followed by brookite, then anatase[6].

While much is known about the structure of pure crystalline oxides, it is not clear that this information translates directly to the thin oxide film which covers metallic Ti. To obtain a durable and reproducible oxide, chemical pretreatments are typically used. These pretreatments (which will be discussed further in Section 4.3) appear to produce oxides which are amorphous[7]. There is some evidence for microcrystallites with anatase-like or rutile-like structures, but there is no long-range order. The stoichiometry of these thin films also appears to differ from the crystalline oxides. When the Auger spectral line shapes of TiO and TiO_2 are compared with spectra obtained from the

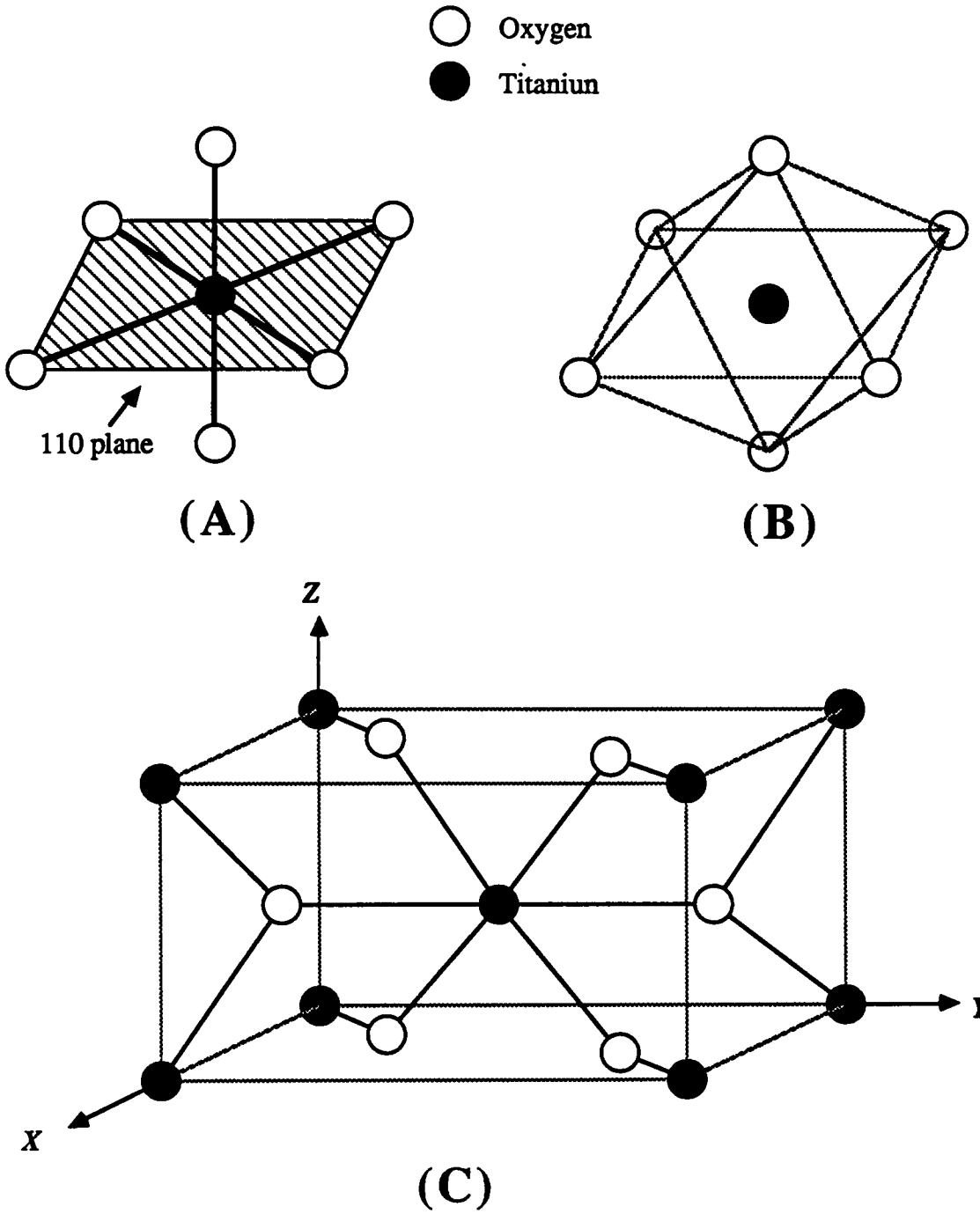

Figure 4.1 Different views of TiO_2: (A) the hexa-coordinate bonding at the titanium atom, (B) the octrahedral shape useful for description of crystal structures, and (C) the unit cell for rutile.

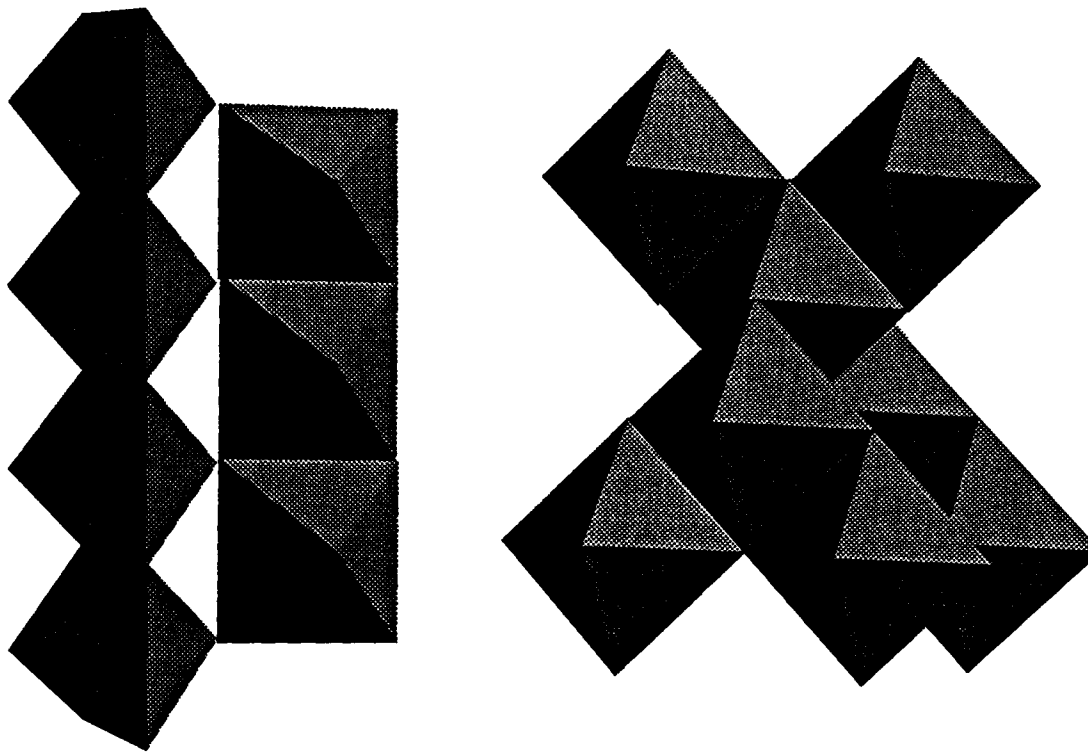

Figure 4.2. An illustration of the packing in the rutile and anatase forms of TiO_2. Rutile (A) shares 2 edges and 6 corners while Anatase (B) shares four edges and four corners.

thin films, the line shapes appear to match the TiO spectra[8]. However, in the same spectra, ratios of the peak intensities for the titanium LMM transition and the oxygen KLL transition indicate a stoichiometry of TiO_2. Atomic ratios obtained from x-ray photoelectron spectra (XPS) of thin films indicate a greater than 2 to 1 ratio for oxygen to titanium[8]. Even though the exact crystalline structure and stoichiometry of the chemically produced oxides is not definitely known, insights gained from the surface chemistry of the crystalline oxides can serve as a guide to the nature of the pretreated oxides.

Typically, the surface of rutile is hydrated and contains two types of hydroxyl groups[9]. Terminal hydroxyl groups fulfill octrahedral coordination for surface Ti^{4+} ions coordinated by five lattice oxygens, and are perpendicular to the surface, which imparts basic character to the hydroxyl group. Hydroxyl groups which share a pair of tetracoordinate surface Ti^{4+} ions (the remaining two oxygens are absent due to termination of the lattice) are designated as bridging groups. This position imparts acidic character to the hydroxyl. Primet *et al.*[10,11] also reports Lewis acid sites which are created by the removal of a terminal hydroxyl or molecular water from the surface. A listing of these proposed sites is shown in Figure 4.3.

If we use this information as a guide to understanding the pretreated surfaces, one might expect an amphoteric surface, since both acidic and basic sites can be formed. The exact acidic or basic strength of the thin film oxides would then depend on which type of site is favorable by the particular pretreatment.

4.3 Titanium Pretreatments

As previously discussed, the reason for pretreating titanium is to obtain reliable, durable, and reproducible oxide layers. The U.S. Army Armament Research and Development Command (AARADCom) have grouped eight pretreatment for Ti-6Al-4V alloy in terms of the durability of epoxy bonds in a 60°C, 95% r.h. environment[12]. These pretreatments are listed in Table 4.1. Also included in Table 4.1 is a sodium hydroxide pretreatment first proposed by Kennedy *et al.*[13] and modified by Filbey[8].

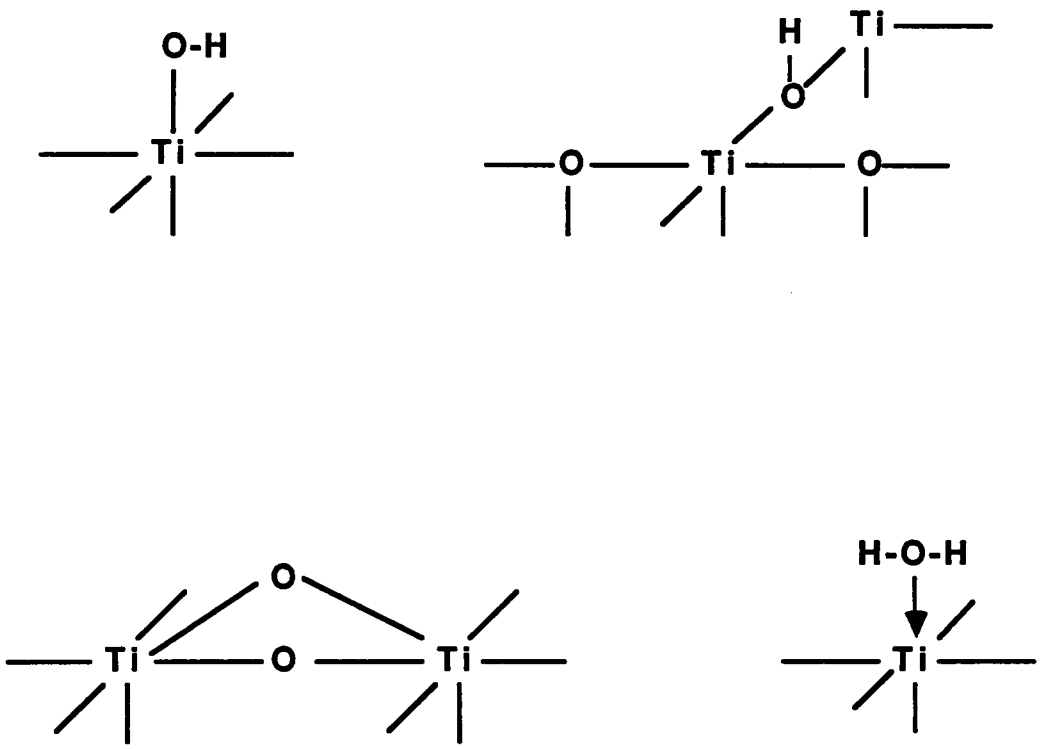

Figure 4.3. Postulated structures for acidic and basic sites on the TiO_2 lattice

Table 4.1. Description of Pretreatments for Titanium and its Alloys.

Designation	Description
CAA	1. Alkaline etch 2. Nitric-HF etch 3. Chromic Acid-HF anodize @ 10 volts
PFS	1. Alkaline clean 2. HF-HNO_3 - Sodium Sulfate etch 3. Trisodium Phosphate-Potassium Fluoride-HF treat 4. Water soak
LP	1. Liquid Hone 2. Alkaline etch 3. Pasa Jell treat
DP	1. Dry Hone 2. Pasa Jell treat
TU	1. Alkaline clean 2. Alkaline etch (Turco 5578)
DA	1. Alkaline clean (Dapcotreat 4023) 2. Conversion coat (Dapcotreat 4000)
PF	1. HNO_3-HF etch 2. Trisodium Phosphate-Potassium Fluoride-HF treat 3. Water soak
MPFS	1. Nitric Acid pickle 2. Alkaline clean 3. HF-HNO_3-Sodium Sulfate etch 4. Trisodium Phosphate-Potassium Fluoride-HF treat 5. Water soak
PSHA	1. Alkaline clean 2. Water soak 3. Nitric-HF etch 4. Sodium Hydroxide anodize @ 10 volts 5. Water soak

Two of these pretreatments are of particular interest to this study, the chromic acid anodization (CAA) and the sodium hydroxide anodization (PSHA). These electrochemical anodizations have been shown to produce macroporous oxides of remarkably similar topology[8] (Figure 4.4). It is important in adhesion research that these oxides have similar surface roughness; the contributions from mechanical interlocking to the bond strength must be equivalent if acid/base effects are to be estimated in actual bonds. Another reason for the use of these pretreatments of titanium is the durability of the resulting oxide. Chromic acid anodized samples have been left exposed to ambient laboratory conditions for 6 months with no change in topology[14]. These pretreatments differ in that the CAA treatment produces an acidic oxide, while the PSHA produces a basic oxide[8]. This combination of attributes makes these oxide surfaces ideal for the study of acid/base interactions.

The anodic oxides show vivid interference color, depending on the pretreatment conditions. It has been suggested that these colors could be used to estimate the thickness of the oxide. Tables, such as Table 4.2, have been established which relate the thickness of oxide film to the colors[15]. This table was not generated with experimental data, rather it was calculated using optical constants for rutile for the various thicknesses. It should be noted that these colors repeat, therefore a particular color may indicate two or more thicknesses. Also the perception of color can vary from observer to observer (this author is slightly green-brown color blind). These limitations, with the fact that the oxide film is amorphous, not crystalline, render Table 4.1 to only qualitative interpretation. If a reproducible color is obtained through the pretreatments, then one can be reasonably confident that an oxide layer has formed, and that this oxide is probably the same thickness as other oxide layers of this color.

The mechanism of anodic oxidation of titanium has been investigated via ^{18}O labelling studies[16]. It is believed that during anodization, the Ti^{4+} cations move throughout the existing oxide layer, and react with water, acting as an oxidizing agent, at the oxide/electrolite interface. This type of growth would be expected to result in an oxide with less residual stress than oxide which grows *into* the metal.

Table 4.2. Interference Color vs. Oxide Thickness for Titanium.[15]

Color	Oxide Thickness (nm)
weak grayish yellows	0-18
OLIVE BROWN	18-25
REDDISH BROWN	25-27
PURPLISH RED	27-30
PURPLE	30-35
BLUE	35-55
weak grayish greens	60-90
GREENISH YELLOW	95-105
GRAYISH ORANGE	110
PURPLISH RED	115-125
PURPLE	125-135
BLUE	135-145
BLUE-GREEN	145-160
GREEN	165-185
grayish yellows	185-195
pinks	195-210
PURPLISH RED	215-225

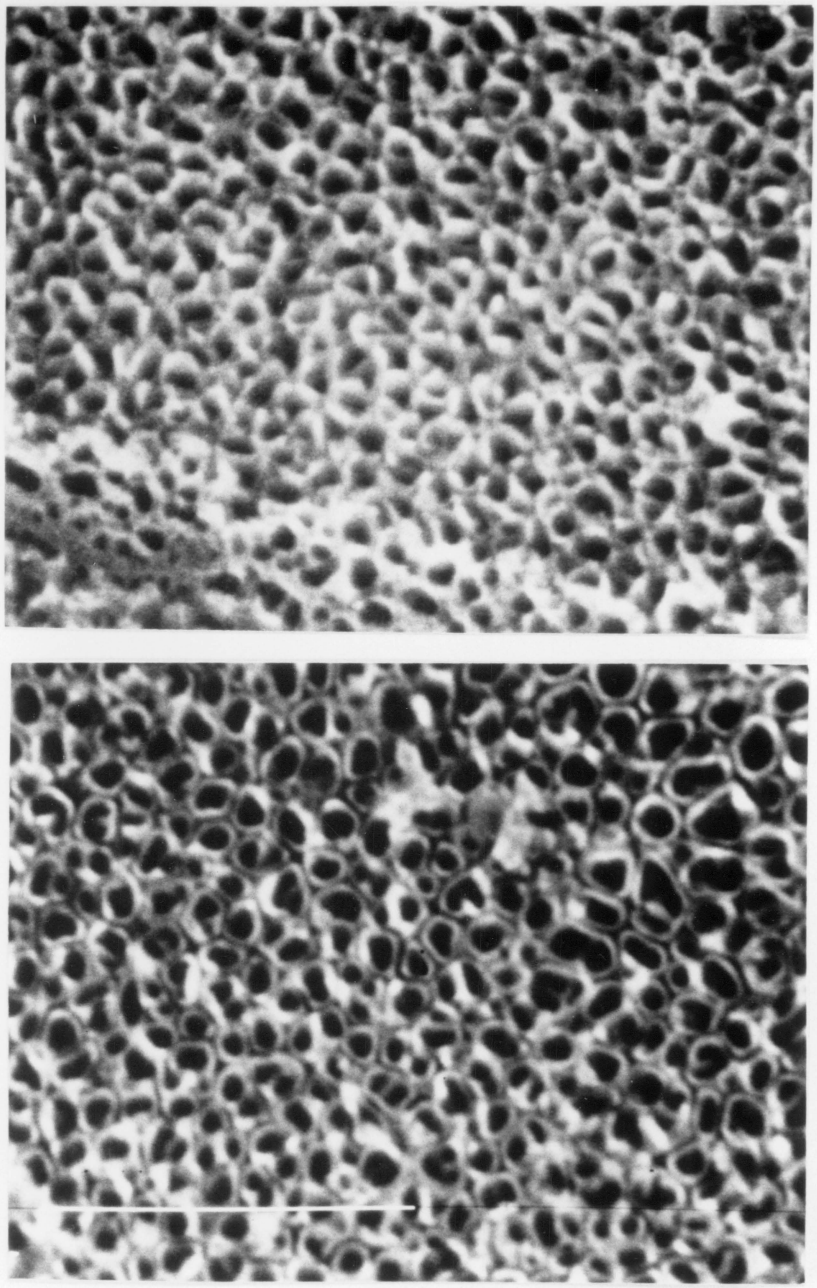

Figure 4.4. Micrographs of PSHA (top image) and CAA pretreated Ti-6Al-4V alloy at 100,000X.

The mechanism of pore formation during anodization is not as well defined. It has been speculated that pore formation is initiated by localized dissolution of the oxide. If the pretreatment is electrochemical, then current flow would increase at the site due to the oxide thinning. This in turn causes localized heating and will favor continued dissolution at the site, sustaining the pore during the pretreatment.

While much has been published on the chemical and physical characterization of Ti-6Al-4V derived oxides, little can be found on pure Ti derived oxide. This is due to the greater technological importance of titanium alloys, particularly Ti-6Al-4V, over pure titanium. In this study, commercially pure, grade 2 titanium will be used. In order to make use of the great body of information on alloy derived oxides, the pure, derived oxide must be produced and characterized.

4.4 Experimental

4.4.1 Materials

All solvents used with the exception of water were ACS reagent grade, obtained from Fisher Scientific. The water used was deionized tap water (typical resistance 4 megaohms/cm). Commercially pure, grade 2 titanium foil (.003 in) on which the oxides were electrochemically grown was obtained from ATEK corporation. Ti-6Al-4V alloy sheet (.06 in) was obtained from Crucible Research. The anodization solutions, discussed in Appendix C, were made from deionized water and ACS reagent grade chemical unless otherwise noted. Indicator dyes were obtained from Aldrich Chemical and made into stock solutions using procedures described in References 18 and 19.

4.4.2 Anodization Techniques

The titanium foil (.003 in) was cut into 6 x 1 inch coupons using foot operated, sheet metal shears which produced a cleaner edge than could be obtained with simple hand shears. The

Ti-6Al-4V alloy (.06 in.) was cut to the same size with motorized shears. After cutting, all samples were cleaned with isopropyl alcohol to remove ink used in markup.

The ridged Ti-6Al-4V backing could be reused. To do so, residual polymeric adhesive from previous testing must be thoroughly removed. This was accomplished by soaking overnight in toluene, wiping down with a toluene saturated Kimwipe™, then vapor degreasing for 3 hours in methylene chloride. After this procedure, the color of the oxide layer was the same as the virgin oxide, and the sample readily showed finger prints upon touching.

A stepwise procedure for both CAA and PSHA anodizations can be found in Appendix C. Latex gloves were worn for both procedures, and the titanium coupons were handled whenever possible with plastic forceps. The pre-anodization alkali etches and soaks were carried out in 250 ml tall form beakers. This allows 5 inches of the 6 inch coupon to be treated.

The actual anodizations were carried out in 3 ℓ or 10 ℓ polyethylene containers. A HP6284A DC power supply was used to adjust the potential and current. A schematic of the anodization setup is shown in Figure 4.5. The Ti-6Al-4V cathode was attached to the side of the bath by means of an alligator clip. The coupons for anodization were first clipped to a brass strip to assure good electrical contact and connectivity between the pieces, and was then suspended from a ring stand, and lowered into the electrolytic bath. Care was taken to assure that neither the alligator clips nor the brass strip came into contact with the electrolyte solution.

The chromic acid anodization required dropwise addition of HF to obtain the desired current density. There was approximately 30 sec lag time between the addition of HF and stabilization of the current.

The sodium hydroxide anodization required the bath to be held at 20°C. This isothermal condition was approximated by preparing two, 2 ℓ bottle of NaOH electrolyte, and chilling one bottle in ice water to $\simeq$5°C. The room temperature electrolyte was then mixed with the cooled solution until a final temperature of $\simeq$18°C was obtained. During the 30 min anodization, the solution would only warm up to 21°C.

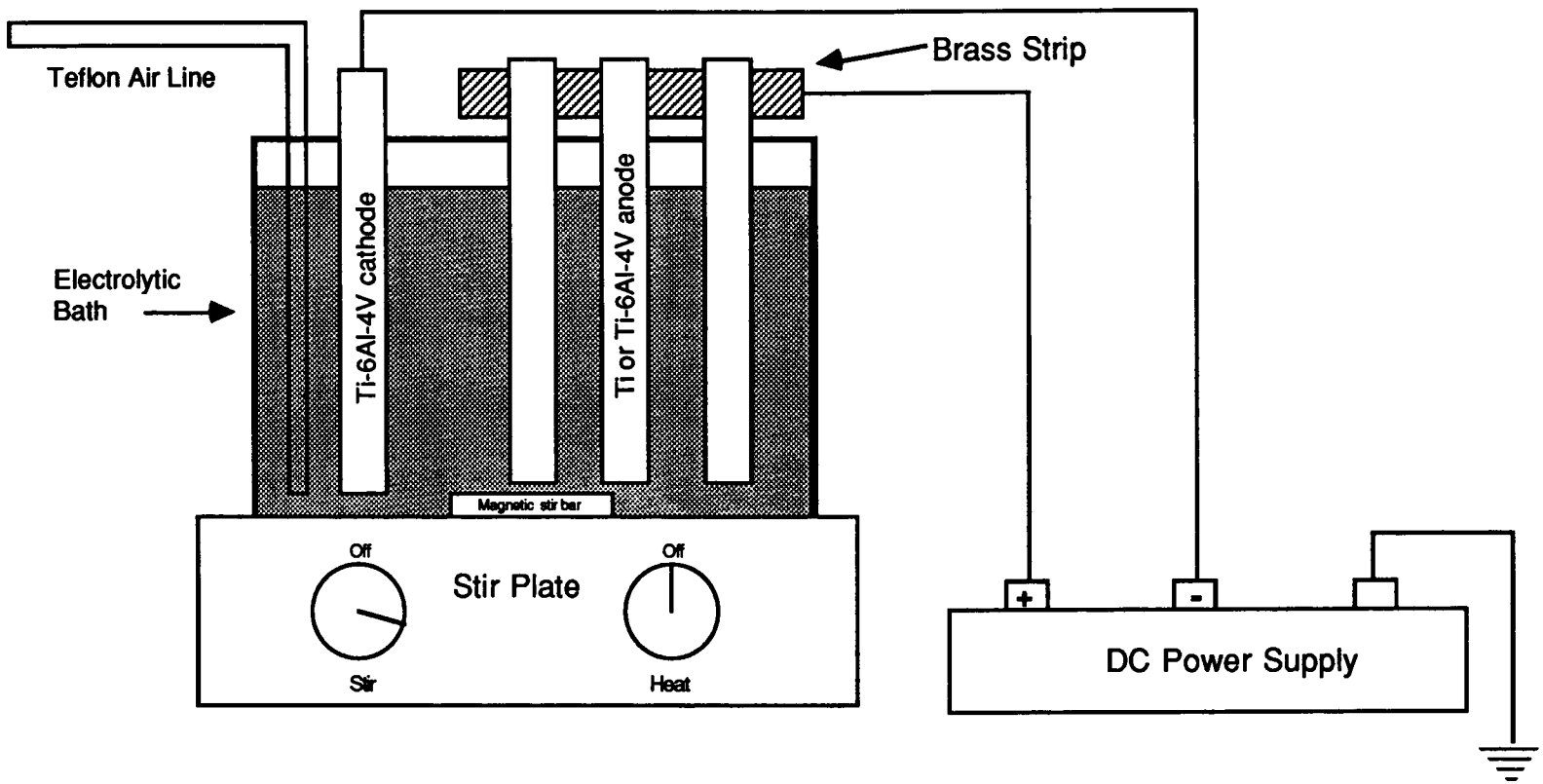

Figure 4.5. Schematic of anodization setup. (The teflon air-bubbler was used only for chromic acid anodizations.)

4.4.3 X-ray Photoelectron Spectroscopy

X-ray photoelectron spectra were obtained using a PHI 5300 ESCA system equipped with a hemispherical analyzer. A magnesium x-ray anode run at a power of 250 W was used for all samples. The spot size of the instrument was 2 x 10 mm. The pretreated foils were cut into rough 1 inch diameter hexagons and mounted onto ESCA probes using double stick tape. The thicker Ti-6Al-4V samples were cut into 1/4 inch disks using a punch, die, and arbor press, and were then mounted onto the probes using the same method.

After the sample had been introduced into the high vacuum chamber, no attempt was made to "clean the surface" with an Argon ion sputter. The spectra obtained were "as is" and would therefore show any contamination picked up during the pretreatment (keeping in mind that the $\simeq 10^{-9}$ torr vacuum will strip off any weakly bound volatile contaminates).

A survey scan of each sample was obtained over a binding energy range from 0 to 1000 eV, with fifteen scans signal averaged for each survey spectra. Narrow scans were done on all significant peaks noted in the wide scan spectra. Again, fifteen scans were averaged for each narrow scan spectra. When analyzing CAA samples, the following elements were always scanned for, regardless of the survey scan: carbon, oxygen, titanium, fluorine, and silicon. For PSHA samples, the elements always scanned for were: carbon, oxygen, titanium, calcium, and silicon.

Relative atomic percents were calculated from the narrow scan spectra. The peak areas for each element were calculated using Perkin-Elmer supplied software. These areas were then corrected by the photoelectron cross-section of each element[20]. The atomic percent for each element was calculated from these corrected area.

4.4.4 Scanning Transmission Electron Microscopy (STEM)

The surface topography of the pretreated Ti and Ti-6Al-4V alloy was studied using STEM. The photomicrographs were acquired in the SEM mode using a Philips EM-420T electron microscope equipped with a Tracor Northern 5500 EDX, Image Analysis system. Foil samples

were cut into 3 x 8 mm pieces and placed into the microscope's probe. The samples were sufficiently conductive, so that coating the samples to prevent charging was not necessary.

Image analysis was accomplished by creating a computerized binary image of the STEM micrographs. This image was processed by first "eroding" to remove any single pixel's features, then backfilling to restore the image (minus the single features). This "cleaned" image was then analyzed in terms of number of pores present, shape, diameter, and net orientation.

4.4.5 Indicator Dyes

Indicator dyes were used in an attempt to quantify the acid/base nature of the oxide surface[17]. The coupons were tested by placing two drops of dye solution[18,19] onto a fresh pretreated surface. The color of the dye, both wet and after drying, was recorded.

4.5 Results and Discussion

The Ti and Ti-6Al-4V alloy samples were pretreated by the CAA and PSHA procedures. The PSHA treated samples were a vivid purple-blue and the CAA samples a red-brown to purple-red. The slight differences in the CAA color probably indicate a thinner oxide and result from the "unforgiving" nature of the CAA process.

When comparing the two anodization methods, the sodium hydroxide anodization (PSHA) was by far the more "forgiving" of the two procedures. A small error in the time in the pre-anodization baths had no effect on the final product. In the actual electrolytic bath, there was no dependence of oxide quality on anode to cathode surface area ratios, or surface area to electrolyte volume ratios. However, there appeared to be a limiting ratio of 1 in^2 of anode to 95 ml electrolyte for the chromic acid anodization (CAA). If this ratio was exceeded, anodization appeared to have no effect on the samples (e.g. no color change). The anode to cathode surface area ratio was not varied, but kept at 3 to 1 as this ratio was used successfully by Filbey[8].

Perhaps the most tedious requirement for the CAA was the necessity to stir the chromic acid electrolyte 12 hours before use. The origin of this requirement remains obscure. After discussions with Dr. J. Mason of Virginia Tech, it is thought that the dissolution process of chromic trioxide, while appearing to the naked eye to be almost instantaneous, is quite involved. He postulated a series of "polymeric" or "clusters" of hydrates of chromic trioxide, which eventually decompose to the common chromate $\rightleftharpoons$ dichromate equilibrium. Apparently, the solution process and therefore the stabilization of the solution's pH takes on the order of 10 hours.

The chemistries of the CAA and PSHA processes are not well defined. Historically, this has been a problem of titanium chemistry. Dr. E. J. Kelly, in his review on the electrochemical behavior of titanium states, *"There are those who maintain that titanium exists for the sole purpose of making electrochemists look bad. ... Hard facts are few and difficult to come by, while controversies abound"*[21]. With this in mind, the following observations are put forth.

There is rapid evolution of gas at both electrodes during the PSHA anodization, indicating that hydrolysis of water, in addition to oxide formation, occurs at basic pH's (> 14). Also, the anode rapidly turns a brownish color as soon as current starts to flow.

During the CAA anodization, no gas is evolved at either electrode. This indicates that other reactions occuring at lower potential are taking place. A likely candidate for the cathodic reaction would be the reduction of the dichromate ion:

$$Cr_2O_7^{-2} + 14\,H^+ + 6e^- \rightarrow 2\,Cr^{+3} + 7H_2O \quad E^0 = 1.33V$$

Qualitative evidence for this is the formation of a green cast to the solution when the anodization is over. Chromium III ions in solution typically have a green color. There is also the possibility for the formation of titanium hydride during the anodization, rather than hydrogen gas, particularly at large negative potential and low pH[21].

$$Ti + 2H^+ + 2e^- \rightarrow TiH_2 \quad E^o = 0.45\,V$$

No further investigation into the electrochemical behavior was pursued. The author has chosen not to rush in where electrochemists have feared to tread.

STEM allowed the topography of the Ti and Ti-6Al-4V samples to be studied in great detail. Micrographs of the various surfaces can be found in Figures 4.6-4.13. Figures 4.6 and 4.9 show micrographs of the CAA and PSHA pretreated oxides at 6,400X magnification, respectively. Apart from the cracks, which were used for proper focus, the two micrographs are markedly similar. Both images reveal a gently rippled surface, devoid of any prominent features. Figures 4.7 and 4.10 show the CAA and PSHA surfaces at 50,000X magnification. At this magnification, the macroporous nature of the oxides are revealed. It is apparent that the CAA pretreated oxides have a more sharply defined pore structure than the PSHA oxide. The macroporous nature of both oxides is readily apparent in Figure 4.12, which shows the surface at 100,000X magnification. Although the PSHA pore structure is less defined than the CAA structure, the pores are approximately the same size. These similar topologies are important to adhesive testing; mechanical interlocking has an important role in adhesion as discussed in Chapter One. If the effect of acid/base interactions is to be observed in a real bond, the mechanical interlocking (and hence the topology) must be taken into consideration.

Figure 4.7 and 4.8 also contain images of CAA pretreated Ti-6Al-4V alloy. Comparisons at 50,000 and 100,000X magnification show the topologies to be virtually identical. The micrographs shown in Figure 4.11 allow comparison of the PSHA treatment of Ti and Ti-6Al-4V. Here the Ti-6Al-4V derived oxide has a better defined pore structure than the titanium, however average pore size is still the same in both cases.

The porosity of these oxide layers were quantified by means of image analysis. A binary representation of the porous surface was created from the micrograph and analyzed in terms of the number of pores present, aspect ratio, size, and orientation. The micrographs, and a summary of this data, can be found in Figure 4.13 and Table 4.3. The average pore is roughly spherical, with a diameter of 270 $\mathring{A}$. This type of surface would be classified as "macroporous" using IUPAC nomenclature. As can be seen in Figure 4.12, the PSHA porosity is very similar. The lesser contrasts in the PSHA image prevents its quantitation for binary analysis.

Wide scan XPS spectra of CAA-Ti and Ti-6Al-4V samples are shown in Figure 4.14, and they appear almost identical. The same elements at the same relative concentrations are observed

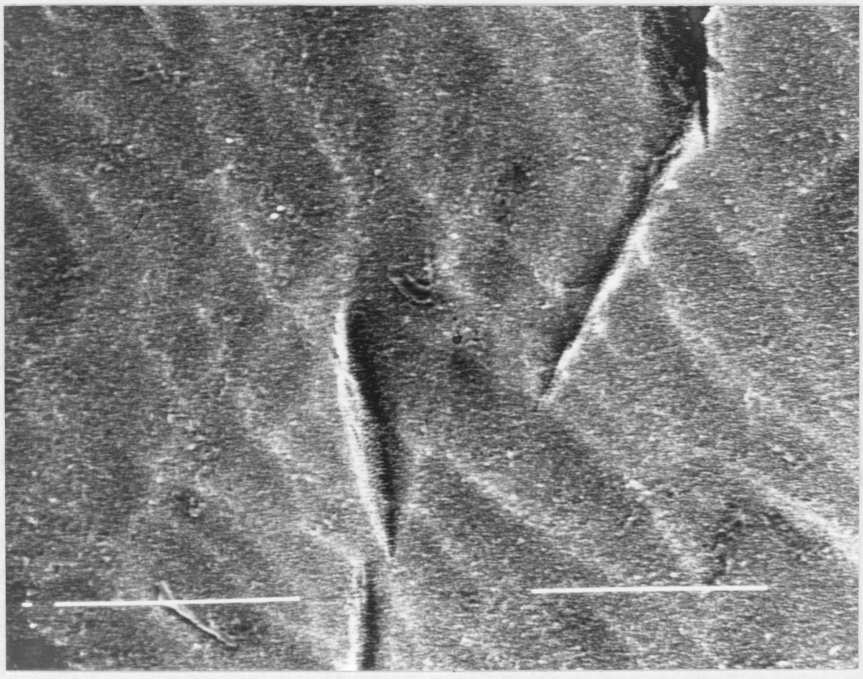

Figure 4.6. SEM micrograph of CAA-Ti surface at 6400X magnification.

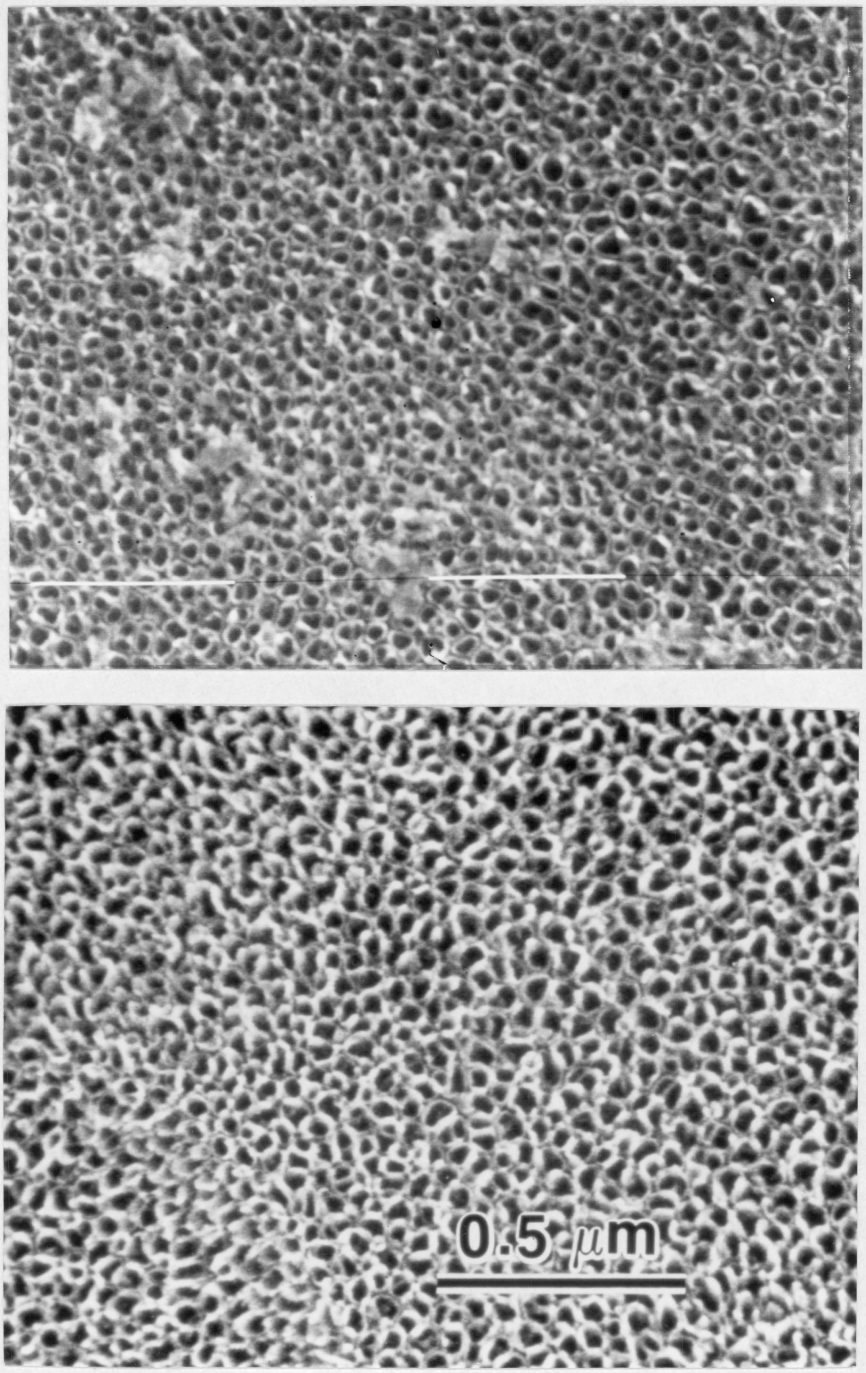

Figure 4.7. SEM micrograph of CAA-Ti (top image) and CAA Ti-6Al-4V (bottom image) at 50,000X magnification.

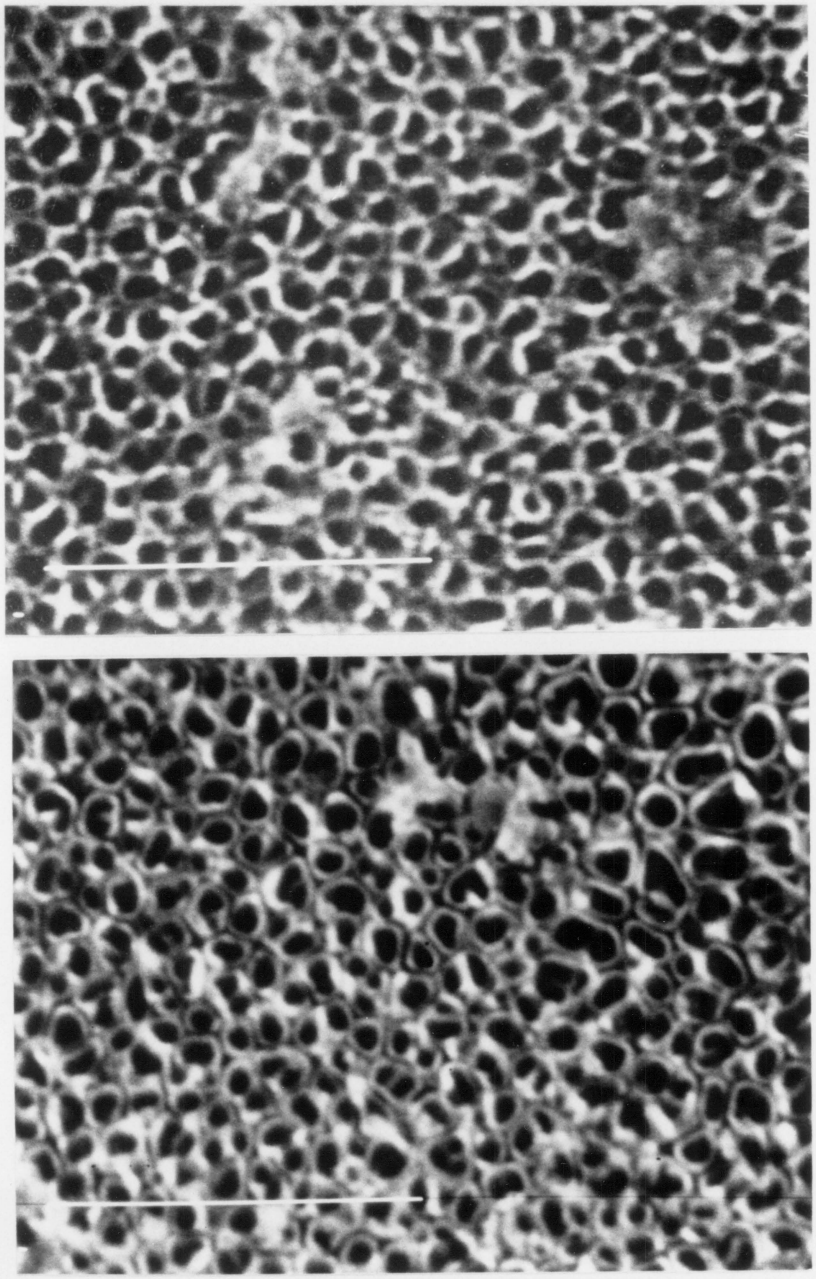

Figure 4.8. SEM micrograph of CAA-Ti (top image) and CAA Ti-6Al-4V (bottom image) at 100,000X magnification.

Figure 4.9. SEM micrograph of PSHA-Ti surface at 6,400X magnification. (Note similarity to CAA surface at same magnification shown in Figure 4.6.)

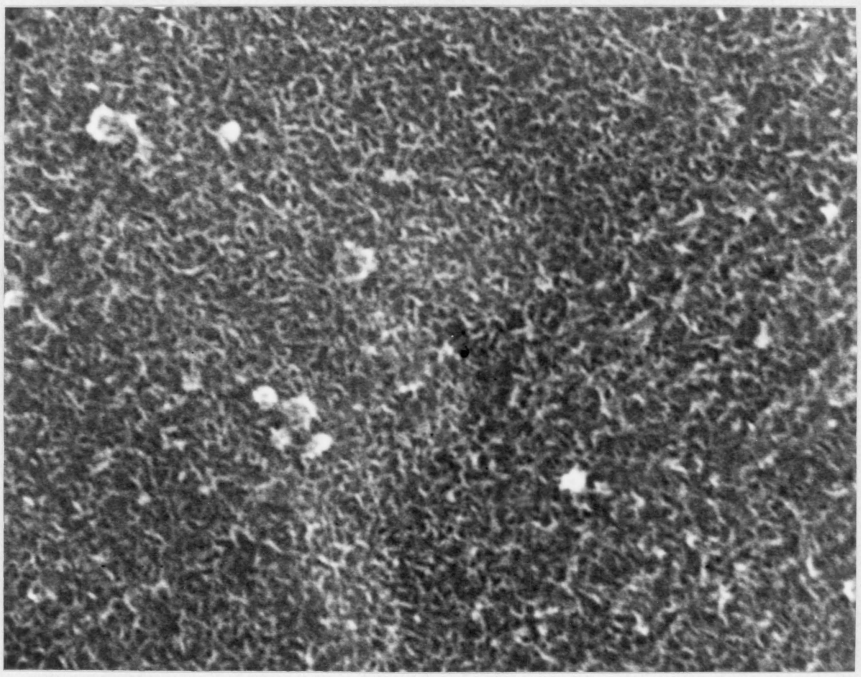

Figure 4.10. SEM micrograph of PSHA-Ti surface at 50,000x magnification.

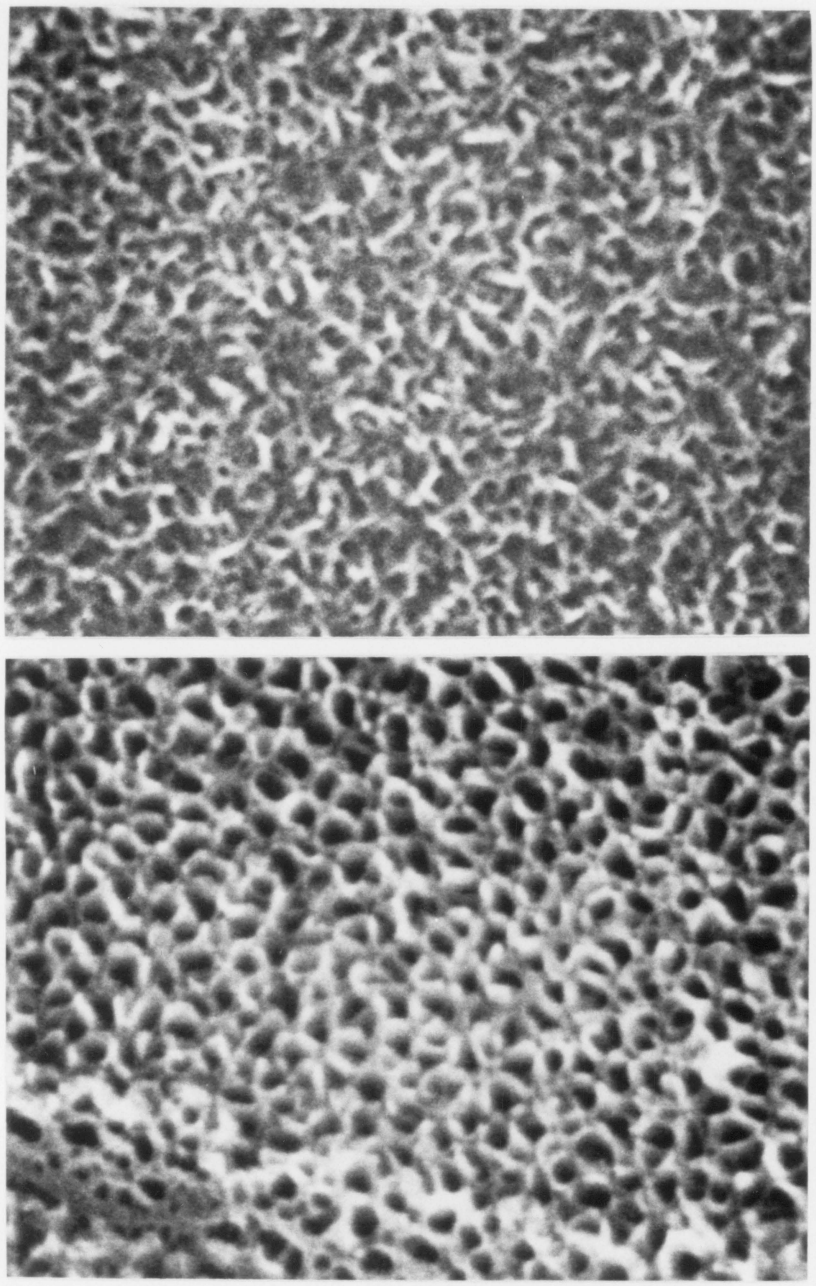

Figure 4.11. SEM micrograph of PSHA-Ti (top image) and PSHA Ti-6Al-4V (bottom image) at 100,000X magnification.

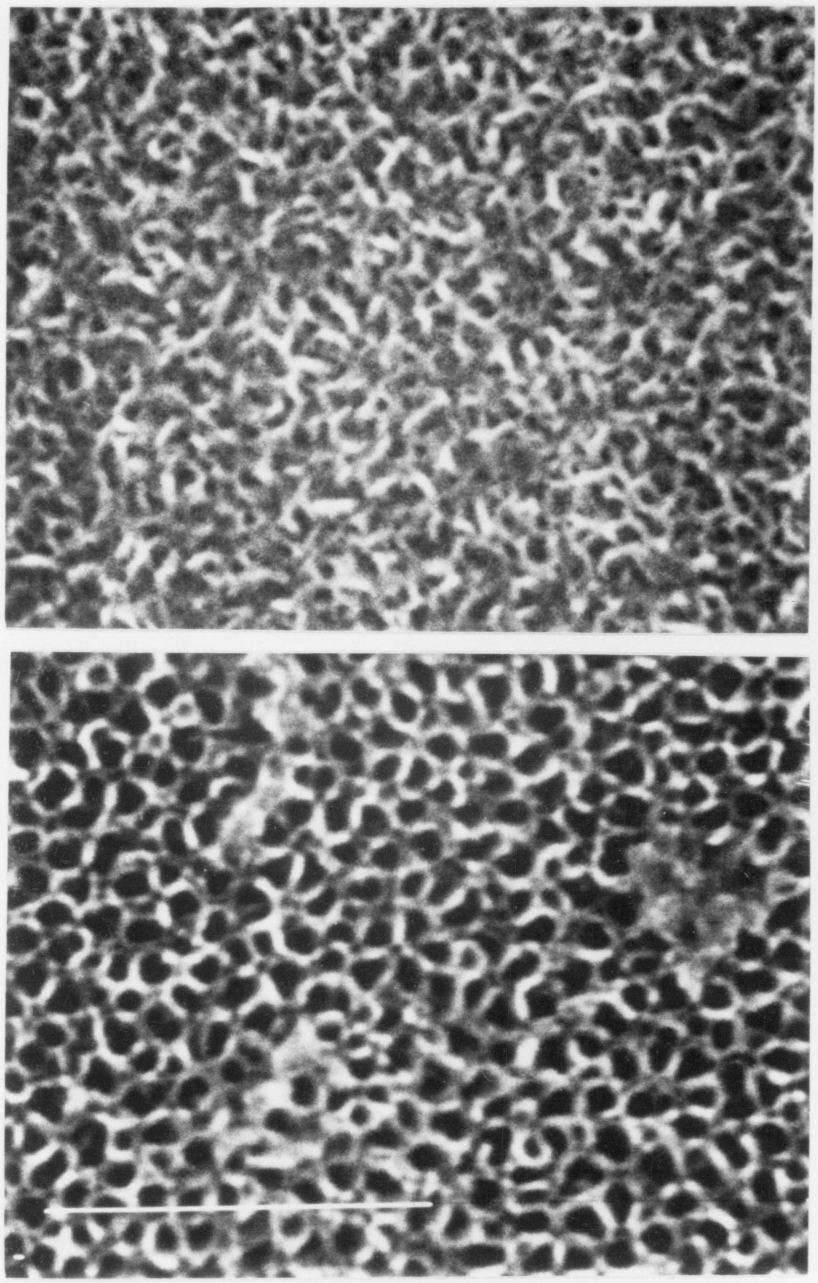

Figure 4.12. SEM micrograph of PSHA-Ti (top image) and CAA-Ti (bottom image) at 100,000X magnification.

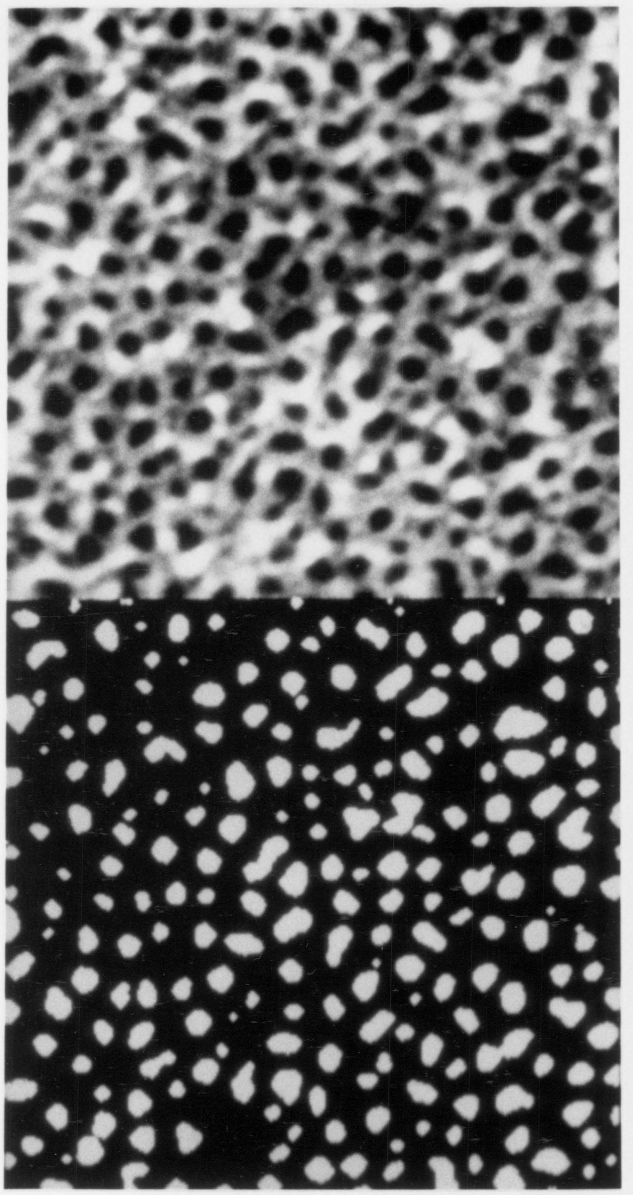

Figure 4.13. SEM micrograph of CAA-Ti surface at 100,000X magnification and corresponding binary representation of the pores.

Table 4.3. Image Analysis Summary for Figure 4.13, CAA Pretreated Titanium.

Magnification	100,000
Field area	0.77×10^{-6} m^2
Number of Particles	230
Average Diameter	270 $\mathring{A}$ ± 100*
Length	330 $\mathring{A}$ ± 127*
Width	230 $\mathring{A}$ ± 85*
Aspect Ratio	1.5 ± .2*
Orientation**	53° ± 53°*

* ± values are one standard deviation
** results indicate no net orientation

in both Ti and Ti-6Al-4V derived oxides. This indicates that the elements used for alloying, Al and V, are not present on the topmost layer of the oxide, and that the same oxide is formed on both metals. Wide scan XPS spectra of PSHA-Ti and Ti-6Al-4V are shown in Figure 4.17. Again, the same elements at the same relative concentrations are observed in both samples. This indicates that this pretreatment likewise forms the same oxide on both metals.

Narrow scan XPS spectras of CAA-Ti samples are shown in Figures 4.15 and 4.16. The presence of a large carbon 1s peak (285 eV) indicates that the surface has been contaiminated to a small extent. The asymmetry of the peak indicates the carbon on the surface is in a variety of chemical states (e.g., single bonded, aromatic, bonded to heteroatoms, etc.). The presence of clear, strong Ti peaks ($2p_{3/2}$ and $2p_{1/2}$, at 459 and 465 eV) indicate, however, that this contamination was slight. XPS is a surface sensitive technique ($\simeq$100 $\mathring{A}$); any heavy contamination layer would reduce or completely eliminate the titanium signal. Therefore, the contamination layer must have been thin and/or discontinuous. The predominate oxygen 1s peak (530 eV) can be assigned to the metal oxygen of TiO_2. The asymmetry of the peak indicates oxygens of different chemical states were present. These can be assigned to the acidic and basic oxygen sites on the surface of the oxide and organic oxygen found in the contamination layer. The fluorine 1s peak (684 eV) arose from the carry over of fluoride ions from the CAA bath. The presence of fluorine is very useful as it can be used as a "tag element" to indicate the presence of virgin oxide surface in future studies.

Narrow scan spectra of the PSHA-Ti samples are shown in Figure 4.19. The appearance of the ubiquitous carbon, titanium, and oxygen peaks appear similar to the CAA samples. Calcium peaks (352 and 348 eV), instead of fluorine, represent the tag element for PSHA. The calcium is assumed to have been carried over for the tap water rinse step in the PSHA procedure.

Both the CAA and PSHA XPS spectra were routinely inspected for silicon compounds since their low surface free energy imparts to them the ability to wet and creep over almost any surface. The presence of such compounds on a surface indicates the potential for the formation of a weak boundary layer upon bonding. Therefore, any sample on which silicon was found, was suspect.

The acid/base nature of the pretreated Ti was determined by observing the color changes of a series of dyes in contact with the oxides[8]. The results shown in Table 4.4 list the colors observed

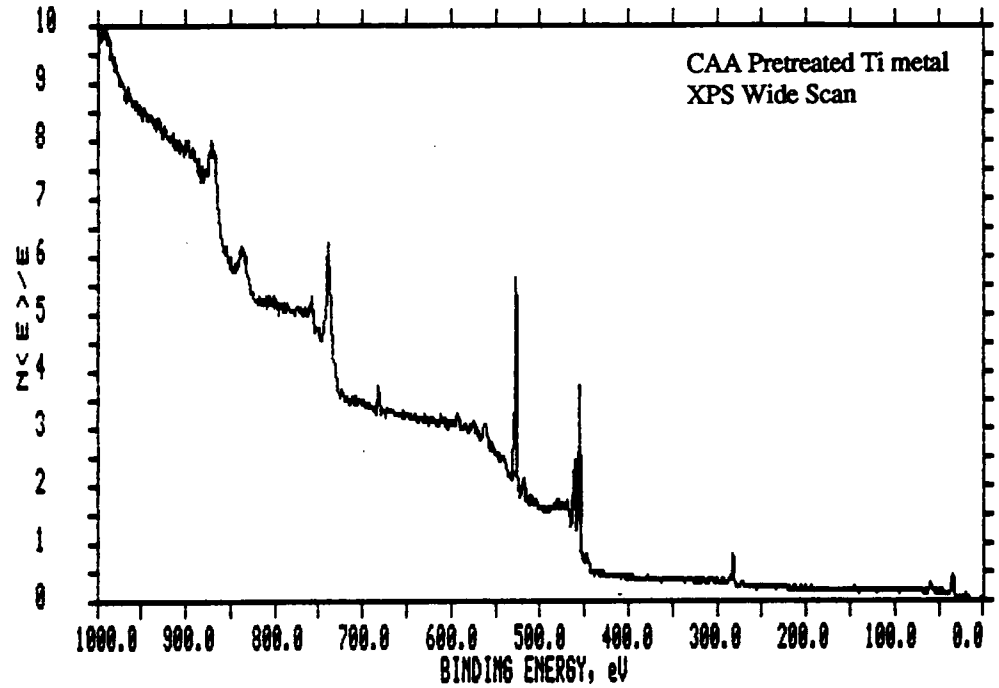

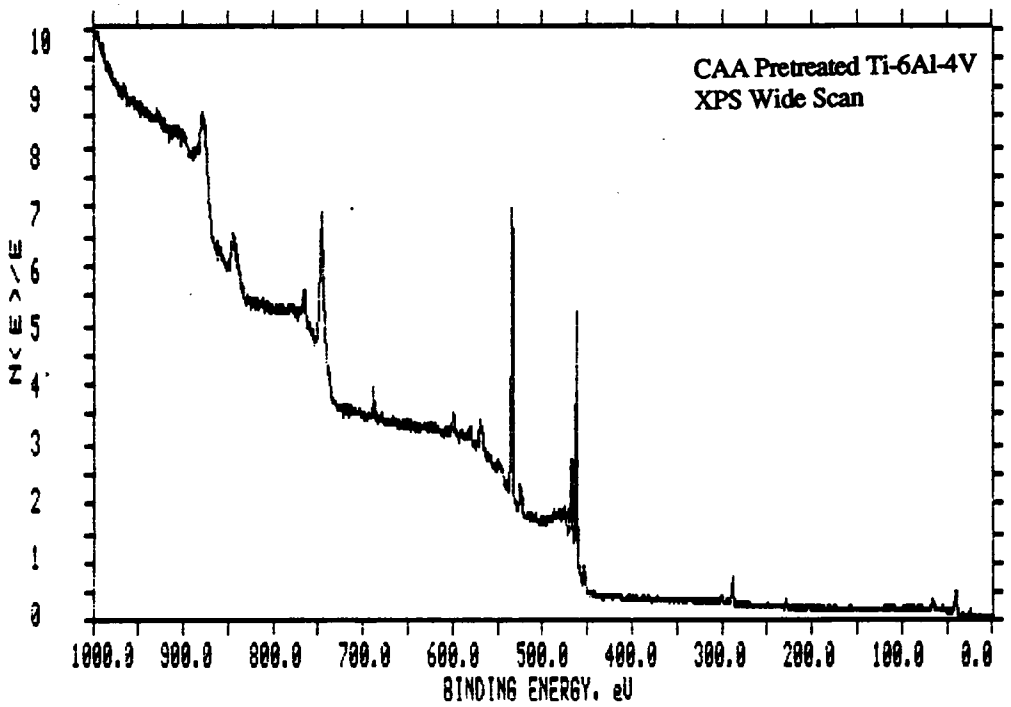

Figure 4.14. Wide scan CAA-Ti and CAA-Ti 6-4.

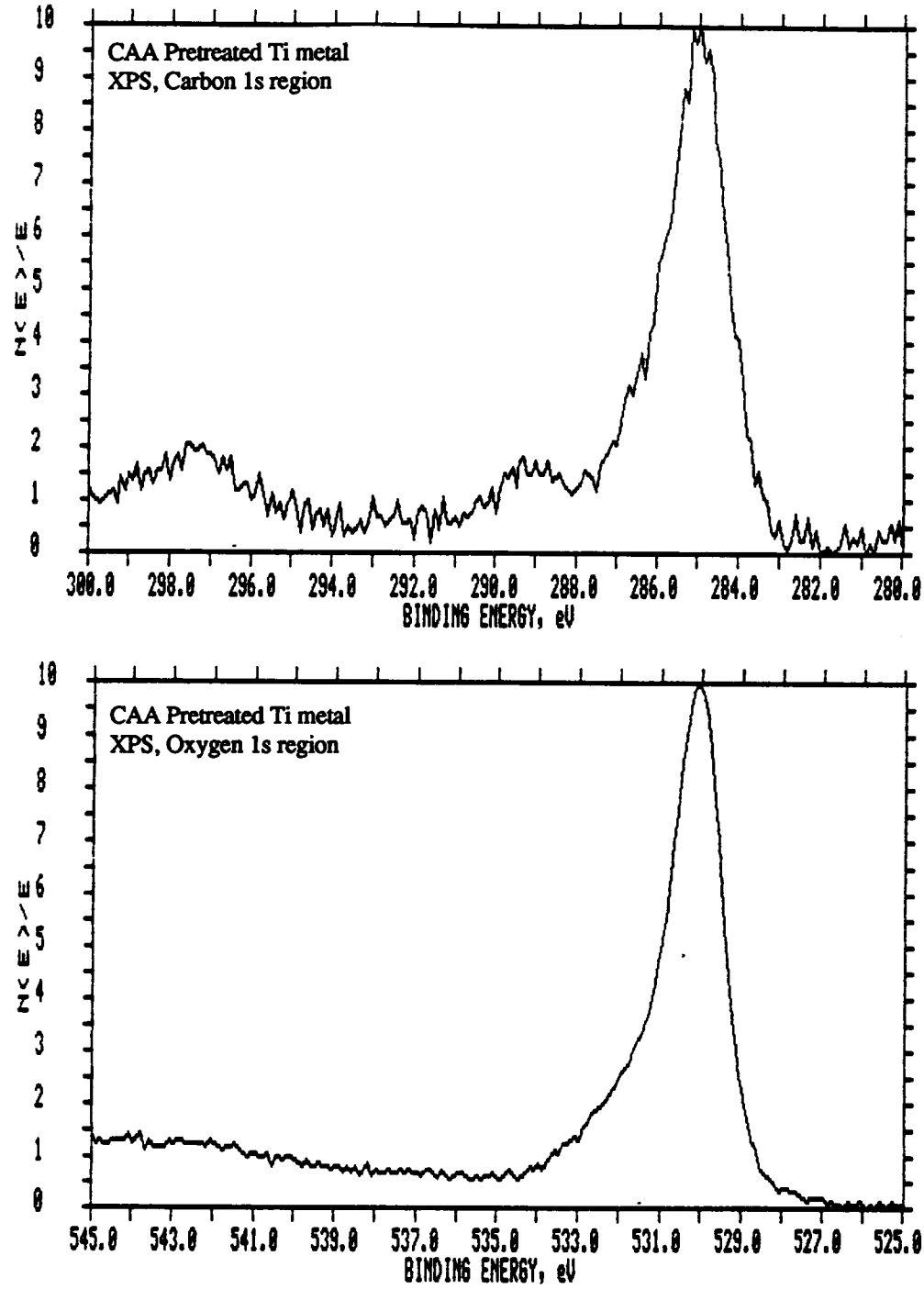

Figure 4.15. Narrow scan of carbon and oxygen peaks found in wide scan CAA-Ti.

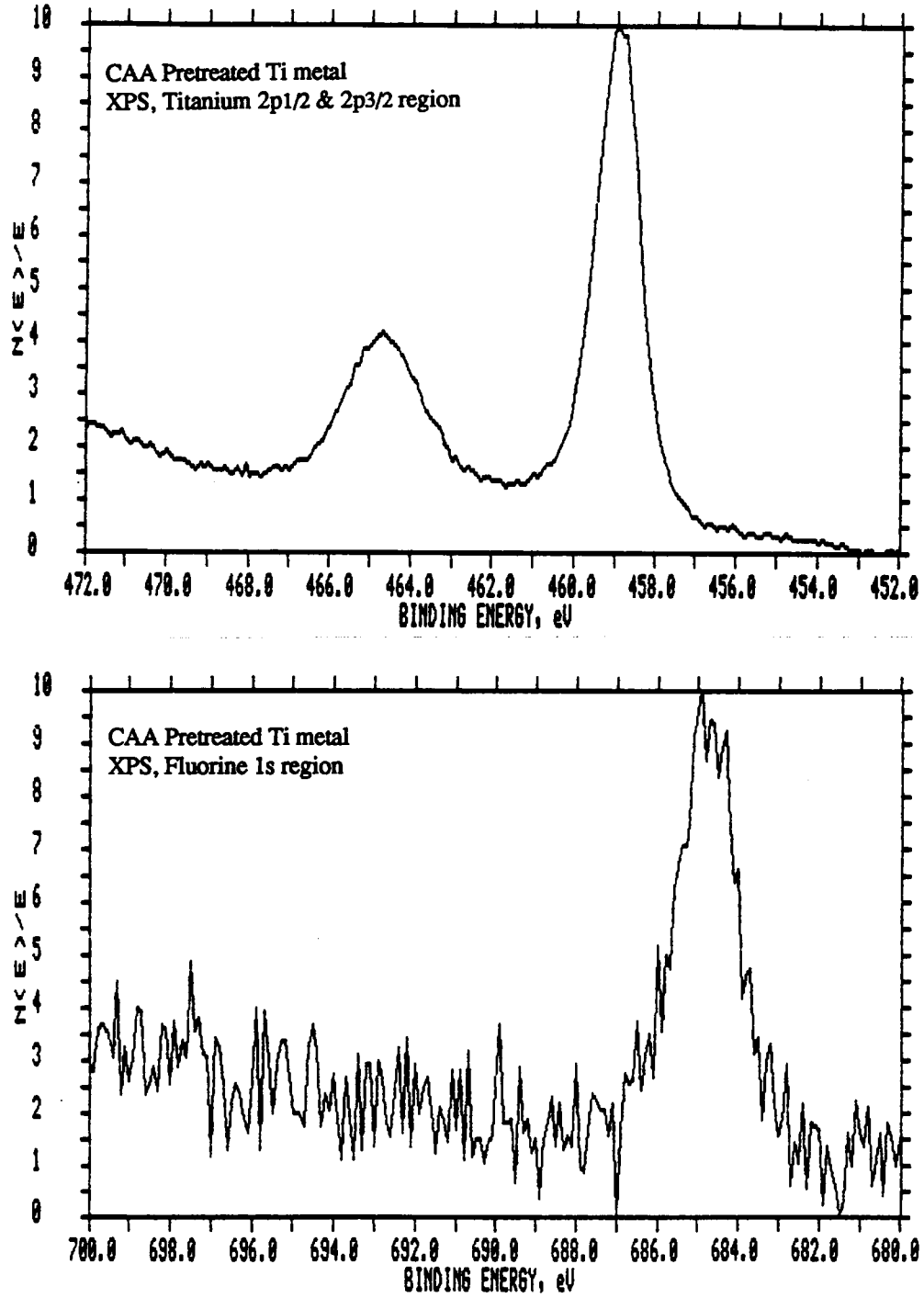

Figure 4.16. Narrow scan titanium and fluorine peaks found in wide scan of CAA-Ti.

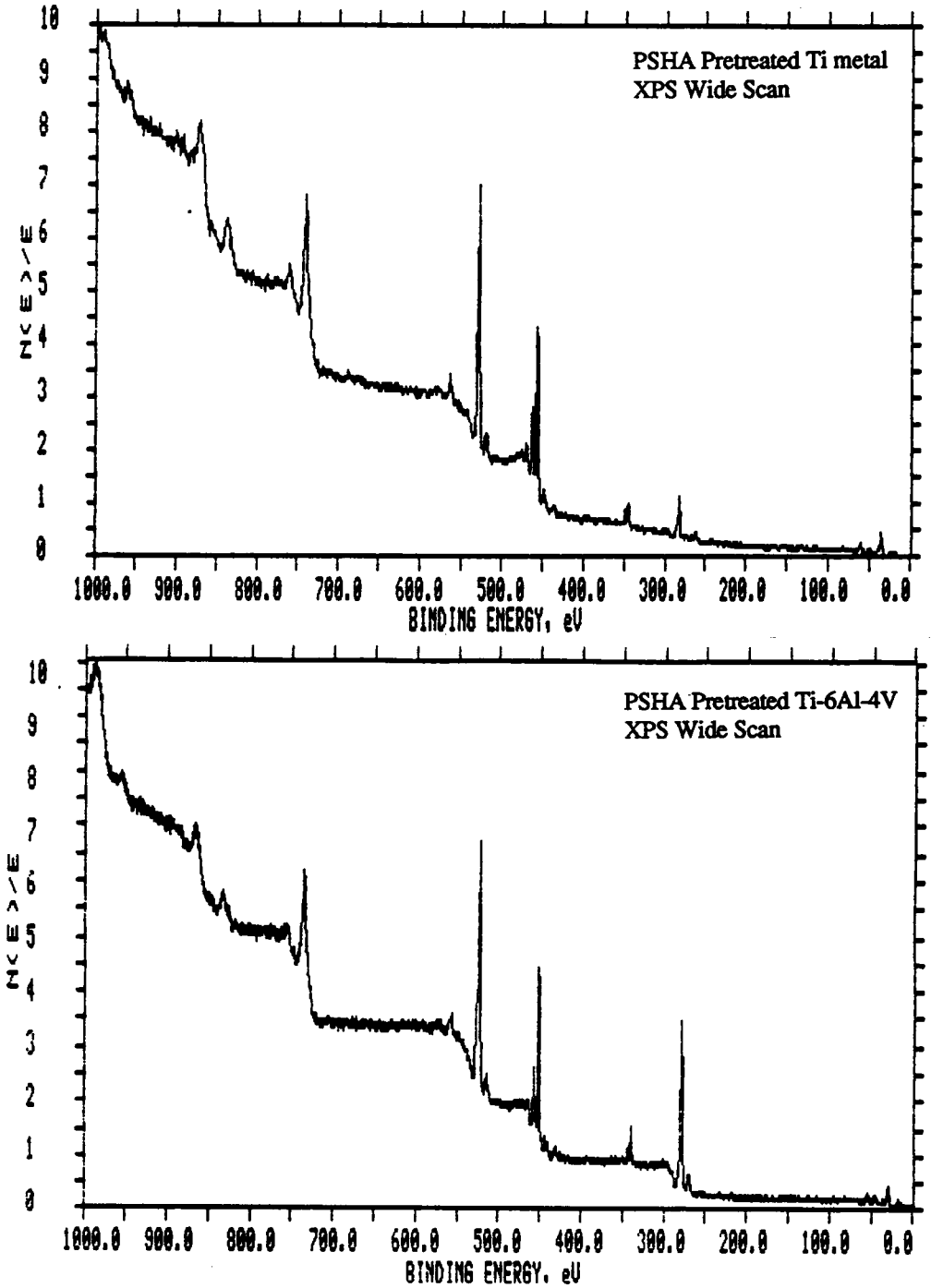

Figure 4.17. Wide scan of PSHA-Ti (top spectra) and PSHA-Ti-6Al-4V.

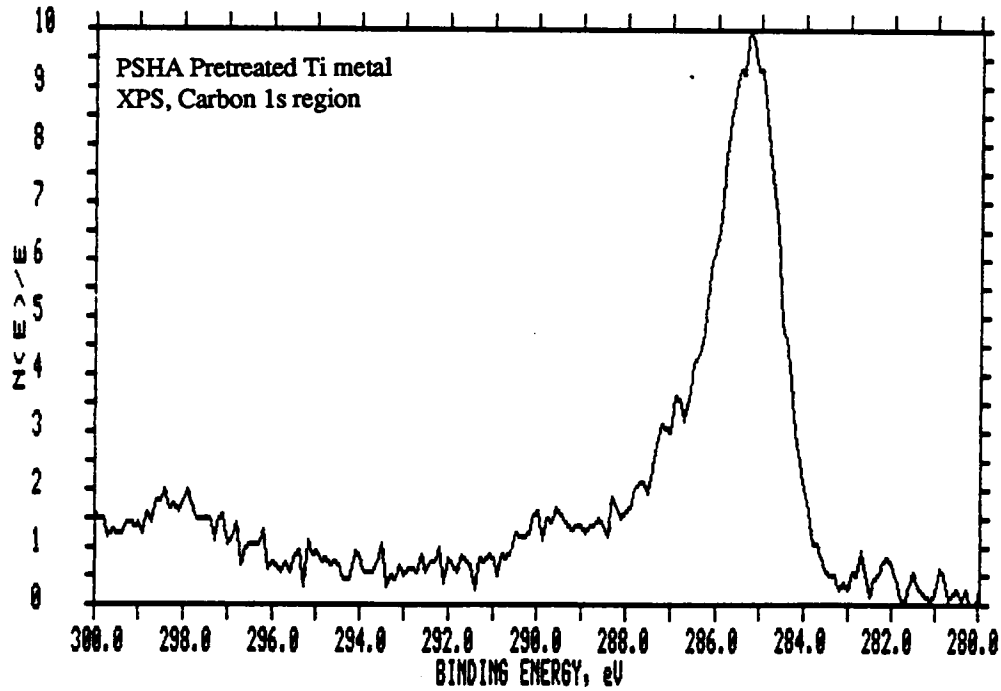

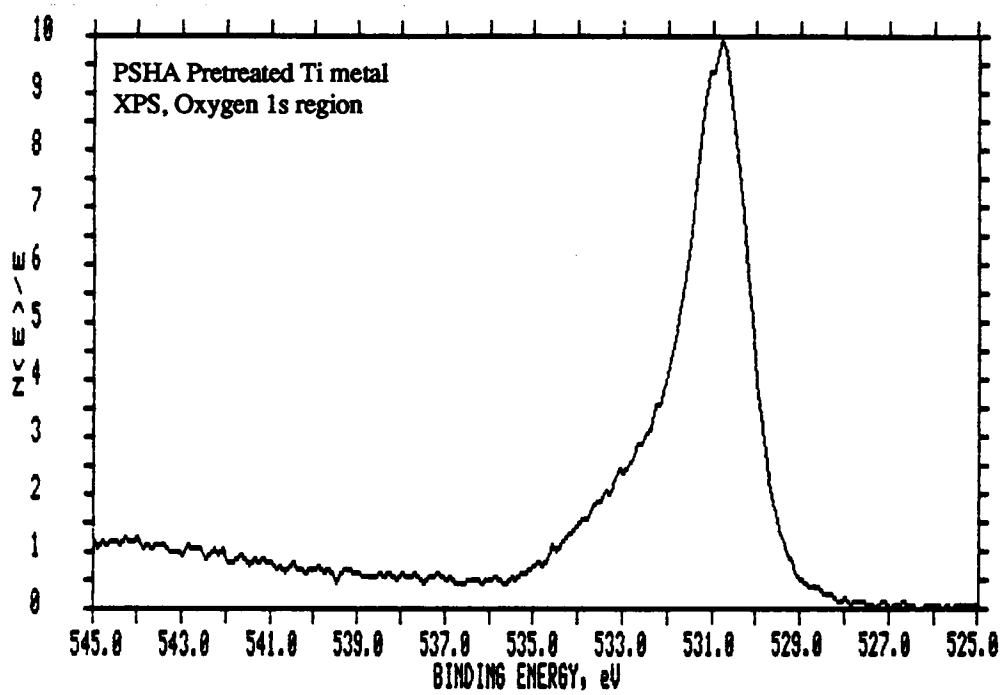

Figure 4.18. Narrow scan of carbon ls and oxygen ls peak found in wide scan PSHA-Ti.

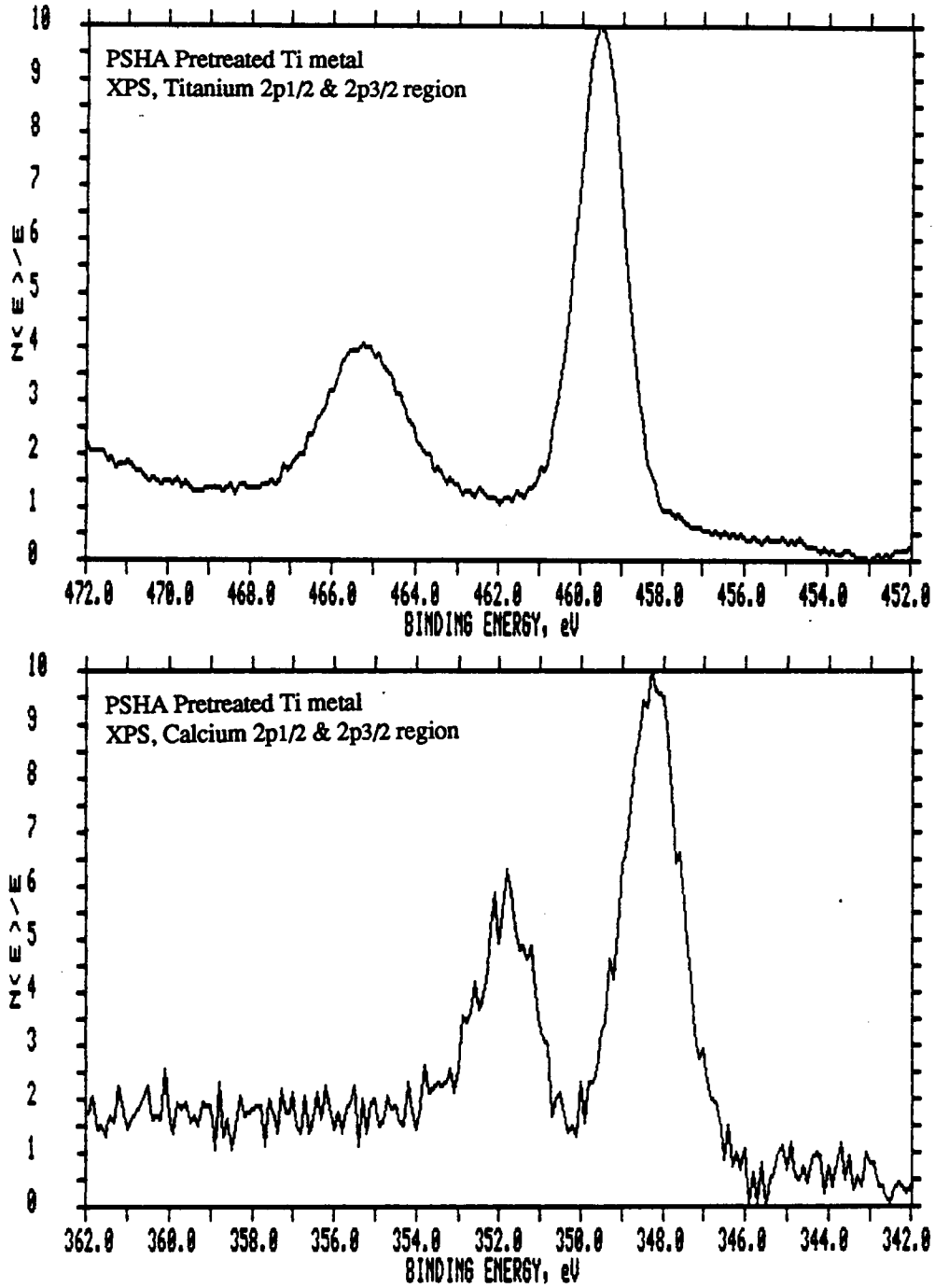

Figure 4.19. Narrow scan of Ti $2p_{1/2}$ and $2p_{3/2}$ and calcium peaks found in PSHA-Ti wide scan.

for each dye on the oxide in both the wet and dry states. The CAA-Ti samples have a surface pH bracketed by the 4-(Phenylazo)diphenylamine, thymol blue and bromophenol blue indicators. This would place the pH in the acidic range of 3.0 to 2.5. The PSHA samples are bracketed by the thymol blue and orange 1 indicators. This would put the surface pH in the basic range of 8-9. Nearly identical results have been obtained for the testing of CAA and PSHA treated Ti-6Al-4V alloys[8]. This is consistent with the fact that the Ti-6Al-4V derived oxides have the same topology and elemental composition as the Ti samples.

4.6 Summary

STEM analysis of PSHA and CAA pretreated titanium demonstrates that oxides of similar topology can be obtained. Both oxide films, while appearing relatively smooth, are actually macroporous. The pores have formed perpendicular to the metal substrate with an average diameter of 270 $\mathring{A}$ and aspect ratio of 1.5. This pore structure is better defined in the CAA anodized samples compared to the PSHA treated one. It is critical that the topologies of the oxides be known, as the contribution to the bond strength must be equivalent if acid/base effects are to be estimated in actual bonds.

Micrographs of CAA treated Ti and Ti-6Al-4V alloys reveal that identical topologies are obtained. In the case of PSHA treated Ti and Ti-6Al-4V alloys, the Ti-6Al-4V derived oxide has a better defined pore structure.

XPS data reveals that, in terms of elements present, the CAA and PSHA surfaces are very similar. The only real difference between them is the presence of calcium on the PSHA samples and fluorine on the CAA samples. This minor difference can be used to advantage in future adhesive testing as their detection indicates the presence of a near-pristine oxide surface. Organic carbon and oxygen are seen on all samples. This fact is important to future testing in that the presence of these elements is not conclusive evidence of residual adhesive on the oxide.

Another important observation of the XPS data is that the Ti and Ti-6Al-4V derived oxides give identical spectra. This, in combination with the STEM and indicator dyes data, is strong

Table 4.4. Results of Indicator Dye Testing.

Indicator	pH Range and Color	CAA-Ti (wet)	CAA-Ti (dry)	PSHA-Ti (wet)	PSHA-Ti (dry)
4-(Phenylazo) diphenyl amine	1.2-2.6 red-yellow	yellow	yellow-green	yellow	yellow
bromophenol blue	3.0-4.6 yellow-blue	green	yellow	blue	blue
bromocresol green	3.8-5.4 yellow-blue	yellow	dark	blue	blue
bromocresol purple	5.2-6.8 yellow-purple	yellow	yellow	blue	blue
bromothymol blue	6.0-7.6 yellow-blue	blue	dark yellow	blue	blue
Orange 1	7.6-8.9 orange-purple	orange	orange	dark orange	brown
Thymol Blue	1.2-2.8 red-yellow	yellow	orange	dark green	dark green
	8.0-9.6 yellow-blue	yellow	orange	dark green	dark green

evidence that these oxide layers are the same and the techniques developed for Ti-6Al-4V alloys can be directly applied to pure Ti metal. Ti metal is available in foil form while Ti-6Al-4V alloy is not. The foil is often a more convenient form for samples and with this information, one can now use the foil to model the alloy.

4.7 Future Directions

As can be ascertained from Section 4.2, the crystalline morphology and stoichiometry of the anodic oxides are not well understood. A great deal of fundamental work aimed at these two topics is definitely needed. The same is true of the anodization processes, in particular, the chromic acid anodization. The CAA procedure calls for an air bubbler. Why is this needed if water is supposed to act as the main oxidizing agent? When anodizing Ti 6Al-4V, neither Al or V appear in the oxide; what is their fate? Why is there no gas evolution, and what happens at the cathode during anodization? These are a few of the fundamental electrochemical questions which presently have no answer.

Aluminum is a very important metal which can be pretreated to produce acidic and basic surfaces[22]. In the same way titanium has been used, aluminum and its alloys could be used. Aluminum has the advantage of being much easier to machine than titanium, making the production of complex bond geometries for advanced testing substantially easier. If durable oxides can be formed by less complicated and time consuming methods, aluminum could be the material of choice for future studies.

Another direction future research should take is the identification of a "reference substrate". Such a reference would act as a benchmark off of which adhesive parameters could be measured (e.g., enthalpy of adsorption, enthalpy of acid/base interaction). Quartz would be a good candidate for this material. It is available in high purity, it can be cut into specific sizes, it allows spectroscopy measurements to be done in the UV through IR, it can be passivated to form a neutral surface, and it is unaffected by most organic solvents. Other possibilities for the reference substrate would be

organo-metallic primes which can be coated onto a substrate, then pyrolized to form a smooth metal oxide surface.

4.8 References

1. R. A. Higgins; *Engineering Metallurgy, 5th ed.*, Hodder and Stoughton (1983).
2. R. M. Brick, A. W. Pense and R. B. Gordon; *Structure and Properties of Engineering Materials, 4th ed.*, McGraw-Hill (1977).
3. A. F. Trotman-Dickenson, Ed.; *Comprehensive Inorganic Chemistry*, Pergamon Press (1973).
4. H. D. Megaw; *Crystal Structures: A working approach*; W. B. Saunders Company (1973).
5. R. C. Evans; *Crystal Chemistry*, Cambridge University Press (1964).
6. A. Navrotsky and O. J. Kleppa; *J. Am. Ceram. Soc., 50*, 626 (1967).
7. M. Natan, K. R. Breen and J. D. Venables; Martin Marietta Laboratories report MML TR 81-42(c), Sept. 1981.
8. J. A. Filbey; "Factors Affecting the Durability of Ti-6Al-4V/Epoxy Bonds," Virginia Tech, Ph.D. dissertation, (1987).
9. T. R. Hayes and J. F. Evans; *J. Phys. Chem., 88 (10)*, 1963 (1984).
10. M. Primet, P. Pichat and M.-V. Mathieu; *J. Phys. Chem., 75 (9)*, 1216 (1971).
11. Ibid, p. 1221.
12. R. F. Wegman and D. W. Levi; *27th National SAMPE Symposium, Materials Overview for 1982*, 440.
13. A. C. Kennedy, R. Kohler and P. Poole; *Int. J. Adhesion and Adhesives, 3 (2)*, (1983).
14. Private communication with Steve McCartney, Virginia Tech, Materials Engineering Department.
15. J. D. Briers; *Optik, 63*, 341 (1983).
16. F. Kovler and M. J. Musselin; *Thin Solid Films, 2*, 211 (1968).
17. J. S. Mason, R. Siriwardane and J. P. Wightman; *J. Adhesion, 11*, 315 (1981).
18. R. C. Weast, Ed.; *Handbook of Chemistry and Physics, 55th ed.*, CRC Press, D-115 (1975).
19. G. F. Kirkbright; *Indicators*, E. Bishop, Ed., Pergamon Press (1972).
20. J. H. Scofield; *J. Electron Spectrosc. and Related Phenomena, 8*, 129 (1976).
21. E. J. Kelly; *Modern Aspects of Electrochemistry, No. 14*, J. Bockris, B. Conway and R. White, Ed., Plenum Press (1982).
22. T. Madeline; "Catalytic Activity of Anodic Oxides on Aluminum," Virginia Tech, Ph.D. dissertation, (1988).

5.0 MACROSCOPIC EFFECT OF ACID/BASE INTERACTIONS - THE PEEL TEST

5.1 Testing of Bonded Joints

Mechanical testing of bonded joints, constructed from materials previously analyzed in terms of their acid/base nature, provides an opportunity to investigate the "real world" significance of acid/base interactions with respect to adhesion science. The testing of a bonded joint is an area where the true interdisciplinary nature of adhesion science is fully revealed. In order to demonstrate the effect of "chemistry" on adhesive performance, a joint design and "mechanical" test appropriate to the "material" that is under investigation must be selected. As can be expected, the mechanical testing of bonded joints is quite complex, and an area of active research.

In practical applications, actual joint designs can be intricate, involving mixed mode loadings and non-uniform stress concentrations in the entire system. Ultimately, the only real test of a bonded structure would be to build a representative sample of the joint for each combination of adhesive, substrate, and surface pretreatment. Such testing would be prohibitively expensive. In practice, one builds simple, standard test specimens which allow the important mechanical properties of the adhesive/substrate system to be explored independently. The peel test is one such standard test.

5.2 Peel Testing

Adhesive joints are inherently weak when subjected to mode I (peel or cleavage) loads. The peel test was developed to take advantage of this since there is a high percentage of tensile (normal) stress in the zone of failure. The entire load is borne over a very narrow strip across the bond. The severity of this test allows one to discriminate between different adhesives in a more sensitive manner than could be achieved in a simple lap-shear test[1,2].

In general, peel testing involves the stripping, at constant rate, of a flexible adherend (peel strip) which has been bonded to a rigid substrate. Some of the common peel test configurations are illustrated in Figure 5.1. The peel force depends not only on the intrinsic adhesion, but on the rate of separation, angle of separation, stiffness of the adherend, viscoelastic nature of the adhesive, temperature, and bond thickness. The stress distribution in peel joints is complex and depends on the mechanical properties of both the adhesive and substrate.

Niesiolowski and Aubrey have assessed the stress distribution in a peel strip by photographic analysis of the peel profile[3]. The deviation of the peel strip, from the position calculated from elementary beam bending theory, was interpreted in terms of the adhesive force, and is shown in Figure 5.2. As can be seen, there are both tensile and compressive stresses acting normal to the bond. Crocombe and Adams have employed large displacement finite element analysis to investigate the peel test[4]. This work has revealed that a maximum stress occurs at the interface adjacent to the flexible peel strip (Figure 5.3), not at the rigid backing. This predicts that any crack will be driven towards the interface, as is found in practice. They also report that the proportions of mode II to the total stress (mode I and mode II) are as large as 30% and are independent of peel load and angle. Their model only considered elastic behavior in both the adhesive and adherend.

The observed response of a joint to a peel test has a strong viscoelastic nature[5-7]. At low rates of separation, or at elevated temperatures, the response of the adhesive is primarily viscous, resulting in cohesive (bulk) failure. The adhesive is often observed to undergo "legging" or filamentation. At higher rates of separation, the response becomes progressively more elastic, filamentation decreases and/or disappears, and failure becomes adhesive (interfacial); that is, it

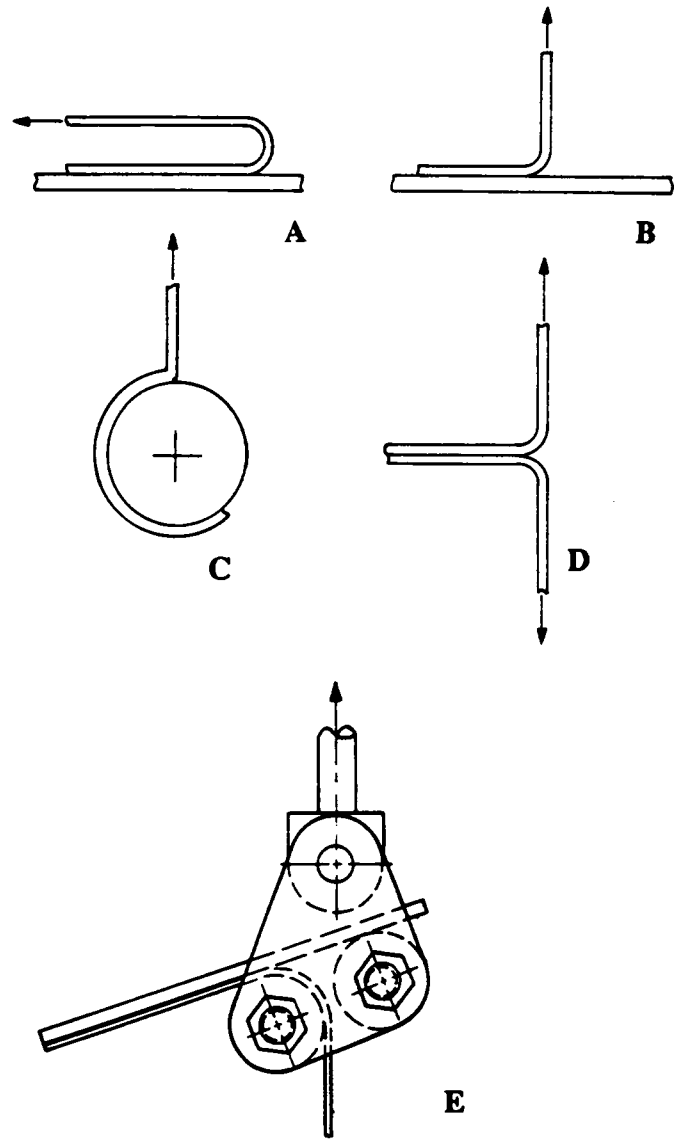

Figure 5.1. Common geometries of the peel test. A. 180° Peel. B. 90° Peel. C. Drum Peel. D. T-peel. E. Floating roller peel.

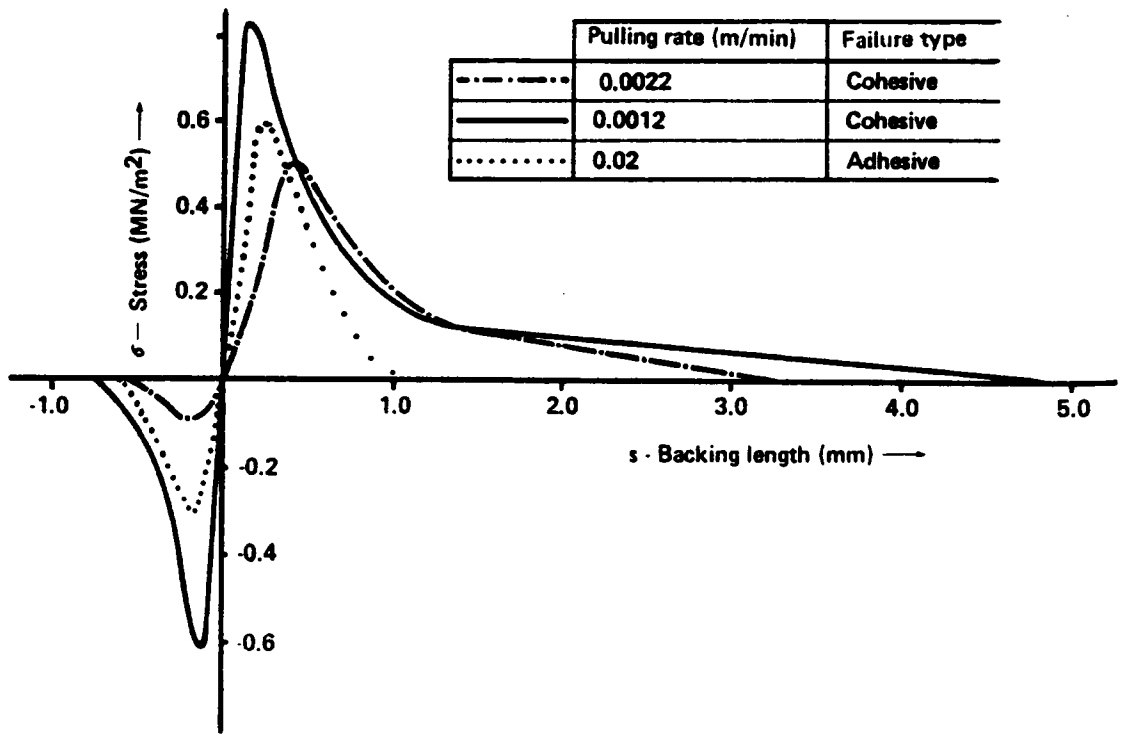

Figure 5.2. Normal stress distribution at three different separation rates (redrawn from Niesiolowski and Aubry[3]).

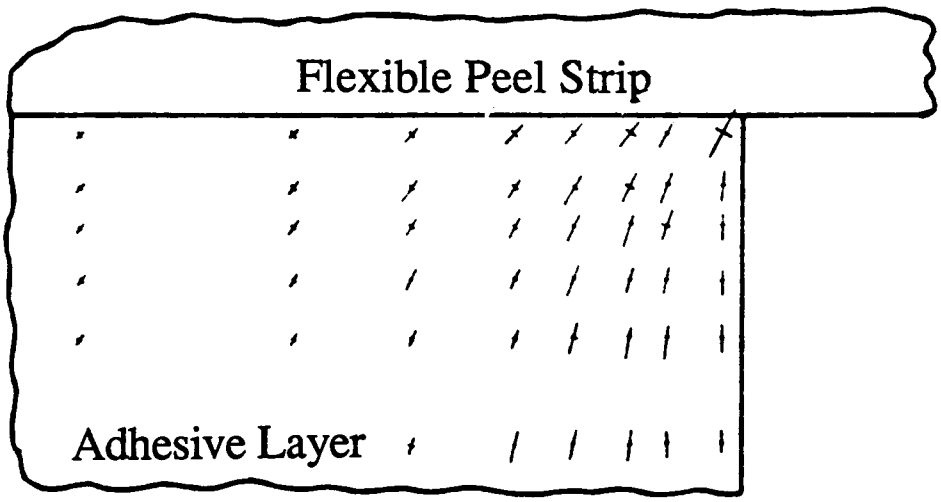

Figure 5.3. Distribution of the adhesive principal stress in the non-cracked peel test. The principal stresses are shown as line vectors (redrawn from Crocombe and Adam[4]).

appears to occur at the adhesive/substrate interface. At even higher rates, a transition to a non-random, oscillating peel force is observed. Figure 5.4 summarizes this behavior in generalized peel force versus separation rate curves. The dotted line at low peel rates represents the cohesive failure, the solid line, an adhesive failure, and the striped line at higher rates represents the oscillating peel force. The peel force shows a decrease immediately after the transition to adhesive failure, then a steady increase with increased peel rate followed by a decrease just before the onset of oscillation.

The lower rate transition from cohesive to adhesive failure has been examined by many researchers. Huntsberger has demonstrated the link of failure mode to viscoelastic processes using poly(n-butyl methacrylate)[6]. He demonstrated that as the test temperature decreases, the relaxation rate of the polymer becomes slower than the rate of force application. When this occured, the stresses concentrate at the interface, and the type of failure changes from cohesive to adhesive.

Gent and Petrich have revealed further evidence confirming the importance of viscoelastic process in the cohesive to adhesive transition, comparing the peel behavior of a linear and crosslinked version of the same adhesive[7]. The crosslinking prevented any liquid-like or viscous flow in the adhesive layer during the time frame of the test. While the linear adhesive (which could undergo flow) showed a cohesive to adhesive transition, the crosslinked version did not; the failure was adhesive at all rates tested. They conclude that liquid-like flow is the cause of cohesive failure, and the transition to interfacial failure occurs when the rate of separation is large enough for the adhesive to behave elastically.

In the same work, Gent and Petrich studied the high speed, oscillatory failure mode, and observed that the crosslinked rubbery adhesive used in the test behaved substantially stiffer when peeled at high rates[7]. They concluded that this stiffening is due to the rubber-to-glass transition brought on by the high rate of deformation.

The regularly oscillating or slip-stick nature of the high speed transition is believed to involve a regular alternation between the rubbery and glassy response of the adhesive[8]. A linear relationship between the "wavelength" of the slip-stick cycle and length of unattached tape has been demonstrated by Wong and Aubrey[9]. They conclude that this is brought about by alternate storage and release of energy by the stretching and relaxing of the unattached portion of the peel strip. The

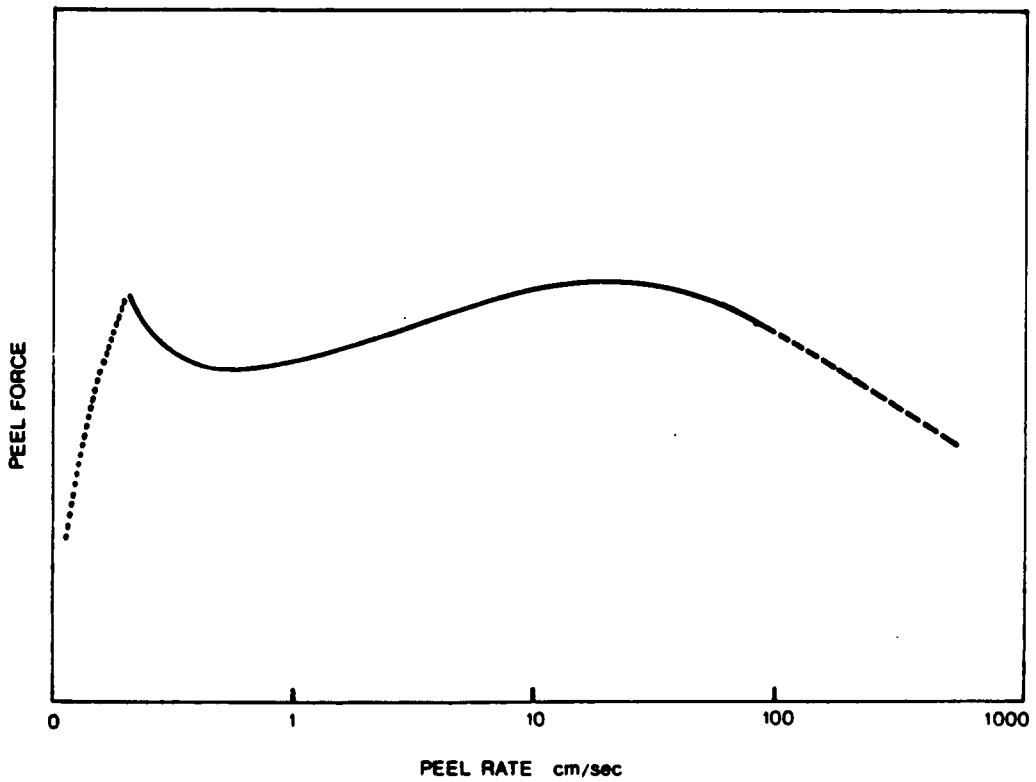

Figure 5.4. Generalized peel force versus peel rate curve (redrawn from Satas[5]).

apparent viscoelastic link between the peel rate, peel force, and temperature has led to the construction of master curves using WLF time-temperature superposition principles. Such studies have been published by Dahlquist[10], Gent[7], Audrey[8], and others.

5.3 Influence of Acid/Base Interactions Via the Peel Test

While the effects of temperature and debond rates on peel testing results are well documented, the use of this test to obtain acid/base information is unknown to the author. The peel test, with its strong viscoelastic dependence, is also a good test of intrinsic or interfacial adhesion. Acid/base interactions will be active in the interphase region of the bonded joint; therefore, any test designed to observe their effect must generate interfacial failure of the bond. The peel test satisfies this requirement. As has been shown by finite element modelling, the stress concentrations in a peel test force cracks towards the interface[4]. In the peel test, the change from cohesive to adhesive failure is accompanied by a sharp drop in the peel load, thus making the change to apparent interfacial failure easy to determine. Finally, the peel test specimen is relatively easy to construct and insensitive to minor flaws in production since, after the debond has moved past a flaw, the experimental results are no longer affected by it.

The property most likely to be affected by the presence of acid/base interactions is *not* the peel load, although historically it has been the parameter of interest. As has been shown, the peel load is dominated by viscoelastic processes so any effect of acid/base interactions would be a slight change on a large "signal". The most likely property to be effected is the rate at which the failure changes from cohesive to adhesive. This view is supported by Gent who states that "improved intrinsic adhesion will shift the low peel rate transition to higher rates of peel"[7].

5.3.1 Effects of Mechanical Interlocking

As discussed in Chapter 1, mechanical interlocking can be an important factor in adhesive phenomena. In any attempt to measure the effect of acid/base interactions, contributions from

mechanical interlocking must be taken into consideration. This can be accomplished by performing the peel test with a neutral adhesive in order to isolate the mechanical contribution. Ideally, a neutral adhesive whose viscoelastic properties matched the actual adhesive exactly should be used, however, in practice, this kind of matching is very difficult. To overcome this, a more relative comparison is employed. The acidic and basic substrates (of potentially different topologies) are bonded with the neutral adhesive. The identical bulk mechanical properties of the neutral adhesive and substrates means the only substantial difference between them will be the interface. The differences between the acidic/neutral and basic/neutral bonds will arise from two factors; the mechanical interlocking at the surface, and dispersion forces active at the surface. Therefore, the differences observed in physical testing with a neutral adhesive can be used as a relative measure of different amounts of mechanical interlock and dispersion forces of the two substrates.

5.3.2 Adhesive/Cohesive Failure

The classical method to determine whether failure is adhesive or cohesive is visual inspection. If the "metal side" of the failure (assuming a metal/adhesive bond) appears free of adhesive then the failure is classified interfacial or adhesive. Recently, there has been a trend to examine failure surfaces using more sophisticated surface science techniques in order to firmly establish the mode and locus of failure. In a peel specimen, there are five potential areas in which failure may initiate and propagate (Figure 5.5). During the propagation of the failure, the crack may jump between areas. The use of surface sensitive techniques is crucial in understanding the failure event. Quite often, examinations employing such techniques reveal that while a surface may visually appear clean (i.e., no adhesive), there are microscopic patches, islands, or complete films still attached to the metal surface; thus what appeared as classic adhesive failure was really mixed-mode or cohesive failure.

In this study of TiO_2/PEHMA bonds, the type of failure will be determined from the X-ray photoelectron spectra (XPS) of the surface. XPS is a surface sensitive technique, with an analytical depth of approximately 100 $\mathring{A}$, therefore, even a slight overlayer of polymer on the substrate would

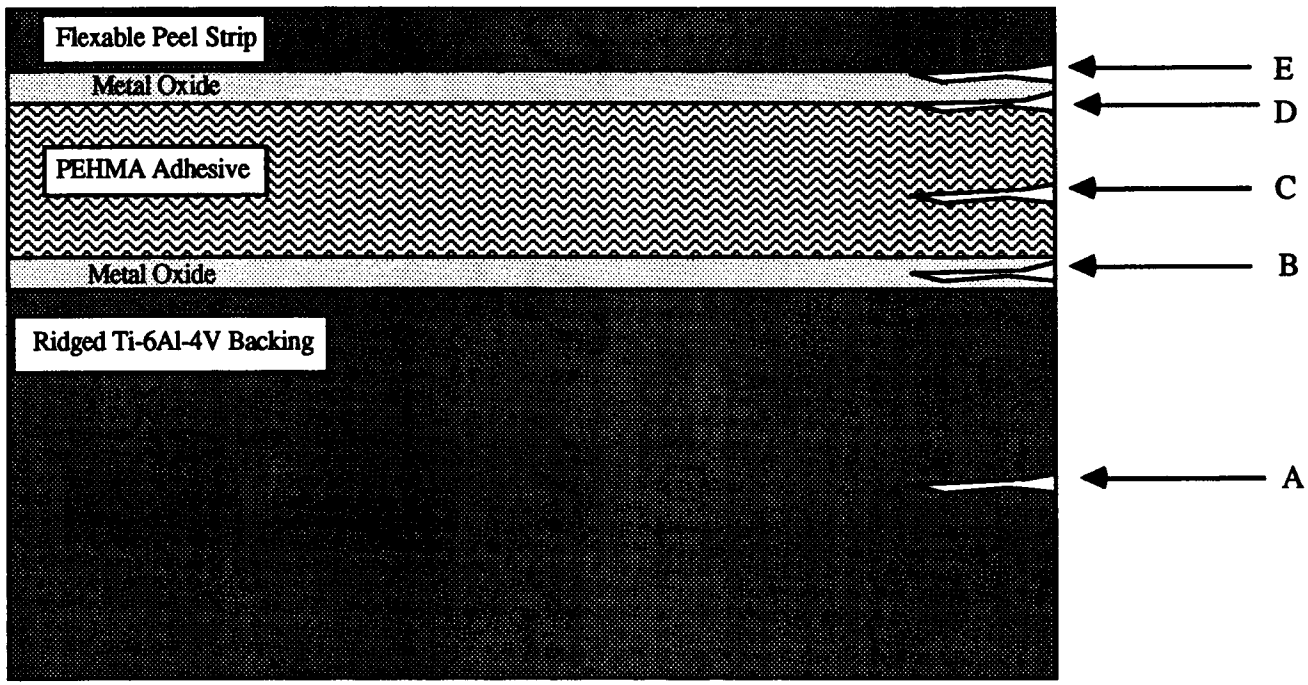

Figure 5.5. Possible locations for the locus of failure in a peel specimen: A. Cohesive in the metal (peel strip or backing) B. Cohesive in the metal oxide (on peel strip or backing) C. Cohesive in the adhesive D. Adhesive at PEHMA / metal oxide interface E. Adhesive at the metal oxide / metal interface

be detected. Clear evidence of the TiO_2 substrate must be indicated for a failure to be classified as adhesive. This means the presence of the tag elements fluorine (for CAA-Ti) and calcium (for PSHA-Ti) and/or clear titanium $2p_{1/2}$, $2p_{3/2}$, and metallic oxygen $1s$ peaks must be apparent. Conversely, the absense of the "tag elements" and/or absence of trace quantities of titanium and inorganic oxygen will be ascribed to cohesive failure.

5.4 Experimental

5.4.1 Materials

The polymer selected for this study was poly(2-ethyl hexyl methacrylate), the same polymer which had been analyzed in the earlier IGC and FTIR studies. The monomer, 2-ethyl hexyl methacrylate, was obtained from Polysciences Inc. and was polymerized, without further purificiation, in bulk via a free radical reaction by Tim Long and Craig DePorter[11]. Two batches of polymer were used in the peel study; the first, by Dr. Long, had a number average molecular weight at 322,000 daltons and a polydispersity of 1.9, the second by Craig DePorter had a molecular weight of 1,280,000 daltons and a polydispersity of 1.9. Triad tacticities of both, revealed by ^{13}C and ^{1}H NMR, were 60% syndiotactic and 40% heterotactic. Both batches of PEHMA, upon receipt, were dissolved in THF, precipitated into a 50/50 methanol-water mixture, dissolved in toluene, filtered and reprecipitated into methanol. This purificiation scheme assured removal of residual monomers, salts, and any particulate impurities.

Hydrogenated poly(isoprene) (HIP) was chosen as the neutral adhesive for two reasons: i) it contained no strong acidic or basic groups nor strong dipoles, and ii) it is an amorphous single phase material. The isoprene monomer was obtained from Goodyear Tire and Rubber Company and purified by passing over activated alumina and molecular sieves, followed by distillation from dibutylmagnesium. The isoprene was then anionically polymerized by Donna Bradley[11] in cyclohexane at 60°C using secondary butyllithium as an initiator under a nitrogen atmosphere. The resulting poly(isoprene) was hydrogenated using a nickel octoate/triethylaluminum catalyst[12]. The

HIP was isolated by decomposing the catalyst with hot aqueous citric acid and decanting off the organic layer. The HIP solution was filtered, precipitated into methanol, dried, redissolved in toluene, filtered and precipitated into methanol. The resulting white, rubbery polymer was dried in a vacuum oven to 100°C for 12 hours. The extent of hydrogenation was determined by ^{1}H NMR to be >99.9% (M_n = 230,000).

The peel strips were made from CP-2 grade titanium foil (.003 in) obtained from ATEK Corporation. The ridge backings were constructed from Ti-6Al-4V alloy sheets (.06 in) obtained from Crucible Research. The anodization techniques and solutions are discussed in Section 4.4 and Appendix C; the reader is referred to these sections for details.

5.4.2 Bond Preparation

Cotton gloves were used during the entire bonding sequence to eliminate the transfer of finger oils to the strips. The peel strips were prepared for bonding by placing five anodized peel strips, flanked by two non-anodized strips on a teflon sheet. The flanking strips prevent "edge effects" while casting the adhesive film. The strips were held flat on the teflon sheet with tape at the ends. A 0.010 in. film of a 5% (wt/vol) solution of PEHMA or HIP in cyclopentane was then cast onto the strips using a doctor's blade. The fresh strips were immediately covered with a watch glass to allow slow evaporation of the solvent and to prevent contamination with dust. The adhesive was allowed to dry overnight at ambient conditions. The strips were then separated using a razor blade and placed into a vacuum oven at 80°C for at least 12 hours to remove residual solvent. A similar procedure was used for the coating of the rigid Ti-6Al-4V backings.

Early in the testing, the vacuum oven was found to be a source for silicon contamination of the bonds. This problem was overcome using two steps. First, all sources of silicone were removed from the vacuum system by changing all tubing, switching to Apiezon T grease for all glass fittings and using a butyl-rubber door gasket. Second, prior to each use, the interior of the vacuum oven was rinsed down with toluene to remove any trace silicone contaminents.

A diagram of the layup used for bonding the peel strip to the rigid backing is shown in Figure 5.6. The foam strips were used to assure even distribution of pressure on all pieces. The bonding was accomplished in a hydraulic press set at 80°C, with a pressure sequence consisting of a 5 min warm-up period at "contact" pressure, then 10 min at 250 PSI. The assembly was then removed from the press and allowed to cool. The bond pieces were tested 24 to 48 hours after bonding.

5.4.3 Mechanical Testing

All peel testing was performed on an Instron model 1123 Universal Testing instrument equipped with an IBM-PC based data acquisition system. A 200 pound tensile load cell was mounted in the crosshead and operated in the 0-10 pound range. The debond rate was assumed to be equal to the crosshead speed of the Instron, and was varied between 0.5 to 20 in/min. Two geometries were used for the peel test; the floating roller test (ASTM: D3167) and the 90° peel test (Instron part 6439-2) which are shown in Figure 5.1. The 90° peel test was restrictive in that the necessity of clamping the 1 in. wide backing along the sides limited the flexible peel strip to a 3/4 in. width. Also, the pulley which aligned the lower clamp to the upper crosshead limited the linear testing distance to 3 inches. The floating roller, however, allowed for a 1 in. wide peel strip and the entire strip to be peeled off the backing.

For low temperature testing (-70°C), an Instron model 3116 environmental chamber was mounted onto the testing frame, with glass wool placed around the chamber's lower jaw exit for more complete insulation. Samples were placed onto the floor of the chamber at room temperature, and then the entire unit was cooled to -70°C via liquid nitrogen blow down. This assured a slow cool down ($\simeq$ 1 hour), and adequate time for the samples to thermally equilibrate. When mounting the samples onto the floating roller testing jig, gloves were worn to limit heat transfer. After the air temperature in the chamber had reequilibrated to the set temperature, the samples were allowed to equilibrate 5 additional minutes before testing.

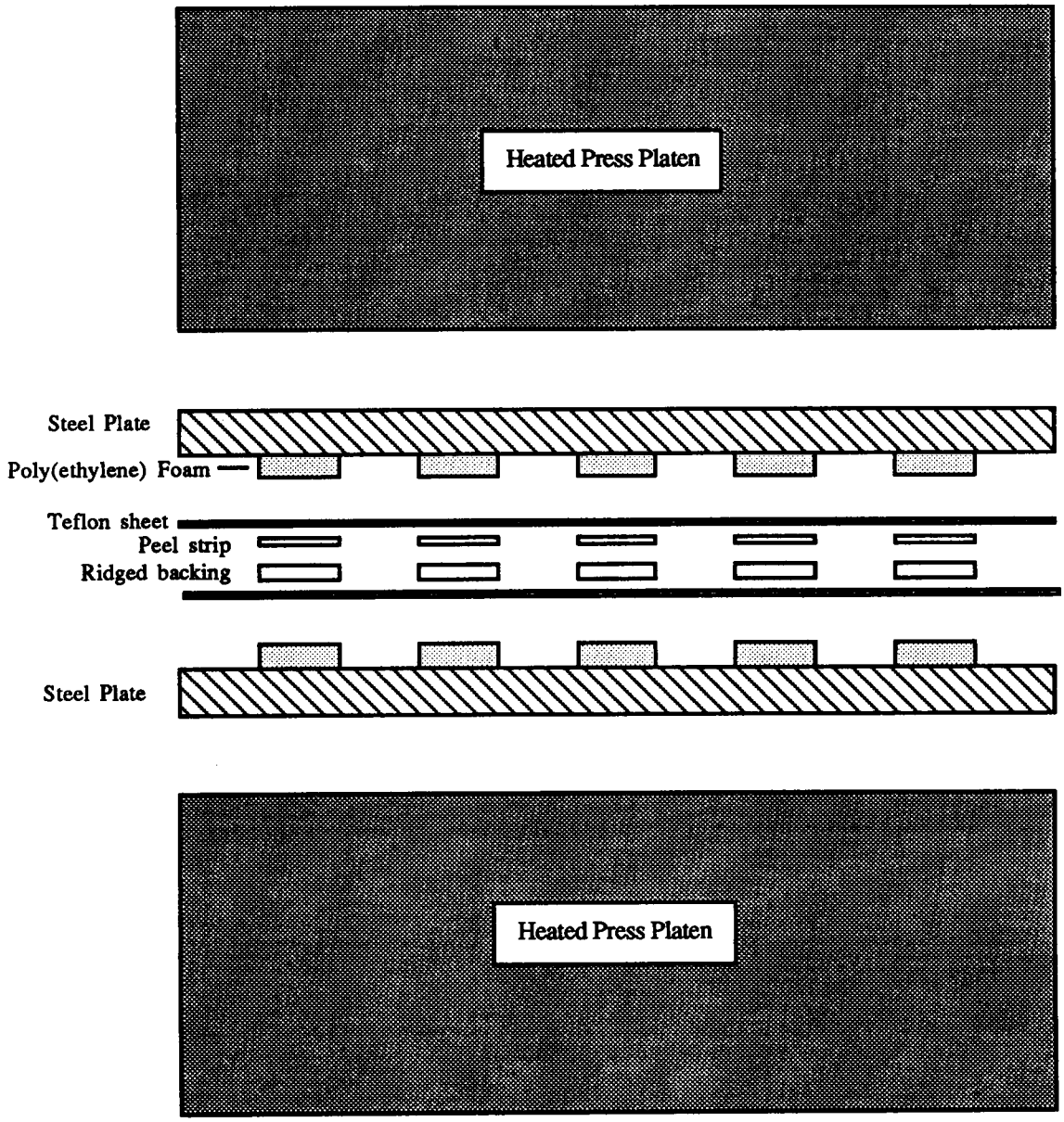

Figure 5.6. Exploded view of bonding assembly for the peel test specimens.

5.4.4 X-ray Photoelectron Spectroscopy

X-ray photoelectron spectra of the failure surfaces were obtained using a PHI 5300 ESCA system equipped with a hemispherical analyzer. A magnesium X-ray anode operated at 250 W was used for all samples. The spot size of the instrument was 2 x 10 mm. The peel strips (after failure) were cut into rough 1 inch diameter hexagons and mounted onto XPS probes using double sided tape. The thicker Ti-6Al-4V samples were cut into 1/4 inch disks using a punch, die, and arbor press, and were then mounted onto the probes using the same method. The "punching" process often produced small burrs and metal flakes which had to be removed from the samples via a tweezers.

A survey scan of each sample was obtained over a binding energy range from 0 to 1000 eV. Fifteen scans were signal averaged for each survey spectra. Narrow scans were performed on any significant peaks noted in the wide scan spectra. Again, fifteen scans were averaged for each narrow scan spectra.

Relative atomic percents were calculated from the narrow scan spectra. The areas for each element were calculated using Perkin-Elmer supplied software. These areas were then corrected by the photoelectron cross-section of each element[13]. The atomic percent for each element was calculated from these corrected area.

5.4.5 Scanning Electron Microscopy (SEM) and Scanning Transmission Electron Microscopy (STEM)

The topography of the failure surfaces were studies using SEM and STEM. Low magnification (< 100X) SEM micrographs were acquired on an International Scientific Instruments SX-40 electron microscope. The sample stage of the SX-40 was large enough so that samples which had been prepared for XPS analysis could be transferred directly to the SEM without further preparation. The use of conductive silver paint on the outside edge of the sample was sufficient to prevent excessive charging. Higher magnification micrographs were acquired using a Philips

EM-420T scanning transmition electron microscope equipped with a Tracor Northern 5500 EDX, Image Analysis system. Peel strips were cut into 3 x 8 mm pieces, sputter coated with gold to prevent charging and mounted into the microscope's probe.

5.5 Results and Discussion

Floating roller peel testing was performed on specimens constructed out of Ti, anodized using the CAA and PSHA pretreatments, and PEHMA (Mn = 332,000). The load versus displacement data (Figure 5.7) indicates that at debond rates of 5.0 in/min and above, the failure propagated in an oscillating, slip-stick fashion. Accompanying the slip-stick failure, the peel strip was observed to "crimp" during the loading or "stick cycle", and emit a sharp "pop" sound when the crack "slips" and propagates. The audible pop indicates that the crack moves significantly faster than the Instron's crosshead speed during the slip. An estimate of the crack speed, based on the sampling speed of the data system and the length of one "slip stick" cycle, puts the crack travelling in excess of 200 in/min. Samples which were failed at debond rates below 5.0 in/min exhibited relatively consistent peel loads interrupted only occasionally by slip-stick failure. This transition, to slip-stick failure at rates above 5.0 in/min, is observed in both PEHMA/CAA-Ti and PEHMA/PSHA-Ti bonds, but appears sharper (e.g., occuring over a smaller range of debond rates) for the CAA pretreated samples. Since this transition is primarily dependent on the bulk properties of the adhesive and the substrate, similar results for both bond types are expected. The thin CAA and PSHA oxide layer should not effect the bulk modulus of the titanium and any interfacial interaction should not effect the bulk viscoelastic nature of PEHMA.

Also common to both PEHMA/CAA-Ti and PEHMA/PSHA-Ti bonds, specimens debonding at rates lower than 5 in/min visually showed small patches of adhesive on the surface, indicating cohesive failure. Thus, to the naked eye, both bond types seem identical.

XPS analysis of the rigid backings (after peel testing) was performed to look for the presence of titanium. The appearance of titanium could indicate that the peel failure was occurring at the backing/adhesive interface, or in the metal oxide layer of the peel strip. Both of these types of

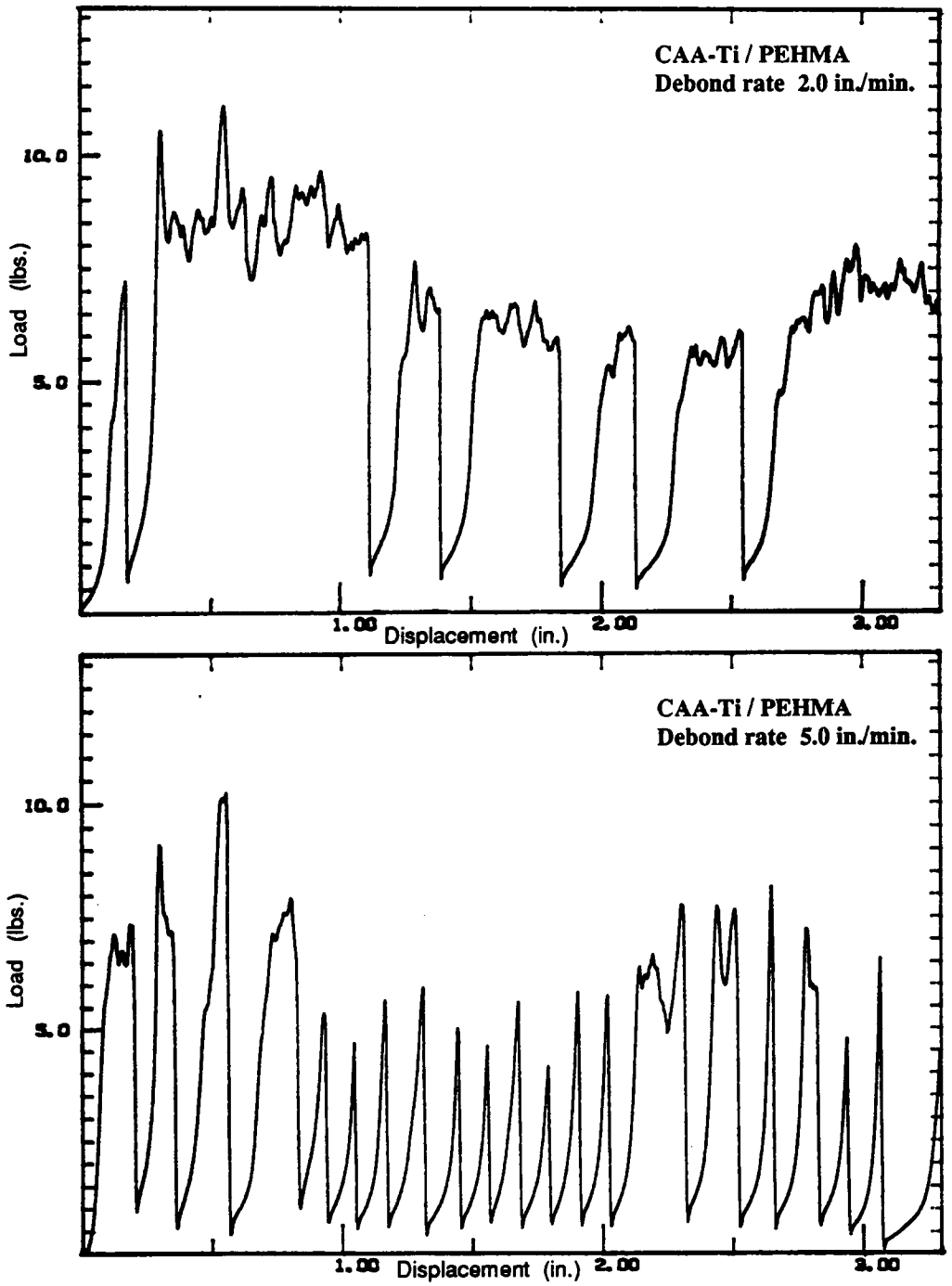

Figure 5.7. Typical load displacement curves for PEHMA/CAA-Ti bond failed in floating roller peel test.

failure were not expected. All samples showed predominately carbon and oxygen on the surface. The occasions on which titanium was observed were random events and were probably due to metal flakes, produced when punching the samples for analysis, adhering on top of the adhesive layer.

XPS analysis of the failed peel strips, however, revealed an important difference between the CAA-Ti and PSHA-Ti bonds. Typical XPS data, on PEHMA/PSHA-Ti peel strips are shown in Table 5.1. At low debond rates (0.5 in/min), the absence of titanium, inorganic oxygen (529 eV) and calcium coupled with the presence of ester oxygens at 532.8 and 533.5 eV indicates cohesive failure; a thin layer of adhesive is still bound to the substrate. This reveals the limitation of simple visual observation of failure surfaces. At the higher peel rate (5.0 in/min), the presence of titanium, calcium, and inorganic oxygen at 529 eV indicate adhesive failure, i.e. at the metal/polymer interface.

The types of failure (i.e., adhesive vs. cohesive) for both pretreatments and average peel loads are summarized in Table 5.2. The most interesting observation from Table 5.2 is that for the CAA-Ti/PEHMA bonds, the failure is cohesive at all rates. Even at the highest Instron speed, the crack does not propagate at the interface, rather, it stays in the bulk adhesive. In contrast, for the PEHMA/PSHA-Ti bonds, the failure mode switches from cohesive to adhesive at rates above 5 in/min.

These results have a clear interpretation in light of the expected acid/base interactions. When the basic PSHA-Ti is bonded with basic PEHMA, favorable acid/base interactions are not possible. Without these interactions, the interface is not strong enough to endure high speed separation and the failure becomes adhesive. When acidic CAA-Ti is bonded with basic PEHMA, favorable interactions are possible. Reinforced by these acid/base interactions, the interface is sufficiently strong to resist adhesive failure until debond rates approach 20 in/min.

As indicated earlier, the failure propagates by a "slip-stick" mechanism at debond rates above 5.0 in/min for both bond types. The peel load data (Table 5.2) does not show a sharp drop at this rate; rather, there is a general decrease with peel rate. When these observations are examined in

Table 5.1. Elemental Composition of PSHA-Ti/PEHMA Failure Surfaces Debonded at 0.5 and 5.0 in/min (Based on XPS Spectra)

Element	Binding Energy (eV)	Atomic Percent	
		0.5 in/min	5 in/min
Carbon	285.0	86	63
Oxygen	529.0	--	29
	532.8 & 533.5	13	--
Titanium	457.0	trace	3.1
Calcium	345.6	--	2.0

Table 5.2. Summary of Floating Roller Peel Test

CAA-Ti/PEHMA Debond Rate (in/min)	0.5	2.0	3.5	5.0	10.0	20.0
Type of failure, visual	•	C*	C*	A	A	A
Type of failure, XPS	•	C	•	C	C	C*
Average peel load (lb/in)**	•	8.5	7.5	7.0	6	5

PSHA-Ti/PEHMA Debond Rate (in/min)	0.5	2.0	3.5	5.0	10.0	20.0
Type of failure, visual	C*	C*	C*	A	A	A
Type of failure, XPS	C*	A*	•	A	•	A
Average peel load (lb/in)**	9.0	9.0	6.5	6	4	5

A = adhesive
C = cohesive
* = mixed mode
• = no data
** = ± 1.0 lb/in

conjunction with the generalized peel curve in Figure 5.4, it appears this transition is brought on by the viscoelastic rubber/glass transition of the polymer.

SEM examination of the PSHA-Ti bonds which underwent adhesive failure revealed an almost featureless surface. At the magnifications necessary to observe the pore structures, the resolution was insufficient to allow focus. The cause of this situation is not clear. A possible explanation is suggested by the XPS data shown in Table 5.1. When the failure was interfacial (5.0 in/min), there was above 60% carbon on the surface of the oxide; this is two to three times the amount of carbon observed on virgin, non-bonded PSHA-Ti. A case could be made that this extra carbon decreases the contrast to the point that resolution is lost at the magnification needed to observe the pores. Visual observation of the bonds which underwent adhesive failure show a dulling of the vivid oxide color present on a virgin surface. This is further evidence is that there is not exact reproduction of virgin oxide upon interfacial failure.

A notable exception to the above observations was found for the CAA-Ti/PEHMA samples which were failed at 20.0 in/min. SEM micrographs of the surface (shown in Figure 5.8), revealed small depressions in which the fracture plane had jumped down to the metal/polymer interface. The pore structure of the oxide layer is clearly visible in the bottom of these depressions. The area surrounding the depression is typical of that seen in cohesive failure; specifically, a gently waving surface covered with microcracks. The micrograph was taken at 30° tilt to normal, and allows a rough estimation of the thickness of the adhesive still adhering to the metal. Using the pores as a guide (they are 300 $\mathring{A}$ in diameter[14]), the layer is on the order of 1000 $\mathring{A}$ thick. There is no data on the adhesive thickness on samples failed at other rates. Energy dispersive analysis of X-rays (EDAX) allows a very coarse estimate of an upper limit to the thickness of a cohesive layer. In a typical SEM, the X-rays analyzed in an EDAX experiment can come from depths up to 2-3 microns. When an EDAX spectrum was acquired on a cohesively failed sample, the observed intensity of X-rays associated with titanium was the same as that for a virgin metal sample. If the adhesive overlays were on the order of 2-3 microns, one would expect the X-ray intensity to be notably reduced. This allows estimation of a coarse upper limit on the adhesive overlay to be placed at 3 microns; the actual thickness is probably significantly thinner.

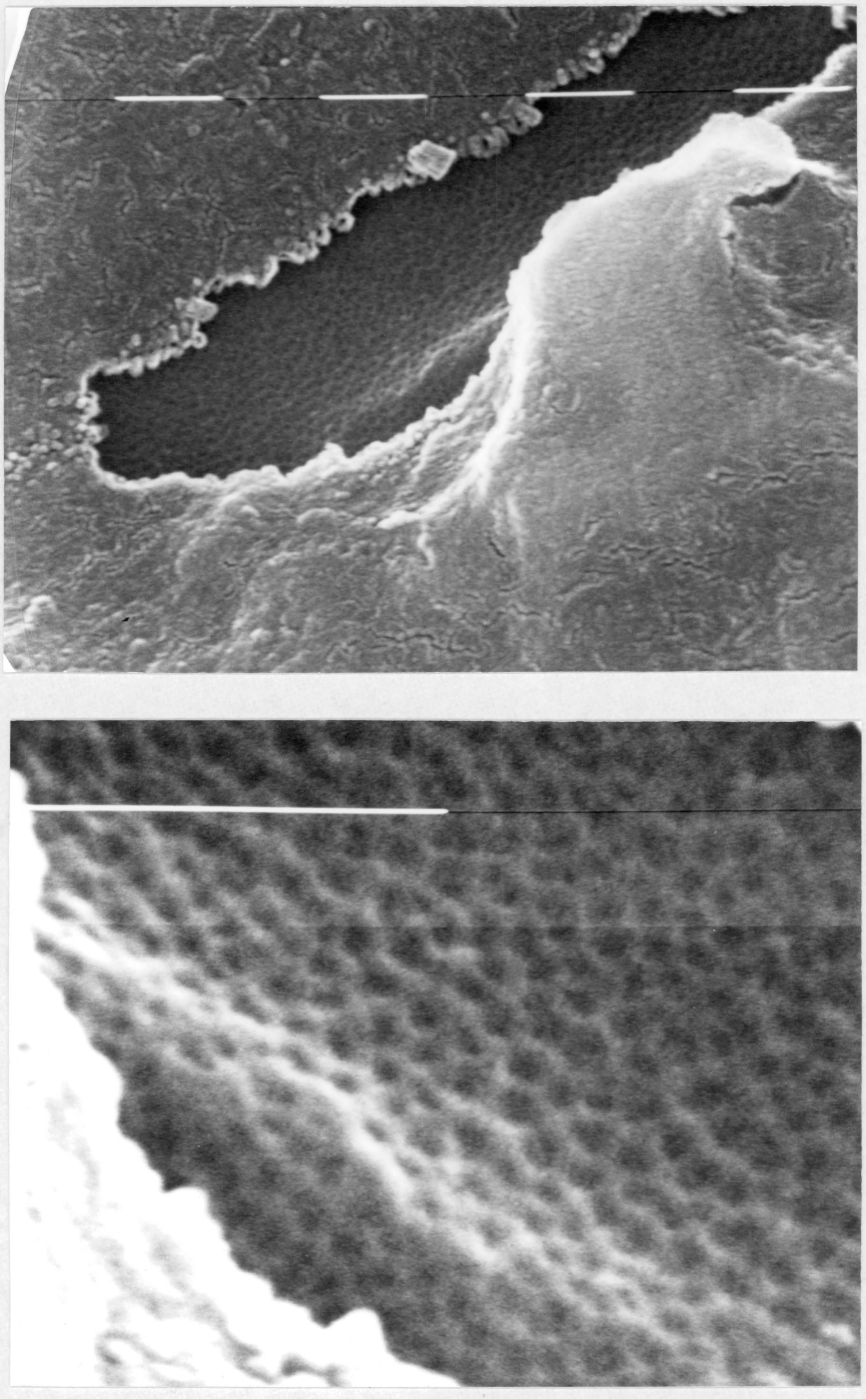

Figure 5.8. SEM micrograph of a CAA-Ti/PEHMA peel strip failed at 20.0 in/min. at 50,000X and 100,000X.

Additional tests were performed using the higher molecular weight PEHMA and the 90° peel test geometry. The 90° test induces a more severe stress concentration than the floating roller test due to the greater angle of peel. The 90° peel test data is summarized in Table 5.3. Mixed adhesive failure is seen in all samples except the PSHA-Ti/PEHMA failed at 20.0 in/min. The mixed adhesive failure was unusual in that the XPS analysis showed strong, clear peaks for titanium, inorganic oxygen and the respective trace elements, and strong clear peaks for organic oxygen. Visually, the sample had small strips of adhesive perpendicular to the direction of peel. The number of these patches decreased with increasing peel rate. Figure 5.9 shows an SEM micrograph of the patches at 24X. The whitish areas in the photo are isolated polymer strips which have charged in the electron beam. The smooth, featureless areas are the metal oxide. The clear, strong titanium oxygen, and trace element XPS peaks indicate that the metal oxide areas are free from any adhesive.

Mechanical interlocking can play an important role in adhesive phenomena. If the two types of pretreated titanium are bonded with a neutral adhesive, any variations between them can be ascribed to mechanical interlocking and/or dispersion force differences. The types of failure for both pretreatments and average peel load for bonds made with a *neutral* adhesive (HIP) are shown in Table 5.4. The average peel load results seem to indicate that the CAA-Ti/HIP bonds support a higher peel load, however, with an uncertainty of ± 3.0 (lb/in) in the measurement, this difference is not significant. Of greater significance is the rate at which the failure type changes. Both PSHA-Ti/HIP and CAA-Ti/HIP bonds changed from cohesive to adhesive failure between 2.0 to 5.0 (in/min) debond rate. These results indicate that the ability to mechanically interlock and/or the dispersion forces active at the surface of the oxides are nearly identical with respect to adhesion. In the testing with the basic adhesive PEHMA, the CAA-Ti bond type clearly demonstrated superior performance. The results from the neutral adhesive testing confirm that superior performance of the CAA-Ti/PEHMA bonds is solely due to favorable acid/base interactions.

Table 5.3. Summary of 90° Peel Test

CAA-Ti/PEHMA Debond Rate (in/min)	2.0	5.0	10.0	20.0
Type of failure, XPS	A*	A*	A*	A*
Average peel load (lb/in)**	4.4	3.1	3.5	1.5

PSHA-Ti/PEHMA Debond Rate (in/min)	2.0	5.0	10.0	20.0
Type of failure, XPS	A*	A*	A*	A
Average peel load (lb/in)***	1.3	1.3	1.0	1.0

A = adhesive
C = cohesive
* = mixed mode
** = ± 1.0 (lb/in)
*** = ± 0.3 (lb/in)

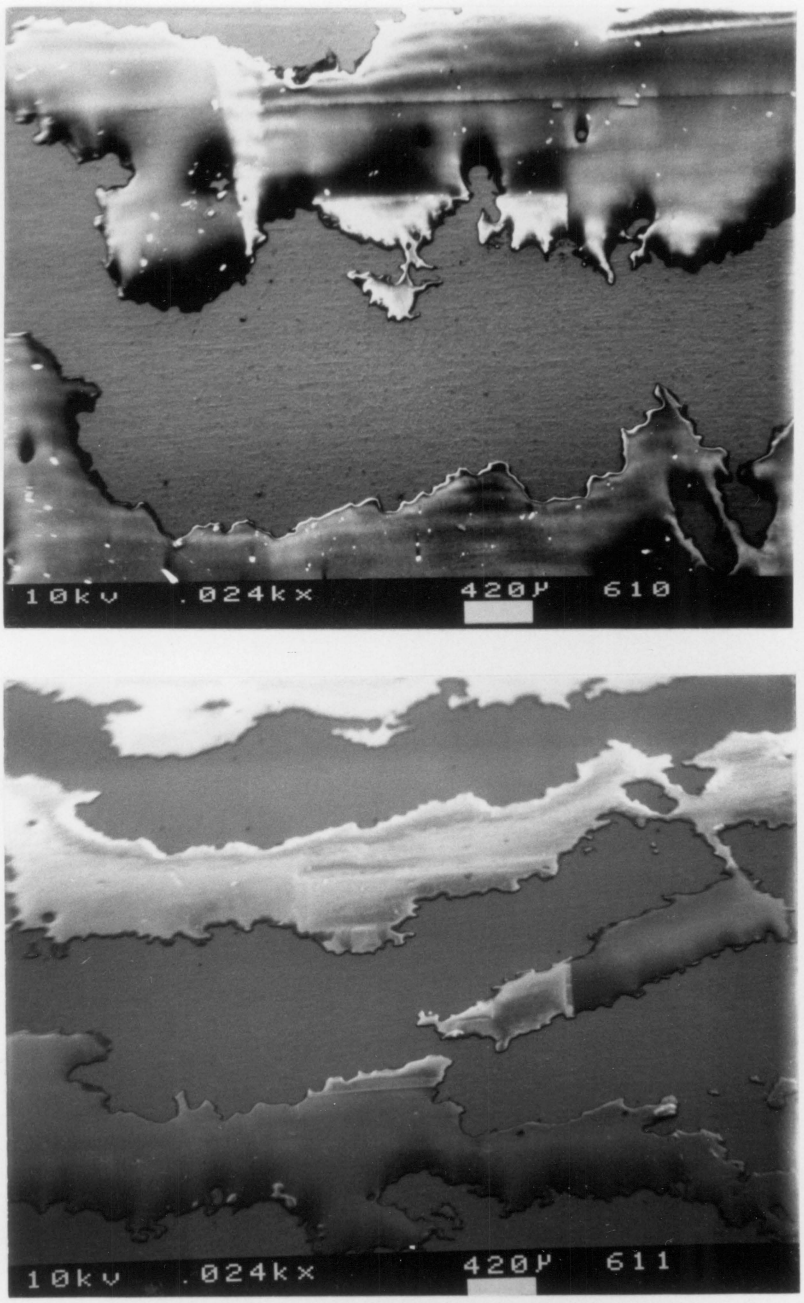

Figure 5.9. SEM micrograph of adhesive strips observed on 90° peel specimens (24X magnification).

Table 5.4. Summary of Neutral Adhesive Testing (-70°C, Floating Roller).

CAA-Ti/HIP	0.5	2.0	5.0	10.0	20.0
Visual failure type	C*	C*	A	A*	A
XPS failure type	C	C	M	A*	A*
Average peel load (lb/in)**	24	20	15	20	17

PSHA-Ti/HIP	0.5	2.0	5.0	10.0	20.0
Visual failure type	•	C*	C*	M	M
XPS failure type	•	C	M	A*	A*
Average peel load (lb/in)**	•	15	16	13	16

A = adhesive
C = cohesive
* = mixed mode
M = ≃50% mixed
** = ± 3.0 (lb/in)

5.6 Summary

It can be concluded that the favorable acid/base interactions that are found in the CAA-Ti/PEHMA contribute to the interfacial performance of the bond. In the floating roller tests of CAA-Ti/PEHMA bonds, cracks did not penetrate or propagate at the interface, but remained in the bulk adhesive. In contrast, the PSHA-Ti/PEHMA bonds did undergo adhesive failure when debonded at rates above 5 in/min. In the 90° peel test where both the CAA-Ti and PSHA-Ti/PEHMA bonds failed adhesively, the CAA-Ti/PEHMA bonds consistently sustained a higher peel load.

It is interesting to note that if the floating roller test data is analyzed only in terms of maximum peel loads and "visual" failure mode, no differences in bond types would be observed. This can be attributed to viscoelastic response of the bonded assembly. The energy dissipated by viscoelastic processes in a soft adhesive overshadow the contribution of favorable acid/base interactions. The XPS results reveal the important differene in interfacial performance of the bond and also the limitations of the naked eye in discerning between adhesive and cohesive failure. The 90° peel test differed from the floating roller test in terms of a more severe stress concentration at the interface due to the higher peel angle. Also, this was coupled with the use of a higher molecular weight adhesive. The "glassy" behavior of the adhesive (i.e. slip-stick at all rates tested) can be attributed to these factors. However, in contrast to the floating roller test, a difference in peel load was observed. One could speculate that this points towards an importance of acid/base interactions in systems where stress is highly concentrated at the interface, and the adhesive exhibits high modulus.

5.7 Future Directions

The peel behavior of uncrosslinked adhesives is still an area of active research. A common problem encountered not only in this work, but in general, is the unsteady magnitude of the peel force. This is not to be confused with the slip-stick phenomenon, but is a noise-like pattern seen

at almost all rates of peel. A "soft machine" peel test has been developed by E. H. Andrews *et al.*[15] which suppresses these oscillations. This novel test method should be pursued as a method to improve data quality.

Gent[16] has recently described improved test of adhesion which can be related to G_a, the fracture energy. The "pull off" peel test appears simple to construct and execute. The "blow-off blister test" is more complex to manufacture, but allows for elastic adherends to be used. However, both tests require no yielding or flow of the adhering strip or adhesive layer for valid G_a measurements. The advantages to these tests is that, if they can be forced to fail interfacially, the fracture energy for adhesive failure is a more quantitative measure of performance than the peel load measurement used in this work.

The idea that acid/base interactions reveal their effects most strongly in systems with high interfacial stress and high modulus adhesives should be pursued. Tentative evidence of this view can be found in Schultz's work with epoxy/carbon fiber composites[17]. In this system of high modulus materials, the ability to withstand high interfacial shear stress correlates strongly with the predicted acid/base interactions.

The effect of acid/base interactions on bond durability should be examined. In many systems, long term exposure to hot, wet conditions result in degradation of the adhesive/substrate interface and interfacial failure of the bond. As acid/base interactions directly effect the interface, their enhancement may reduce and/or retard bond degradation under these conditions.

5.8 References

1. R. D. Adams, A. D. Crocombe and J. A. Harris; *Adhesion, 7*, ed. K. W. Allen, Applied Science Publishers (1983).
2. J. A. Filbey; *Factors Affecting the Durability of Ti-6Al-4V/Epoxy Bonds*, Virginia Tech Ph.D. Dissertation, p. 170 (1987).
3. F. Niesiolowski and D. W. Aubrey; *J. Adhesion, 13* (1981).
4. A. D. Crocombe and R. D. Adams; *J. Adhesion, 12* (1981).
5. D. Satas; *Handbook of Pressure Sensitive Adhesive Technology*, ed. D. Satas, Van Nostrand Reinhold Co. Inc. (1982).
6. J. R. Huntsberger; *J. Polym. Sci., A1*, 2241 (1963).
7. A. N. Gent, R. P. Petrich; *Proc. Roy. Soc., A 310*, 433 (1969).
8. D. W. Aubrey; *Adhesion 3*, ed. K. W. Allen, Applied Science Publishers (1979).
9. D. W. Aubrey, G. N. Welding and T. Wong; *J. Appl. Polym. Sci., 13* (1969).
10. J. O. Hendricks and C. A. Dahlquist; *Adhesion and Adhesives*, Vol. 2, ed. R. Houwink and G. Salomon, Elsevier Publishing Co. (1967).
11. From the Polymer Synthesis Group at Virginia Tech under the direction of Dr. J. E. McGrath.
12. J. M. Hoover; *Morphological Effects on Gas Transport through Poly(methylmethacrylate)-Poly(dimethylsiloxane) Graft Copolymers and Instruments for their Synthesis and Permeability Characterization*, Ph.D. dissertation, Virginia Tech (1987).
13. J. H. Scofield; *J. Electron Spectrosc. and Related Phenomena, 8*, 129 (1976).
14. Chapter 4 of this work.
15. E. H. Andrews, T. A. Khan, and H. A. Majid; *J. Mater. Sci., 20* (1985).
16. A. N. Gent; *J. Adhesion, 23* (1987).
17. J. Schultz, L. Lavielle and C. Martin; *J. Adhesion 23*, 45 (1987).

6.0 Conclusions

The fundamental study of Lewis acid/base interactions presented in this dissertation demonstrates their role in macroscopic adhesive phenomena. The model systems investigated were representative of real substrates and soft, single phase adhesives. The model adhesive, poly(2-ethyl hexyl methacrylate) (PEHMA) was analyzed in terms of its acid/base nature using two techniques: Inverse gas chromatography and Infrared spectroscopy.

From the inverse gas chromatography-derived enthalpy for acid/base interactions,between the model adhesive and selected acidic and basic solvent molecules, it was concluded that PEHMA exhibits the properties of a Lewis base. These values are shown in Table 2.2 and 2.3. The experimental results demonstrate that reliable acid/base information on polymeric systems is available using such chromatographic techniques.

Infrared spectroscopy results confirmed that a reference-state free carbonyl frequency can be established for non-volatile compounds. This allowed the use of the solvent shift effect to gain information about acid/base interactions in polymeric systems. By observation of the solvent shift of the carbonyl stretching frequency, the basic nature of the model adhesive, PEHMA, was again revealed. These solvent shifts, along with the corresponding enthalpies for acid/base interaction derived from the shifts, are shown in Table 3.3. These enthalpies are in good agreement with those independently determined via IGC, and thereby confirm the credibility of these experiments. Comparison of the IGC and infrared-derived enthalpies for acid/base interactions allowed verification of an empirical relation (Equation [3.7), which converts spectral shift information into thermodynamic enthalpies of interaction.

The average Drago E_B and C_B values calculated for PEHMA were 0.27 $(kcal/mol)^{1/2}$ and -0.70 $(kcal/mol)^{1/2}$, respectively. The E_B value is reasonable in that it is a positive value, and only slightly lower than E_B values reported for other aliphatic esters. The negative C_B value is not reasonable as Drago's model does not allow for values less than zero. Statistical modelling of the enthalpic data, based on Equation [3.13], indicates that a contributing factor to the negative C_B value is the relative unimportance of the covalent (C_B) portion of the interaction. The donor strength (f_B), based on Gutmann's model obtained from Equation [3.15] was 0.03 ± 0.01 arbitrary SI units. There is no listing of donor strength for alphatic ester for comparison purposes.

The model substrate, commercially pure grade 2 titanium, was pretreated using chromic acid (CAA) and sodium hydroxide (PSHA) anodization. STEM and XPS analyses of PSHA and CAA pretreated titanium confirmed that oxides of similar topology and elemental composition can be obtained using these anodizations. Indicator dye results confirmed that the CAA pretreatment produces oxide surfaces in the acidic range of pH 3.0 to 2.5. The PSHA pretreatment sample was found to be the basic range of pH 8.0 to 9.0.

It can be concluded from the peel test results that the favorable acid/base interactions found in the CAA-Ti/PEHMA bonds contribute to the interfacial performance of the bond. In the floating roller test, cracks did not propagate at the interface of the CAA-Ti/PEHMA samples, but remained in the bulk adhesive (Table 5.2). In contrast to that, the PSHA-Ti/PEHMA samples did undergo adhesive failure when debonded at rates above 5 in/min. The comparison of visually observed failure and XPS determined failure illustrated the limitations of the naked eye in discerning between adhesive and cohesive failure. When bonds where examined in the more severe 90° peel test, both bond types failed adhesively (Table 5.3), however, the CAA-Ti/PEHMA samples consistently sustained a higher peel load.

In summary, as predicted by the adsorption theory of adhesion, the production of specific interactions (i.e. Lewis acid/base) when two materials are brought into intimate contact can effect the observed adhesion between the two materials. In spite of the viscoelastic dominance of peel test results when testing a soft adhesive, favorable acid/base interactions are manifested in improved interfacial performance of the bond.

Appendix A.

A.1 Derivation of Equation [2.3]

The derivation of this Equation was first demonstrated by Littlewood[1] where one starts with two fundamental Equations:

$$\partial G = -S\partial T + V\partial P \qquad [A.1]$$

and:

$$G = H + TS \qquad [A.2]$$

From Equation [A.1] it is seen that:

$$\left(\frac{\partial G}{\partial T}\right)_p = -S \qquad [A.3]$$

Substituting that into Equation [A.2] yields:

$$G = H + T\left(\frac{\partial G}{\partial T}\right)_p \qquad [A.4]$$

We will now introduce the relation:

$$\left[\frac{\partial\left(\frac{G}{T}\right)}{\partial T}\right]_p = -\frac{G}{T^2} + \frac{1}{T}\left(\frac{\partial G}{\partial T}\right)_p \qquad [A.5]$$

Using the information in Equation [A.4] and substituting yields:

$$\left[\frac{\partial\left(\frac{G}{T}\right)}{\partial T}\right]_p = -\frac{H}{T^2} \qquad [A.6]$$

since:

$$\frac{\partial(1/T)}{\partial T} = \frac{1}{-T^2} \qquad [A.7]$$

then:

$$\left[\frac{\partial\left(\frac{G}{T}\right)}{\partial(1/T)}\right]_p = \left[\frac{\partial\left(\frac{G}{T}\right)}{\partial T}\right]_p \frac{\partial T}{\partial(1/T)} = H \qquad [A.8]$$

in terms of ΔG_m:

$$\left[\frac{\partial\left(\frac{\Delta G_m}{T}\right)}{\partial\, 1/T}\right]_p = \Delta H_m \qquad [A.9]$$

From GC theory, it is known that:

$$\Delta G_m = RT \ln(\gamma^\infty) \qquad [A.10]$$

where:

$$\gamma^\infty = \frac{273.16R}{V_g^o M_2 P_1^o} \qquad [A.11]$$

Substituting into Equation [A.9]:

$$\frac{\partial R \ln \gamma^\infty}{\partial(1/T)} = \Delta H_m = R\frac{\partial \ln \gamma^\infty}{\partial(1/T)} + \ln \gamma^\infty \frac{\partial R}{\partial(1/T)} \qquad [A.12]$$

which reduces to:

$$\Delta H_m = R \frac{\partial \ln \gamma^{\infty}}{\partial (1/T)} \qquad [A.13]$$

Substituting Equation [A.11] into Equation [A.13] and simplifying yields:

$$\Delta H_m = -R\left[\frac{\ln P_1^o}{\partial (1/T)} + \frac{\partial \ln V_g^o}{\partial (1/T)}\right] \qquad [A.14]$$

Since:

$$-R\left(\frac{\partial \ln P_1^o}{\partial (1/T)}\right) = \Delta H_v \qquad [A.15]$$

we can rewrite Equation [A.14] to read:

$$\Delta H_m = \Delta H_v + -R\frac{\partial \ln V_g^o}{\partial (1/T)} \qquad [A.16]$$

$$[\Delta H_m - \Delta H_v] = -R\frac{\partial \ln V_g^o}{\partial (1/T)} \qquad [A.17]$$

$$-\Delta H_s = -[\Delta H_m - \Delta H_v] = R\frac{\partial \ln V_g^o}{\partial (1/T)} \qquad [A.18]$$

which yields our final relation:

$$\frac{-\Delta H_s}{R} = \frac{\partial \ln V_g^o}{\partial (1/T)} \qquad [A.19]$$

A.2 GC Theory, Infinite Dilution

A non-interacting probe injected onto a column will elute at time t_m. The retention volume of this non-interacting probe will be given by:

$$V_m = \dot{V} t_m = al \qquad [A.20]$$

where $\dot{V}$ is the flow rate, l the length of the column and a the volume of gas per unit length of the column. This retention volume is typically called the "dead volume". A probe which interacts with the stationary phase will elute with a longer retention time t_p. The retention volume of the interacting probe, corrected for the dead volume of the column, is given by:

$$V_r = (t_p - t_m)\dot{V} \qquad [A.21]$$

If a soap bubble flow meter is used, a correction for saturation of the carrier gas with water must be made to the flow rate:

$$\dot{V}_{corr} = \dot{V}\left(\frac{P_o - P_{H_2O}}{P_o}\right) \qquad [A.22]$$

where P_o is the outlet pressure of the column and P_{H_2O} the vapor pressure of water at the temperature of the flow meter. A correction must also be made for the pressure drop across the column. The James Martin J factor for gas compressibility is:

$$J_2^3 = \frac{3}{2}\left[\frac{\left(\frac{P_i}{P_o}\right)^2 - 1}{\left(\frac{P_i}{P_o}\right)^3 - 1}\right] \qquad [A.23]$$

where P_i is the inlet pressure for the column.

The net retention volume takes these corrections into account:

$$V_N = J_2^3 (t_p - t_m) \dot{V}_{corr} \qquad [A.24]$$

A more useful quantity which takes the amount of stationary phase into consideration is the specific retention volume:

$$V_g^o = \left(\frac{273.16}{T_c W_l}\right) V_N \qquad [A.25]$$

where T_c is the column temperature and W_l the mass of polymer on the column. The specific retention volume is the elution volume corrected to 0°C per gram of polymer on the column.

At low concentration of probe (infinite dilution) the probe will obey a linear partition function:

$$q = \beta c \qquad [A.26]$$

where q is the probe concentration in the polymer (mol/g), c the concentration in the carrier gas (mol/ml) and β the partition coefficient per unit mass of polymer (ml/g). The GC retention volume can be written in terms of this partition coefficient:

$$V_r = \beta w_l \qquad [A.27]$$

and the specific retention volume can be written:

$$V_g^o = \left(\frac{273.16}{T}\right)\beta \qquad [A.28]$$

A.3 Solution Theory, Infinite Dilution

Present-day polymer solution theories have their origins in vapor-pressure measurement on mixtures of small molecules. The simplest case is that of Raoult's law, where the activity of a component is equal to its mole fraction in solution.

$$P_1 = X_1 P_1^0 = a_1 P_1^0 \qquad [A.29]$$

where P_1^0 is the vapor pressure of the pure component 1, P_1 the vapor pressure over the solution, X_1 the mole fraction of 1 and a_1 the activity of I. This law is generally valid only for mixtures of non-polar liquid of similar size, shape and structure, such as benzene and toluene. In other systems, at lower concentration, linear behavior may still exhibit where the activity is proportional, although not equal, to the mole fraction. This is expressed by Henry's law:

$$P_1 = \gamma_1 X_1 P_1^0 \qquad [A.30]$$

where γ_1 is now the activity coefficient of component 1. We can see that γ_1 is an activity coefficient based on a mole fraction description of the solution.

In light of IGC experiments, when bulk absorption is the dominant mechanism, the theory of gas-liquid partition chromatography may be applied to calculate various thermodynamic results. The concentration of the solvent probe (component 1) in the gas chromatographic column is not known but is low enough (infinite dilution) that Henry's law will be valid. As polymers typically form highly non-ideal solution, a method to assure that Henry's law is valid is to vary the injected sample size and extrapolate to zero concentration. To remind ourselves that we are working in infinite dilution, we rewrite [A.30]:

$$P_1 = \gamma_1^{\infty} X_1 P_1^0 \qquad [A.31]$$

Littlewood has shown that in the region where Henry's law is valid, the relationship between the activity coefficient, partition coefficient and specific retention volume may be written as:

$$\frac{a_1}{x_1} = \gamma_1^{\infty} = \frac{RT}{\beta M_2 P_1^0} = \frac{273.16R}{V_g^o M_2 P_1^o} \qquad [A.32]$$

where M_2 is the molecular weight of the stationary phase.

There is a problem with applying Equation [A.32] in its present form to calculate the activity coefficient. It would seem to suggest that as $M_2 \rightarrow \infty$ (i.e., high polymer), $\gamma_1^{\infty} \rightarrow 0$. The problem

lies in that we have chosen a mole fraction reference to determine γ_1^∞. A more suitable reference would be any concentration variable which does not involve the number of moles of polymer.

We can convert from mole fraction to weight fraction knowing that:

$$ {}^{w}\gamma_1^\infty = (\gamma_1^\infty)\frac{M_2}{M_1} = \Omega_1^\infty \qquad [A.33] $$

If we now apply this to Equation [A.32] we obtain

$$ \Omega_1^\infty = \frac{273.16R}{V_g^o M_2 P_1^o}\frac{M_2}{M_1} = \frac{273.16R}{V_g^o M_1 P_1^o} \qquad [A.34] $$

Rather than P_1^o, the fugacity f_1^o should be used according to the Equation.

$$ \ln f_1^o = \ln P_1^o + \frac{(B_{11} - V_1)P_1^o}{RT} \qquad [A.35] $$

We now write:

$$ \ln \Omega_1^\infty = \ln\left(\frac{a_1}{w_1}\right)^\infty = \ln \frac{273.16R}{V_g^o M_1 P_1^o} + \frac{P_1^o}{Rt}(B_{11} - V_1) \qquad [A.36] $$

A.4 Polymer Solution Theory: Flory-Huggins Lattice Model

Perhaps the most widely used solution model for polymers is the Flory-Huggins lattice model[2]. This approach starts with a statistical mechanics description of the solution. The free energy of mixing is factored into a combinatorial (or athermal) and non-combinatorial (or thermal) contribution.

$$ \Delta G_m = \Delta G_{m,\ combinatorial} + \Delta G_{m,\ non\text{-}combinatorial} \qquad [A.37] $$

The combinatorial term arises for the entropy change upon mixing and is given by:

$$\Delta G_m \, combinatorial = -T\Delta S \, combinatorial \qquad [A.38]$$

The solution is viewed as a lattice, with each site occupied by a solvent molecule or by a polymer composed of r segments. The volume fractions of the solvent (1) and polymer (2) are given by:

$$\phi_1 = \frac{N_1}{N_1 + rN_2}, \quad \phi_2 = \frac{rN_2}{N_1 + rN_2} \qquad [A.39]$$

where N_1 and N_2. equal the number of molecules, and r the ratio of molar volume of polymer to the molar volume of solvent. The change in entropy calculated from the model is:

$$\Delta S_m = -k\,(N_1 \ln \phi_1 + N_2 \ln \phi_2) \qquad [A.40]$$

and therefore substituting [A.40] into [A.38] yields:

$$\Delta G_m, \, combinatorial = kT(N_1 \ln \phi_1 + N_2 \ln \phi_2) \qquad [A.41]$$

$$\Delta G_m \, non\text{-}combinatorial = \Delta H_m \qquad [A.42]$$

The non-combinatorial term comes from replacing solvent-solvent energy contacts of energy ε_{11} and segment-segment energy contacts of energy ε_{22}, with polymer-solvent contacts of energy ε_{12}. The exchange energy is given by:

$$\varepsilon = \varepsilon_{12} - \frac{1}{2}(\varepsilon_{11} + \varepsilon_{22}) \qquad [A.43]$$

If each molecule has z nearest neighbors with which it can interact, then the total non-combinatorial free energy of mixing for N_1 molecules of solvent with N_2 molecules of polymer is:

$$\Delta G_m, \; non\text{-}combinatorial = \frac{N_1 rN_2}{N_1 + rN_2} z\,\varepsilon = (N_1 + rN_2)\phi_1\phi_2 z\,\varepsilon \qquad [A.44]$$

We can now express the Gibbs free energy of mixing by:

$$\begin{aligned}\Delta G_m &= kt(N_1 \ln \phi_1 + N_2 \ln \phi_2) + (N_1 + rN_2)\phi_1\phi_2 z\varepsilon \\ &= kt(N_1 \ln \phi_1 + N_2 \ln \phi_2 + (N_1 + rN_2)\phi_1\phi_2\chi_{12})\end{aligned} \qquad [A.45]$$

where χ_{12} is the Flory-Huggins interaction parameter and is given by:

$$\chi_{12} = \frac{z\varepsilon}{kt} \qquad [A.46]$$

By differentiating Equation [A.45], the activity of the solvent may be obtained.

$$\begin{aligned}\ln a_1 &= \frac{G_1 - G_1^o}{RT} = \frac{1}{kT}\left(\frac{\partial \Delta G_m}{\partial N_1}\right)_{P_1 T_1 N_2} \\ &= \ln \phi_1 + \left(1 - \frac{1}{r}\right)\phi_2 + \chi_{12}\phi_2^2\end{aligned} \qquad [A.47]$$

For an infinitely dilute solution of solvent in polymer (e.g., the IGC experiment), $\phi_1 \rightarrow 0$ and $\phi_2 \rightarrow 1$,

$$\ln(a_1)^{\infty} = \ln \phi_1 + \left(1 - \frac{1}{r}\right) + \chi_{12} \qquad [A.48]$$

Equation [A.48] must now be recast in terms of weight fractions. In order to do this, we define:

$$\phi_1 = \frac{w_1 v_1}{w_1 v_1 + w_2 v_2}, \quad r = \frac{M_2 v_2}{V_1} \qquad [A.49,50]$$

where v_1 and v_2 are the specific volumes of the solvent and polymer, M_2 the number average molecular weight of the polymer and V_1 the molar volume of the solvent. If we again take the limit as $\phi_1 \rightarrow 0$ and $\phi_2 \rightarrow 1$, we now write the weight fraction activity coefficient:

$$\ln\left(\frac{a_1}{w_1}\right)^{\infty} = \ln \Omega^{\infty} = \ln \frac{v_1}{v_2} + \left(1 + \frac{V_1}{M_2 v_2}\right) + \chi_{12} \qquad [A.51]$$

Combining Equations [A.51] with [A.36] gives an expression for χ_{12} in terms of GC retention volumes and was first derived by Patterson *et al.*[3].

$$\chi_{12}^{\infty} = \ln\left(\frac{273.16Rv_2}{P_1^o V_g^o V_1}\right) - \left(1 - \frac{V_1}{M_2 v_2}\right) - \frac{P_1^o}{RT}(B_{11} - V_1) \qquad [A.52]$$

A.5 References

1. A. B. Litlewood, C. S. G. Phillips, and D. T. Price; *J. Chem. Soc.* (1955).
2. P. J. Flory; *Principles of Polymer Chemistry*, Cornell University Press (1953).
3. D. Patterson, Y. B. Tewari, H. P. Schreiber, and J. E. Guillet; *Macromol. 4 (3)* (1971).

Appendix B.

The following relation for the estimation of Lewis acid/base interaction has been postulated by DiPaola-Baranyi *et al.*[1]. Its validity is not readily apparent; however, a breakdown of its logical steps shows its soundness.

$$\Delta H_{f(A|B)} = \left[\Delta H_s^P - \Delta H_s^M\right]_{sam} - \left[H_s^P - \Delta H_s^M\right]_{ref} \qquad [B.1]$$

Each enthalpy of solution terms on the right-hand side of Equation [B.1] can be broken down into individual contributions from intermolecular forces (i.e., the dispersion force contribution for solvent X, ΔH_D^X, the dipole interaction term for solvent X, ΔH_d^X, and so on). Using this pseudo-Hess' Law approach and assuming the additivity of group contributions, it becomes apparent that each like enthalpy term or difference in like enthalpy terms finds its match in the sample and reference portions of [B.1]. Then for all individual contributions, except one, the subtraction results in their canceling to zero. The exception, the enthalpy for the formation of acid/base interactions, is thereby isolate. For a more systematic mathematical description of this process, we can expand the sample portion of [B.1] into enthalpic contributions from dispersion forces, dipole/dipole interactions, vaporization and acid/base interactions and write:

$$\begin{aligned}\left[\Delta H_s^P - \Delta H_s^M\right]_{sam} = {} & \left[\Delta H_D^P - \Delta H_D^M\right]_{sam} + \left[\Delta H_{d|d}^P - \Delta H_{d|d}^M\right]_{sam} \\ & + \left[\Delta H_v^P - \Delta H_v^M\right]_{sam} + \left[\Delta H_{f(A|B)}^P - \Delta H_{f(A|B)}^M\right]_{sam}\end{aligned} \qquad [B.2]$$

The model probe molecule is neutral, and by definition has no acid/base sites or permanent dipoles, so it follows that:

$$\Delta H^{M}_{f(A/B)} = 0 \qquad [B.3]$$

$$\Delta H^{M}_{d/d} = 0 \qquad [B.4]$$

Substituting [B.3] and [B.4] into [B.2]:

$$\begin{aligned}\left[\Delta H^{P}_{s} - \Delta H^{M}_{s}\right]_{sam} = {} & \left[\Delta H^{P}_{D} - \Delta H^{M}_{D}\right]_{sam} + \left[\Delta H^{P}_{d/d}\right]_{sam} \\ & + \left[\Delta H^{P}_{v} - \Delta H^{M}_{v}\right]_{sam} + \left[\Delta H^{P}_{f(A/B)}\right]_{sam}\end{aligned} \qquad [B.5]$$

The second part of [B.1] can be expanded in a similar manner:

$$\begin{aligned}\left[\Delta H^{P}_{s} - \Delta H^{M}_{s}\right]_{ref} = {} & \left[\Delta H^{P}_{D} - \Delta H^{M}_{D}\right]_{ref} + \left[\Delta H^{P}_{d/d} - \Delta H^{M}_{d/d}\right]_{ref} \\ & + \left[\Delta H^{P}_{v} - \Delta H^{M}_{v}\right]_{ref} + \left[\Delta H^{P}_{f(A/B)} - \Delta H^{M}_{f(A/B)}\right]_{ref}\end{aligned} \qquad [B.6]$$

Since both the model probe and the reference polymer are neutral:

$$\Delta H^{P}_{f(A/B)} = 0 \qquad [B.7]$$

$$\Delta H^{M}_{f(A/B)} = 0 \qquad [B.8]$$

$$\Delta H^{M}_{d/d} = 0 \qquad [B.9]$$

$$\Delta H^{P}_{d/d} = 0 \qquad [B.10]$$

Substituting [B.7] through [B.10] into [B.6] yields:

$$\left[\Delta H^{P}_{s} - \Delta H^{M}_{s}\right]_{ref} = \left[\Delta H^{P}_{D} - \Delta H^{M}_{D}\right]_{ref} + \left[\Delta H^{P}_{v} + \Delta H^{M}_{v}\right]_{ref} \qquad [B.11]$$

Combining [B.5] and [B.11]:

$$\left[\Delta H_s^P - \Delta H_s^M\right]_{sam} - \left[\Delta H_s^P - \Delta H_s^M\right]_{ref} = \left[\Delta H_D^P - \Delta H_D^M\right]_{sam} - \left[\Delta H_D^P - \Delta H_D^M\right]_{ref} + \left[\Delta H_v^P - \Delta H_v^M\right]_{sam} - \left[\Delta H_v^P - \Delta H_v^M\right]_{ref} + \left[\Delta H_{d/d}^P\right]_{sam} + \left[\Delta H_{f(A/B)}^P\right]_{sam} \quad [B.12]$$

It is obvious if the heats of vaporization for the probe and model are determined over the same temperature range that:

$$\left[\Delta H_v^P - \Delta H_v^M\right]_{sam} - \left[\Delta H_v^P - \Delta H_v^M\right]_{ref} = 0 \quad [B.13]$$

Dispersion forces are non-specific on the atomic level, and they can be related to the number of electrons and their polarizability. Since these differences between the probe and the model are constant and the dispersion forces are non-specific:

$$\left[\Delta H_D^P - \Delta H_D^M\right]_{sam} = \left[\Delta H_D^P - \Delta H_D^M\right]_{ref} \quad [B.14]$$

and therefore:

$$\left[\Delta H_D^P - \Delta H_D^M\right]_{sam} - \left[\Delta H_D^P - \Delta H_D^M\right]_{ref} = 0 \quad [B.15]$$

rewriting [B.12] we now have:

$$\left[\Delta H_s^P - \Delta H_s^M\right]_{sam} - \left[\Delta H_s^P - \Delta H_s^M\right]_{ref} = \left[\Delta H_{d/d}^P\right]_{sam} + \left[\Delta H_{f(A/B)}^P\right]_{ref} \quad [B.16]$$

We see that we have reproduced Equation [B.1] with the addition of a term for the heat of dipole/dipole interactions. We now must examine the relative magnitude of these terms.

Water has one of the largest dipole moments, approximately 10 times that of normal organic compounds. At 1.82 debyes this roughly corresponds to an interaction energy of 0.7 kJ/mol[2]. Typical hydrogen bond strengths are on the order of 3-30 kJ/mol[3]. This would indicate that the typical enthalpy resulting dipole/dipole interaction is 1 to 2 orders of magnitude *smaller* than the

enthalpies for acid/base interaction. Therefore, in systems where acid/base interactions are expected, Equation [B.16] is effectively equal to [B.1].

We now must view Equation [B.1] in terms of the physical realities of the experiment. Have we accounted for all potential contributions to the enthalpies? The answer is no, yet these additional terms out cancel each other. There could be interactions between the probe molecules and the steel column, injector, detector and with the solid support. Fortunately, as these would be identical for both the sample and reference column, they will have no net effect on the measurement. Also, with an intelligent selection of solid support, good quality steel and well-behaved probes, these effects are minimal.

B.1 References

1. G. DiPaola-Baranyi, J. E. Guillet, H. Jeberien and J. Klein; *Makromol. Chem., 181*, 215 (1980).
2. G. M. Barrow; *Physical Chemistry, 3rd Ed.*; McGraw-Hill.
3. J. March; *Advanced Organic Chemistry, 2nd Ed.*; McGraw-Hill.

Appendix C.

C.1 Titanium Pretreatments

Chromic Acid Anodization (CAA):

1. Wipe with methyl ethyl ketone (MEK)
2. Soak in sodium hydroxide solution (13 g/250 ml) at 70°C for 5 minutes
3. Rinse three times in deionized water
4. Pickling step: Immerse in pickle solution (15 ml conc. HNO_3, 3 ml 49% w/w HF, 82 ml H_2O) at room temperature for 2 minutes (Titanium foils for only 1 min.)
5. Anodize in chromic acid solution (50 g CrO_3/1000 ml)
   - Ti-6Al-4V cathode
   - Room temperature
   - 10 volts
   - 20 minutes
   - Current: 26.9 amp/sq. m., 49% w/w HF is added to attain the desired current density
   - Air bubbler and mechanical stirring
6. Rinse three times in deionized water
7. Blow dry with prepurified N_2 gas until visibly dry

Sodium Hydroxide Anodization (PSHA):

1. Wipe with MEK
2. Immerse in SuperTerj (30 g/l) at 80°C for 15 minutes
3. Rinse three times in deionized water
4. Soak in deionized water at 50°-60°C for 15 minutes
5. Pickling step: Immerse in pickle solution (15 ml conc. HNO_3, 3 ml 49% w/w HF, 82 ml H_2O) at room temperature for 2 minutes
6. Anodize in NaOH solution (5 M)
   - Ti-6Al-4V cathode
   - 20°C
   - 10 volts
   - 30 minutes

- Current: Not controlled, for 8 sq. in. immersed the current decreased to a constant 0.4 amp by 11 minutes
- simple mechanical stirring

7. Rinse in running tap water for 20 minutes
8. Rinse in deionized water
9. Blow dry with prepurified N_2 gas until visibly dry

The vita has been removed from the scanned document